The Meteorological Data of the Neumayer Station (Antarctica) for 1992, 1993, and 1994

Gert König-Langlo and
Andreas Herber

Ber. Polarforsch. 187 (1996)
ISSN 0176 - 5027

List of Contents

1. INTRODUCTION

Since March 1981 a meteorological observatory program is carried out at Georg-von-Neumayer Station (70°37´S, 8°22´W) continuously. Data reports have beeen presented by Gube-Lenhardt et al. (1986), Gube-Lenhardt (1987), Helmes (1989), König-Langlo (1992) and Schmidt et al. (1994). On 16 March 1992 the programme was transferred to the new Neumayer Station (70°39´S, 8°15´W) in a close neighbourhood of the former one.

Neumayer Station is located 8 kilometer southeast of Georg-von-Neumayer Station, (Fig.1). Both establishments are situated at the Ekström Ice Shelf which has a homogenous, flat surface, sloping gently upwards to the south. Thus the environment of both stations is similar. Nevertheless the different distances to the free ocean in the north and to the Atka Bay in the east may become obvious in some atmospheric quantities.

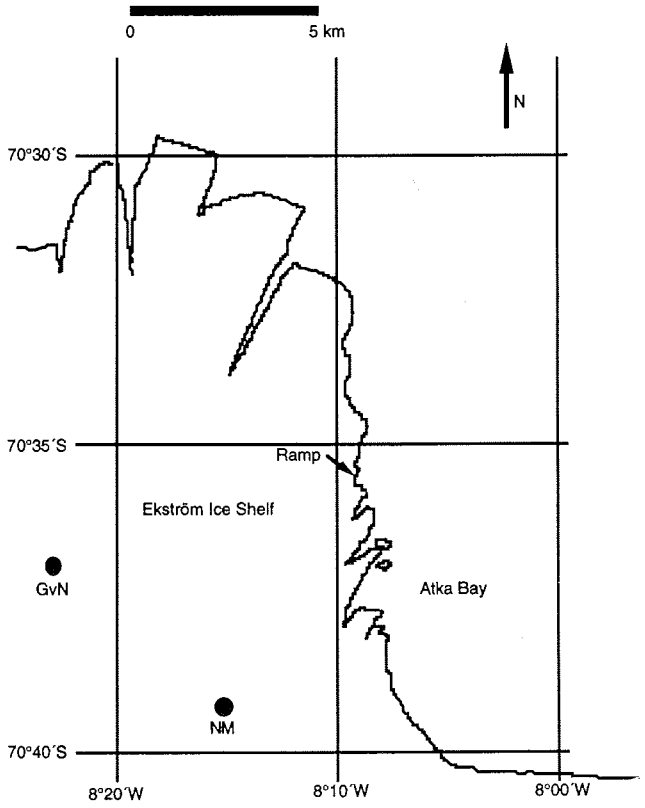

Fig. 1 The geographic location of the "Georg-von-Neumayer" (GvN) and the "Neumayer" (NM) Stations

Starting with the new station the meteorological observatory programme was extended mainly in two points:

- The surface radiation measurements were improved significantly (see Chapter 2.3) to fulfill the demands of the "**B**aseline **S**urface **R**adiation **N**etwork" **BSRN**, (WMO, 1991).
- The ozone soundings started in 1985 at the Georg-Forster Station (70°46´S, 11°41´E) are carried out at Neumayer Station since 1992.

The stations´s annual course of the sun elevation (without refraction) is shown in Fig. 2. The maximum incidence angle is 42.8° at the 22nd of December. The sun stays permanently above the horizon from 19th of November to 24th of January (polar day) and permanently below the horizon from 19th of May to 27th of July (polar night).

This report presents a description of the meteorological data obtained during the years 1992 through 1994. The full data sets are archived in the **M**eteorological **I**nformation **S**ystem at the **A**lfred-**W**egener-**I**nstitute (**MISAWI**). This information system provides a quick and easy access to all data, data subsets, statistics and derived quantities for all users.

Additionally MISAWI offers an interactive interface to the internet which is implemented in the World Wide Web under the address of the AWI home page (http://www.awi-bremerhaven.de).

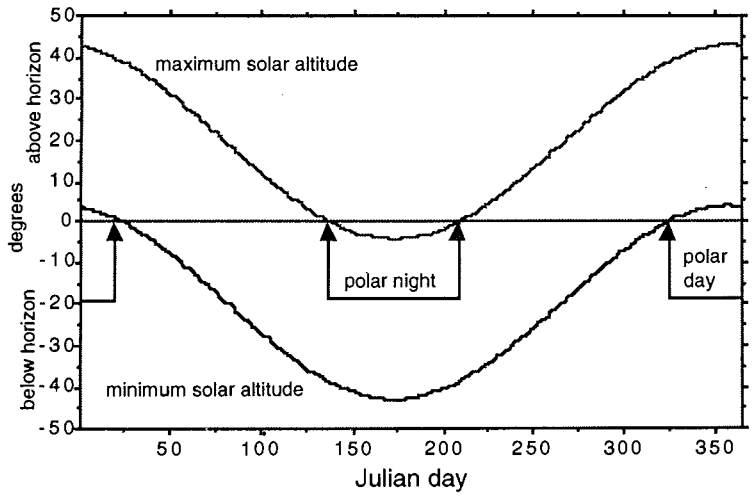

Fig. 2 Annual course of sun elevation at Neumayer

2. *MEASUREMENTS, OBSERVATIONS and INSTRUMENTATION*

The meteorological observatory was operated by:

- Christoph Kleefeld and Harald Rentsch 1992/93
- Jörg Hofmann and Uwe Terzenbach 1993/94
- Jens Fickert and Valeri Goldberg 1994/95

The measurements and observations are subdivided into three groups, namely synoptic observations, upper air soundings and radiation measurements. Fig. 3 portrayes a scheme of the meteorolgical observatory.

2.1) Synoptic Observations

Synoptic observations are carried out routinely every 3 hours. They include measurements of air temperature (at 2m and 10m height), air pressure (values are reduced to mean sea level), wind vector (at 2m and 10m height), dew point temperature (at 2m height), clouds (cloud amount, type and height), horizontal visibility, present and past weather snowdrift and whiteout.

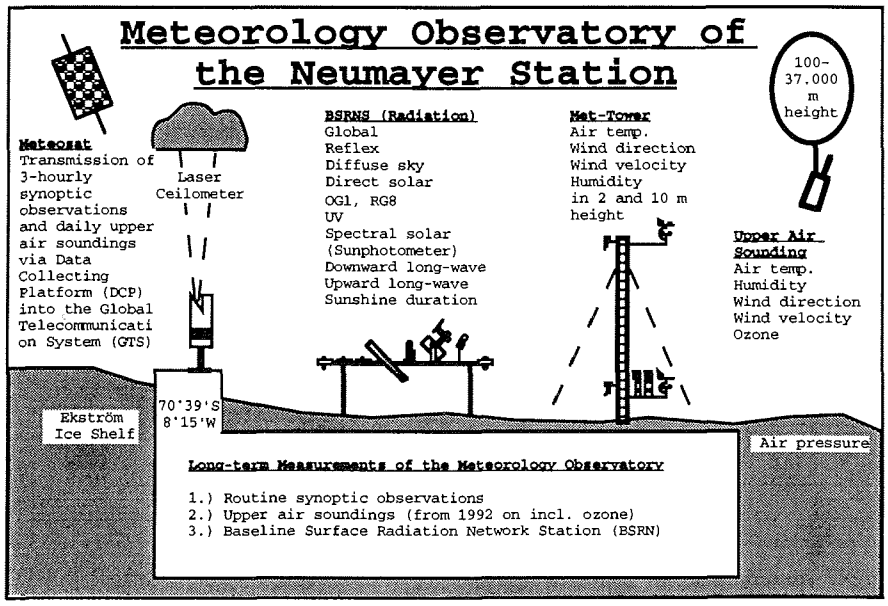

Fig. 3 The meteorological observatory of Neumayer

The full program is carried out at 0, 9, 12, 15, 18, 21 UTC. During night time at 3 and 6 UTC the visual observations are omitted. These data are generally coded (FM12-SYNOP) and transferred directly into the Global Telecommunication System (GTS) by a Data Collecting Platform (DCP). Additionally, they are broadcasted by short-wave communication to other Antarctic stations. In this report all data (2 automatic and 6 full observations per day) are taken into account.

Temperature measurements are carried out with PT-100 platinum resistance sensors with an accuracy of 0.1°C (Thies 2.1265.10). The thermometers are ventilated artificially and protected against radiation.

Relative humidity is measured with two pernix hair hygrometers (Lambrecht 800L100) mounted in naturally ventilated radiation shields and by one Assmann psychrometer. The hygrometers are frequently regenerated alternately and checked against the psychrometer. In spite of this procedure the uncertainty ranges from 5 to 10% due to the harsh polar environmental conditions.

Surface air pressure is detected by using two quartz systems (Digiquartz, 215-AW002). Routinely the Digiquartzes are checked with two absolute instruments (Friedrichs normal barometer 2K, Fuess hypsometer). The digiquartzes are installed inside the station but connected to a pipe which ends outside the station at a depth of about half a meter below the snow surface. Thus influences due to wind induced pressure fluctuations or effects caused by the air-conditioning inside the station can be eliminated.

For the reduction of the air pressure to mean sea level an instrument height of 36m is applied untill 16 March 1992 (height of Georg-von-Neumayer Station) and of 42m since16 March 1992 (height of Neumayer Station). Compared with the uncertainties of the instrument height other errors in the pressure measurements can be neglected.

The wind vector is determined by a combined instrument consisting of a cup anemometer and a wind vane (Thies 4.3323.11.41).

Cloud base heights below 12000 feet are determined by a ceilograph (Impulsphysik LD-WHX 05). Bases above the 12000 feet level are estimated visually.

2.2) Upper Air Soundings

Routinely once daily (about 10:00 UTC) a radiosonde is launched to measure vertical profiles of air pressure, temperature, relative humidity and the wind vector. The resulting TEMP message is also transferred into the GTS via a DCP. Normaly, one ozonesonde is launched every week to measure the vertical ozone profile through the troposphere and the lower stratosphere.

Upper air soundings are carried out with VAISALA RS80-15N radiosondes which directly measure air pressure, air temperature and relative humidity. The wind vector is determined with the aid of the OMEGA navigation system, the height information is calculated using the hydrostatic approximation.

Helium filled balloons (TOTEX 350g, 600g) are used to obtain an ascent velocity of about 5m/s. Typically the balloons burst at heights between 20 and 35km. To reach such height levels also during wintertime when the stratosphere is extremely cold, the balloons are pretreated by heating and oil dipping.

For the ozone soundings a VAISALA RS80-15NE radiosonde is connected via an interface (RSA11 OZONE) to a VAISALA ECC sonde. A 1200g TOTEX balloon is used for these ascents.

All balloons were filled inside an inflation shed equipped with a sliding door 3m wide and 4m high. During strong wind conditions (>20m/s), only 350g balloons could be launched with a reasonable chance of success.

The data reception and evaluation is carried out by a DigiCora System (VAISALA, Finland).

2.3) Radiation Measurements

The following radiation quantities are measured every minute and stored in form of 5 minute averages:

- global (solar) radiation with glas-filter (305 - 2800nm)
- global radiation with OG1-filter (530 - 2800nm)
- global radiation with RG8-filter (695 - 2800nm)
- UV radiation (300 - 370nm)
- diffuse sky radiation (305 - 2800nm)
- direct solar radiation (305 - 2800nm)
- reflected solar radiation (305 - 2800nm)
- downward long-wave radiation (4 - 50µm)
- upward long-wave radiation (4 - 50µm)
- sunshine duration.

Nearly all radiation sensors are ventilated with slightly preheated air (Eigenbroth, FRG) to minimize hoar frost problems and zero offset effects during cloud- and windless conditions. The radiation measurements are carried out with:

- 5 pyranometers (CM11, Kipp&Zonen, Netherlands) for global radiation (glas, OG1-, RG8-filter), diffus sky radiation and reflected solar radiation,
- 1 normal incidence pyrheliometer (NIP, Eppley, USA) for direct radiation,
- 1 UV-meter (TUVR, Eppley, USA) for broadband UV radiation,
- 2 pyrgeometers (PIR, Eppley, USA) for upward and downward long-wave radiation,
- 1 photoelectric sunshine detector (Solar 111b, Haenni and Cie., Switzerland).

The normal incidence pyrheliometer is mounted on a sun tracker (ST-1, Eppley, USA) which follows the azimuth direction of the sun automatically. The diffuse sky radiation is obtained using a shadow ring with a diameter of 58cm and a width of 5cm. From the pyrgeometers the thermopile output and the body temperatures of the instruments are recorded separately.

All instruments are calibrated at the Deutscher Wetterdienst at Hamburg Sasel. After one year of operation the sensors are exchanged with newly calibrated instruments.

Together with the radiation data 5 minute averages of the surface air pressure, relative humidity (2m), air temperature (2m and 10m) and the wind vector (2m and 10m) are recorded. The

minimum value of the ceilometer record within the 5 minute intervals is taken as the cloud base height.

In addition to the continuous radiation measurements sun photometer measurements are performed whenever the sun is located between 4° and 20° above the horizon and is not hidden by clouds. The measurements are carried out by applying the **A**chtkanal-**B**oden-**A**tmosphären-**S**onnenphotometer (**ABAS**) of Leiterer and Weller (1988).

The sun photometer operates in the spectral range between 380nm and 1100nm. With the aid of the Bouguer-Lambert's law the atmospheric optical depth can be derived from the measured direct solar radiation. Airmass corrections are taken into account by the method of Kasten and Young (1989).

Rayleigh scattering effects and the absorbtion of atmospheric trace gases, like water vapour and ozone, are considered according Froehlich and Shaw (1980) before the aerosol influence on the optical depth is estimated.

The instruments are calibrated at a high level Alpine site in Europe (Zugspitze-Alps, Germany) and, by the Langley procedure, in Antarctica. The uncertainty of the measurements is less than 0.008 for the aerosol optical depth.

3. DATA PROCESSING and ARCHIVING

3.1) Data Processing

Close to the radiation sensors their analog signals of the radiation sensors are amplified inside a heated and thermostated box. In a second box of the same kind the interfaces for all sensors mounted on the meteorological tower are installed. The analog/digital conversion of the preconditioned signals take place in the meteorological observatory inside the station, see Fig. 4.

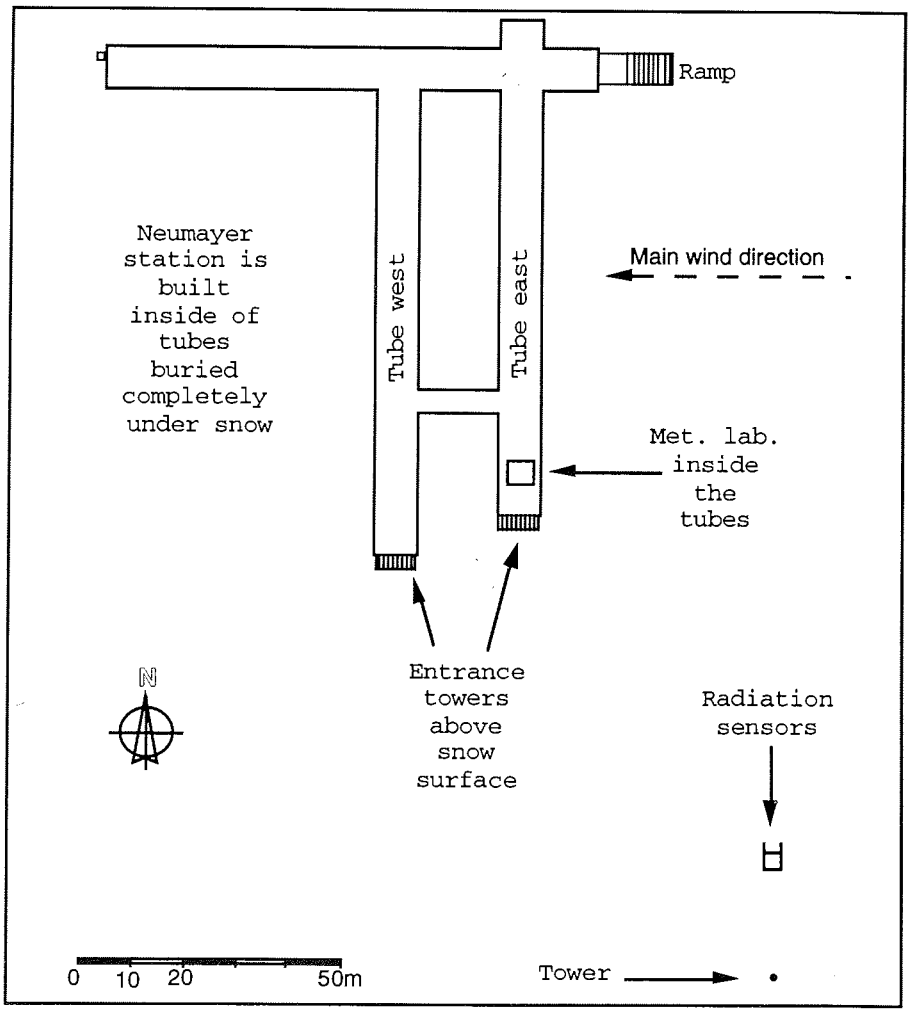

Fig. 4 Neumayer station and the surrounding area

The same computer (Compac 286) which houses the two A/D-plug-in boards (DAS-20, Kethley, USA) also samples the digital signals from the ceilometer and the digiquartz interfaces using a 4 channel serial interface board (DIB COM 4-I, COMES, Germany). The data aquisition program provides the following functions:

- sampling every channel once a minute,
- transforming the signals into physical units,
- checking for error limits,
- displaying actual data numerically,
- preparing 5-minute averages,
- visualysing requested data of the day and background information such as sun elevation, etc.,
- feeding an information terminal in the mess room,
- providing wind values for the wind power generator of Neumayer,
- coding an FM-12 message every three hours. (During daytime visual information is added by the observers),
- sending the FM-12 message to an interface of a **D**ata **C**ollecting **P**latform (**DCP**) for injection into the **G**lobal **T**ele-communication **S**ystem (**GTS**),
- archiving data on a local harddisk as back-up,
- transfering data into the network of the Neumayer station (ethernet) for further postprocessing steps on a computer cluster (SUN, SPARC IPX).

The on-line visualisation helps to detect malfunctions like mispointing of the solar tracker, hoar frost deposition on radiation instruments, etc and to immediately correct such defects. Thus a rather high data quality with data gaps of less than 1% can be assured.

The data processing of the routine upper air soundings is carried out almost automatically by the DigiCora System. For the DCP a compressed data set according to the FM35 TEMP-code is prepared. The full data set consisting of pressure, temperature, humidity and wind vector measurements in 10 second intervals is first stored on a personal computer (Tandon 286) and later transfered via ethernet into the SUN cluster.

The ozone soundings require special processing steps including visual inspections. A compressed data set according to the

TORONTO-code is prepared and transfered in near real time to WMO at Geneva.

Every day the following amount of data is aquired:

- 1 kByte for the 3-hourly meteorological observations,
- 50 kByte for the 5-minute averages from the radiation and meteorological sensors,
- 200 kByte of raw data from the ceilometer including the backscatter profile from 107 levels every minute and
- 100 kByte for the radiosonde data.

1992 a data link between Neumayer and AWI in Bremerhaven has been established via a satellite modem connection. Because of the high transmission costs only the 3-hourly meteorological observations and the weekly ozone profiles (TORONTO-code) are transferred routinely while the other data are transported to Bremerhaven once a year by ship.

The total amount of all data collected during one year ranges between 100 - 200 MByte. It easily fits on one magneto optical disk or exabyte tape. After final postprocessing steps at AWI all data - except the raw values of the ceilometer - are imported to the **M**eteorological **I**nformation **S**ysten of the **A**lfred-**W**egener-**I**nstitut (**MISAWI**).

3.2) Data Archiving

MISAWI consists out of 3 databases, namely:

- "ObseDB" for the 3-hourly synoptic weather observations,
- "RadiosondenDB" for the upper air soundings including the ozone concentrations,
- "StrahlungDB" for the 5-minute averages of the radiation and atmospheric surface data.

Synoptic data are available since 28 January 1981, upper air data since 21 February 1983 and some radiation quantities since 13 March 1982. After 16 March 1992 all radiation components exist to the standard of the global "**B**aseline **S**urface **R**adiation **N**etwork" (**BSRN**).

3.3) Database Description

In this section the structure of MISAWI is described briefly to offer all nesessary information to any reader who wish to use MISAWI for their individual data analysis.

A database system allows continuous access to any data without being concerned about the structure of the files or how to access any single value within a record. The users only need to give the identification of a particular piece of information (attributes like date, hour, temperature, etc.) they want to select or work with.

For the "ObseDB" database the following attributes are stored in table "GemDaten":

ObseDB.GemDaten

FM12-Code	Attribute Name	Units
(administration)	Obse_ID#	-
(administration)	Messort_ID#	-
Year, MiMi,YY,GG	DatumUhrzeit	-
h	Wolkenuntergrenze	WMO-code
VV	HorSicht	WMO-code
d d	Windrichtung	degrees
f f	Windgeschw	m / s
TTT	Temperatur	°C
$T_dT_dT_d$	Taupunkt	°C
PPPP	Luftdruck	hPa
a	ArtLuftdruckAenderung	WMO-code
p p p	BetragLuftdruckAenderung	hPa
w w	GegenWetter	WMO-code
W_1	VergWetter1	WMO-code
W_2	VergWetter2	WMO-code
C_L	TiefeWolken	WMO-code
C_M	MittlereWolken	WMO-code
C_H	HoheWolken	WMO-code
N	GesamtBedeckung	octa
N_h	BedeckungClCm	octa
(administration)	DatenValidiert	-

In table "Station" the following special observations are available:

ObseDB.Station

FM12-Code	Attribute Name	Units
(administration)	Obse_ID#	-
$T_XT_XT_X$	MaxTemperatur	°C
$T_nT_nT_n$	MinTemperatur	°C
S_8	GegenwSchneetreiben	WMO-code
S'_8	VergSchneetreiben	WMO-code
96111	Whiteout	WMO-code

Joins between the two tables can be constructed easily by using the unique index Obse_ID#.

In the "RadiosondenDB" database each sounding is described with attributes such as Aufstieg_ID#, date, time, height of tropopause, precipitable water content, etc. in table "Aufstieg" (sounding). The profile data of each sounding are stored in the table "Messung" (measurement) containing up to 1200 tuples per sounding with the following attributes:

RadiosondenDB.Messung

Value	Attribute Name	Units
(administration)	Aufstieg_ID#	-
(administration)	ZeilenNr#	-
pressure	Druck	hPa
height	Hoehe	meter
temperature	Temperatur	°C
rel. humidity	RelFeuchte	%
wind direction	Windrichtung	degrees
wind speed	Windgeschw	m/s
water vapour content	Wasserdampfgehalt	g/cm^2
ozone concentration	Ozon	mPa

Other evaluative values such as potential temperature, dewpoint, specific humidity, virtual temperature and wind components are available in the virtual table "ViewMessung". The additional table "HDF" contains interpolated values of the mean pressure levels and table "FH" of fixed heights. Joins between the tables can be constructed using the unique index Aufstieg_ID#.

The "StrahlungDB" consists mainly of 3 tables with measurements and derived quantities. In the table "Strahlung" (radiation) the following attributes exist:

StrahlungDB.Strahlung

Value	Attribute Name	Units
(administration)	Strahlung_ID#	-
(administration)	Messort_ID#	-
date and time	DatumUhrzeit	-
global radiation	Global	W/m^2
reflected global radiation	Reflex	W/m^2
diffus sky radiation	Diffus	W/m^2
direct solar radiation	Direkt	W/m^2
global with OG1-filter	OG1	W/m^2
global with RG8-filter	RG8	W/m^2
UV radiation	UV	W/m^2
pyrgeometer signal $\Downarrow$	GegenSignal	W/m^2
pyrgeometer temperature $\Downarrow$	GegenTemp	°C
pyrgeometer signal $\Uparrow$	AusSignal	W/m^2
pyrgeometer temperature $\Uparrow$	AusTemp	°C
sunshine duration	Sonne	minutes
cloud base height	Wolkenhoehe	meter
solar elevation	Sonnenhoehe	degrees
relative air mass	Luftmasse	-
extraterrestrial insolation	AstroEin	W/m^2
surface albedo	Albedo	%
derived surface temperature	Temp0	°C

From the signals of the pyrgeometers (PS) and their body temperatures (PT) the downward and upward long-wave radiation (L) is virtually implemented in table "ViewStrahlung" by using:

$$L = PS + 5.67 * 10^{-8} * (PT + 273.15)^4$$

The extraterrestrial insolation and solar elevation is derived after Iqbal (1983), while the relative air mass was calculated after Kasten (1966). To obtain reliable albedo values, the albedo is archived only for cases when the global radiation exceeds 50 W/m^2. Temp0 denotes the black body temperature of the snow surface calculated from $L\Uparrow$.

Table "Mast" (tower) contains the 5-minute averages of the meteorological tower and associated values.

StrahlungDB.Mast

Value	Attribute Name	Units
(administration)	Messort_ID#	-
date and time	DatumUhrzeit	-
temperature in 10m	Tem10	°C
wind speed in 10m	FF10	m/s
wind direction in 10m	DD10	degrees
temperature in 2m	Tem2	°C
wind speed in 2m	FF2	m/s
wind direction in 2m	DD2	degrees
relative humidity in 2m	RelFeuchte1	%
relative humidity in 2m	RelFeuchte2	%
station air pressure	Stationsdruck	hPa

In many cases daily averaged radiation quantities are important. They are available in table "Tagesmittel" (daily averages).

StrahlungDB.Tagesmittel

Value	Attribute Name	Units
(administration)	Messort_ID#	-
date and time	DatumUhrzeit	-
global radiation	Global	W/m^2
reflected global radiation	Reflex	W/m^2
diffus sky radiation	Diffus	W/m^2
direct solar radiation	Direkt	W/m^2
global with OG1-filter	OG1	W/m^2
global with RG8-filter	RG8	W/m^2
UV radiation	UV	W/m^2
downward long-wave	Gegen	W/m^2
upward long-wave	Aus	W/m^2
sunshine duration	Sonne	hours
extraterrestrial insolation	AstroEin	W/m^2
ext.sunshine duration	AstroSonne	hours

To minimize effects of missing measurements the following averaging scheme is applyed:

- 3-hourly averages are constructed (0-3, 3-6, ..., 21-00 UTC) if at least one 5-minute value (normally 36) exists within the averaging interval.

- daily averages are calculated on the basis of the 8 3-hourly averages.
- if one or more 3-hourly averages per day is missing, no daily averages is calculated.

While the raw data are loaded into the database system they are subject to quality-control procedures by the database management system. The data are examined and checked under pre-defined conditions and all suspect cases are flagged for manual review, correction (if required) and updating of the data set. There are, for example:

- checks for impossible format codes,
- tolerance tests: many attributs which are reported by code have defined limits, e.g. cloud amount, visibility. Other attributs may have implied upper or lower limits, e.g. $0 \leq$ wind direction ≤ 360. For parameters with no definite limits, such as air temperature and atmospheric pressure, a table is established, according to location and time, of approximate limits beyond which the occurence of a value is unlikely,
- internal consistency tests: some parameters are checked for consistency against associated parameters within each observation, e.g. Global > Reflex, Global > OG1 > RG8 > UV, FF10 > FF2, etc.

Finally, a graphic quick-look helps to detect unreliable values. After correction the data are restored into the database and various computations are made:

- evaluation of related parameters,
- evaluation of mean and extreme values,
- interpolations.

All original (corrected) and a part of the derived values are stored in the database. With the aid of the database language **S Q L** (**S**tructured **Q**uery **L**anguage) it is rather easy to export any desired information or data subset.

For users whithout sql-experiences an interactive interface to the internet is implemented in the World Wide Web below the address of the home page of the AWI (http://www.awi-bremerhaven.de). This interface offers certain pre-defined export statements which make data export extremely fast and easy.

4. RESULTS

4.1) Synoptic Observations

Monthly and annual means and extrema for the years 1992, 1993, and 1994 are listed in Tabs. 1a-c and 2a-c.

- Tabs. 1a-c contain monthly and annual mean values and standard deviations based on the 3-hourly synoptic observations. The same scheme has been used in the previous report on this subject (König-Langlo, 1992), while in an older report (Helmes, 1989) the monthly values were based on daily means and the annual values on monthly means. Thus the standard deviations cannot be compared directly.

- At 00 and 12 UTC the maximum and minimum temperature (Max.Temp and Min.Temp) of the last 12 hours are coded in the routine observations. The monthly and annual mean of Max.Temp. and Min.Temp. are included in Tabs. 1a-1c without standard deviations because these values are taken only twice a day.

- It is obvious that wind directions should not be averaged. Thus in Tabs. 1a-c only the averaged wind speed (absolute values) and the averaged wind components ($u>0$ = wind from west to east, $v>0$ = wind from south to north) are listed. The resultant wind (see Helmes, 1989) can be calculated from these components.

- Tabs. 2a-c contain the extrema of the 5-minute averages. In the previous report on this subject (König-Langlo, 1992) all extreme values of Tabs 2a-c were based on 10-minute averages, taken every 3 hours. Thus the extrema can not be compared directly.

- Observations of the cloud amount are rather uncertain while it is dark. Especially during the polar night (19th of May through 27th of July) only observations with moon or stars visible can be assessed accurately. Therefore, means during this period are unrealistically low and the yearly means based on 3-hourly values may differ from yearly means based on unweighted monthly means.

Month	Temperature (°C)		Max. Temp. (°C)	Min. Temp. (°C)	Relative Humidity (%)		Pressure (hpa)		Wind speed (m/s)		U_Wind (m/s)	V_Wind (m/s)	Cloud amount (n/10)
1	-2,2	2,2	-0,7	-3,7	86	9,2	990,0	7,5	7,1	5,0	-5,1	0,4	7,9
2	-7,3	3,8	-5,2	-10,1	90	8,0	992,2	5,3	8,0	5,3	-6,7	1,4	7,5
3	-9,9	4,6	-7,8	-12,4	90	7,9	981,1	7,8	11,1	6,9	-7,9	0,8	8,4
4	-19,9	6,9	-16,7	-23,7	81	8,2	986,8	8,6	7,6	5,6	-4,1	1,6	5,4
5	-17,3	7,5	-14,7	-19,9	75	8,7	990,8	7,2	9,4	5,2	-6,4	2,1	7,4
6	-19,5	7,0	-17,1	-22,9	77	6,3	994,6	10,1	9,1	5,2	-6,9	0,8	7,1
7	-25,2	9,9	-22,1	-28,2	78	5,6	981,3	9,9	8,8	6,3	-5,8	1,1	7,0
8	-31,4	7,3	-27,9	-35,1	75	4,3	980,1	9,6	7,9	5,4	-2,9	2,0	5,3
9	-24,8	7,0	-21,3	-28,8	80	2,8	985,6	9,4	8,8	5,5	-5,6	1,5	5,4
10	-18,1	10,5	-14,2	-22,7	81	6,6	983,5	8,9	9,3	6,4	-6,2	1,1	5,8
11	-10,6	5,4	-8,0	-14,8	79	8,7	979,0	10,1	8,0	6,6	-4,0	0,8	6,8
12	-5,3	3,7	-2,2	-9,1	82	9,3	985,6	5,4	5,9	3,9	-2,2	1,5	6,3
year	-16,0	10,9	-13,3	-19,5	81	9,0	985,8	9,8	8,4	5,8	-5,3	1,3	6,6

Tab.1a Monthly means for the year 1992 from synoptic observations. First value = mean, second value = standard deviation with respect to the 3-hourly observations.

Month	Temperature (°C)		Max. Temp. (°C)	Min. Temp. (°C)	Relative Humidity (%)		Pressure (hpa)		Wind speed (m/s)		U_Wind (m/s)	V_Wind (m/s)	Cloud amount (n/10)
1	-4,2	3,3	-1,9	-7,4	83	7,7	995,7	5,7	5,8	3,1	-2,9	1,2	6,6
2	-10,1	5,8	-7,5	-14,3	82	8,3	986,2	6,7	5,4	3,2	-2,0	2,1	5,8
3	-16,0	5,1	-12,6	-19,5	82	6,5	988,5	7,9	5,9	2,9	-1,9	2,2	5,5
4	-21,4	8,1	-18,7	-24,7	87	7,6	987,4	6,9	9,1	7,1	-6,1	1,6	5,0
5	-20,3	7,7	-17,5	-23,5	85	8,9	983,9	11,7	9,9	6,3	-6,2	0,4	5,1
6	-20,9	8,5	-18,8	-23,3	83	8,2	983,2	12,1	10,9	6,8	-8,1	0,1	5,0
7	-25,5	7,5	-23,3	-28,7	78	5,4	979,4	10,7	10,6	7,0	-6,1	1,1	5,1
8	-24,6	5,9	-21,9	-27,9	78	8,8	979,8	7,7	9,7	6,6	-2,6	2,3	5,6
9	-23,1	6,6	-20,5	-26,7	79	7,4	979,0	11,3	9,4	7,0	-6,6	1,8	7,3
10	-6,5	4,5	-14,3	-19,3	84	6,6	977,8	8,1	9,8	6,7	-7,1	0,7	7,4
11	-10,5	3,8	-8,4	-13,9	81	9,2	986,6	5,8	9,0	5,7	-5,2	0,5	6,6
12	-5,0	3,5	-3,1	-8,0	81	10,4	983,5	6,0	6,8	4,2	-3,2	1,3	6,5
year	-16,5	9,4	-14,1	-19,7	79	10,4	984,2	10,0	8,5	6,1	-4,8	1,3	6,1

Tab.1b Monthly means for the year 1993 from synoptic observations. First value = mean, second value = standard deviation with respect to the 3-hourly observations.

Month	Temperature (°C)		Max. Temp. (°C)	Min. Temp. (°C)	Relative Humidity (%)		Pressure (hpa)		Wind speed (m/s)		U_Wind (m/s)	V_Wind (m/s)	Cloud amount (n/10)
1	-5,2	3,6	-3,5	-8,1	84	8,7	989,5	4,3	6,1	3,7	-4,5	-0,1	7,1
2	-7,2	2,7	-5,4	-9,7	85	9,8	984,8	5,6	9,5	5,3	-7,3	-0,3	7,4
3	-14,7	5,5	-12,2	-16,8	86	7,6	981,7	7,4	10,0	6,1	-5,5	1,4	5,9
4	-16,4	6,1	-14,3	-18,2	88	7,6	984,6	9,2	10,9	6,2	-8,6	-0,2	6,8
5	-23,9	7,4	-21,2	-26,7	88	7,4	987,6	9,7	10,2	6,3	-5,9	1,4	3,3
6	-21,5	6,3	-18,5	-24,3	86	8,0	997,8	9,6	9,2	7,2	-6,6	1,2	4,3
7	-24,8	6,4	-21,8	-27,5	84	6,9	986,8	7,5	8,1	4,6	-4,1	1,3	4,9
8	-24,5	7,6	-21,6	-27,3	89	5,2	980,3	11,5	10,1	6,6	-6,2	0,7	4,8
9	-21,2	8,2	-19,0	-23,8	80	7,4	988,4	11,6	11,0	6,2	-5,9	0,4	4,8
10	-17,0	4,5	-14,7	-19,9	85	6,2	982,3	6,4	8,9	4,5	-6,2	-0,7	7,3
11	-10,9	5,5	-8,3	-14,4	88	9,5	990,7	7,2	8,2	4,7	-4,3	0,3	6,0
12	-4,6	2,9	-2,7	-6,7	88	8,6	983,3	8,7	6,9	3,8	-2,9	-0,2	8,1
year	-16,1	9,3	-13,7	-18,7	86	8,2	986,5	9,7	9,1	5,7	-5,6	0,4	6,0

Tab.1c Monthly means for the year 1994 from synoptic observations. First value = mean, second value = standard deviation with respect to the 3-hourly observations.

Month	Max. Temp. (°C) Maximum		Min. Temp. (°C) Minimum		Pressure (hpa) Maximum		Pressure (hpa) Minimum		Maximum Windspeed (m/s) Speed	(deg) Dir.	
1	4,3	21.1	-12,0	15.1	1005,3	3.1	974,1	18.1	21,6	90	12.1
2	-0,4	14.2	-19,7	8.2	1005,8	28.2	979,0	12.2	21,6	100	24.2
3	0,9	12.3	-26,4	14.3	995,3	5.3	956,9	30.3	27,3	90	28.3
4	-4,6	1.4	-36,0	15.4	1003,8	26.4	969,1	16.4	28,3	90	30.4
5	-0,2	27.5	-33,8	13.5	1006,0	18.5	974,0	24.5	26,8	90	15.5
6	-5,3	22.6	-39.8	19.6	1014,0	17.6	973,4	11.6	22,6	80	22.6
7	-5,6	5.7	-44,5	23.7	1005,3	1.7	960,7	24.7	32,4	90	1.7
8	-11,1	11.8	-47,3	18.8	995,9	23.8	948,5	9.8	31,9	90	9.8
9	-9,6	17.9	-43,6	27.9	1002,5	20.9	959,3	16.9	26,2	90	11.9
10	0,8	16.10	-42,6	6.10	1001,9	13.10	961,0	17.10	26,2	90	15.10
11	0,2	29.11	-27,0	1.11	994,4	15.11	945,3	8.11	31,4	90	7.11
12	2,5	6.12	-16,5	2.12	994,7	31.12	968,0	13.12	18,0	100	13.12
year	4,3	21.1	-47,3	18.8	1014,0	17.6	945,3	8.11	32,4	90	1.7

Tab.2a Monthly extremes for the year 1992 from synoptic observations. First value = extreme, second value = date. Maximum windspeed is shown with the associated wind direction.

Month	Max. Temp. (°C) Maximum		Min. Temp. (°C) Minimum		Pressure (hpa) Maximum		Pressure (hpa) Minimum		Maximum Windspeed (m/s) Speed	(deg) Dir.	
1	1,2	3.1	-17,1	24.1	1010,2	20.1	985,7	30.1	16,5	90	9.1
2	-0,3	11.2	-24,7	20.2	1002,8	1.2	975,2	20.2	16,5	80	11.2
3	-5,9	4.3	-29,1	29.3	1004,3	29.3	971,0	2.3	17,0	90	22.3
4	-2,5	29.4	-38,7	14.4	998,6	12.4	968,4	22.4	29,8	90	27.4
5	-5,6	21.5	-39,1	18.5	1012,5	31.5	952,1	24.5	28,8	90	24.5
6	-6,3	12.6	-42,6	20.6	1015,2	1.6	951,4	13.6	27,3	80	5.6
7	-11,0	7.7	-41,8	21.7	997,9	26.7	954,2	4.7	32,4	90	4.7
8	-12,2	3.8	-41,0	13.8	994,4	28.8	960,4	4.8	31,4	80	30.8
9	-11,9	30.9	-39,2	11.9	995,4	29.9	949,4	22.9	32,9	90	21.9
10	-8,4	8.10	-33,0	19.10	1002,1	7.10	965,5	11.10	28,3	90	1.10
11	-1,6	24.11	-23,8	5.11	996,9	13.11	970,8	11.11	27,3	80	11.11
12	1,0	16.12	-18,2	5.12	996,3	30.12	971,1	14.12	20,6	80	12.12
year	1,2	3.1	-42,6	20.6	1015,2	1.6	949,4	22.9	32,4	90	4.7

Tab.2b Monthly extremes for the year 1993 from synoptic observations. First value = extreme, second value = date. Maximum windspeed is shown with the associated wind direction.

Month	Max.Temp. (°C) Maximum		Min. Temp. (°C) Minimum		Pressure (hpa) Maximum		Pressure (hpa) Minimum		Maximum Windspeed (m/s) Speed	(deg) Dir.	
1	-0,9	8.1	-23,8	21.1	1001,0	1.1	982,9	27.1	16,0	80	25.1
2	-2,0	10.2	-25,8	3.2	995,3	23.2	970,0	19.2	21,6	80	17.2
3	-5,8	18.3	-31,6	31.3	994,2	29.3	962,1	11.3	24,7	90	10.3
4	-7,1	4.4	-32,9	13.4	1001,6	8.4	959,0	10.4	26,8	80	18.4
5	-11,0	26.5	-40,0	14.5	1007,6	18.5	971,9	6.5	26,2	90	23.5
6	-9,1	22.6	-34,3	25.6	1017,0	26.6	969,1	9.6	35,5	80	8.6
7	-13,3	12.7	-40,7	31.7	1007,2	1.7	970,5	10.7	20,1	80	11.7
8	-8,6	26.8	-43,7	7.8	998,1	10.8	936,2	11.8	29,3	90	4.8
9	-9,9	28.9	-42,3	3.9	1013,0	27.9	961,9	5.9	29,3	90	5.9
10	-9,0	28.10	-30,7	6.10	999,3	16.10	964,8	22.10	21,6	240	16.10
11	-1,5	9.11	-27,0	6.11	1007,8	18.11	977,2	4.11	24,2	80	8.11
12	-0,6	13.12	-15,8	1.12	998,7	3.12	957,1	27.12	18,0	90	26.12
year	-0,6	13.12	-43,7	7.8	1017,0	26.6	936,2	11.8	35,5	80	8.6

Tab.2c Monthly extremes for the year 1994 from synoptic observations. First value = extreme, second value = date. Maximum windspeed is shown with the associated wind direction.

4.1.1) Surface Air Temperature
Figs. 5a-5c show the monthly mean surface temperatures as well as the associated extrema for 1992, 1993 and 1994. Additionally, the monthly mean values for the period between 1982 and 1992 are presented. All values base on 5-minute averages and are taken during the routine 3-hourly synoptic observations. The extrema in Figs. 5a-5c differ slightly from the values in Tabs. 2a-2c, where the extrema of Max.Temp and Min.Temp are shown (see section 4.1).

The standard deviations indicate a larger temperature variability during winter than during summer. The monthly means of each year agree closely with the 10 year averages.

4.1.2) Relative Humidity
There is no distingish regular variation of relative humidity (Figs. 6a-6c) detectable. The monthly means range between 75% and 90%. Interannual changes are also rather small.

The currently existing methods for measuring air humidity yield large uncertainties especially at low air temperatures (see also section 2.1). Therefore, special attention has been given to humidity data at low (< -25°C) temperatures.

4.1.3) Air Pressure
Figs. 7a-7c present the monthly mean pressure data at sea level which are always below 1000hPa due to the location of Neumayer close to the circumpolar low pressure belt. According to van Loon et al. (1984a, 1984b) a half-year cycle in the pressure data should exist. To a certain extend this cycle is detectable in the 10 year averages, but hidden behind synoptic pertubations if only single years are regarded.

4.1.4) Wind
Figs. 8a-8c contain monthly averages of wind speed (absolute values of the wind vector) and the zonal (u) and meridional (v) wind components. Additionally, the monthly means of wind speed averaged between 1982 and 1992 are displayed. During the summer months December, January and February the wind speed is mostly lower than in winter. The mean zonal wind component is easterly (negative) throughout the entire year. The meridional component is weak but due to catabatic winds mainly from the south (positive).

As can be seen in the histograms of wind direction (Figs. 9a-9c) the easterly winds prefer a rather distinct direction around 90 degrees. The catabatically influenced southerly winds occur with a much lower directional constancy. Northerly winds are very rare.

4.1.5) Present Weather Observations
According to the FM12 instructions (Deutscher Wetterdienst 1982, WMO 1983a, 1983b) the present weather observations (ww) are coded in numbers between 0 and 99. In Figs. 10a-10c the annual courses of weather phenomena are shown. Codes between 36 and 39 - indicating snow drift - are predominant (see also Fig. 11). Longer intervals without snowdrift hardly exist. Also, snow fall — coded between 70 and 79 — occurs frequently troughout the year. Furthermore, significant phenomena such as fog (40 - 49) and showers (80 - 90) are seldom (0 - 3 denotes insignificant weather). Thunderstorms (91 - 99) do not exist.

4.1.6) Clouds
According to the FM12 code clouds are classified into three categories with reference to their height:

- C_l: low clouds of the type Stratocumulus, Stratus, Cumulus and Cumulonimbus (0 - 2 km),
- C_m: medium clouds of the type Altocumulus, Altostratus and Nimbostratus (2 - 4 km),
- C_h: heigh clouds of the type Cirrus, Cirrocumulus and Cirrostratus (3 - 8 km).

Each cloud layer is subdivided into 10 different classes. Class 0 in Figs. 12a-12c means, that no clouds in the specified layer exist. Typical low clouds are Stratocumulus and Stratus (5, 6, 7), whereas Cumuli are rare (1, 2, 3). Cumulonimbi (9) do not exist. Typical medium clouds are Altocumulus (3, 4, 7) and Altostratus (1, 2). In the highest layer Cirrus in the form of filaments, strands or hooks (1) are predominant.

As already mentioned in section 4.1 observations of clouds are hindered by darkness. Monthly mean observations during polar night are not comparable with values during polar day. Thus, no annual courses of these observations are plotted.

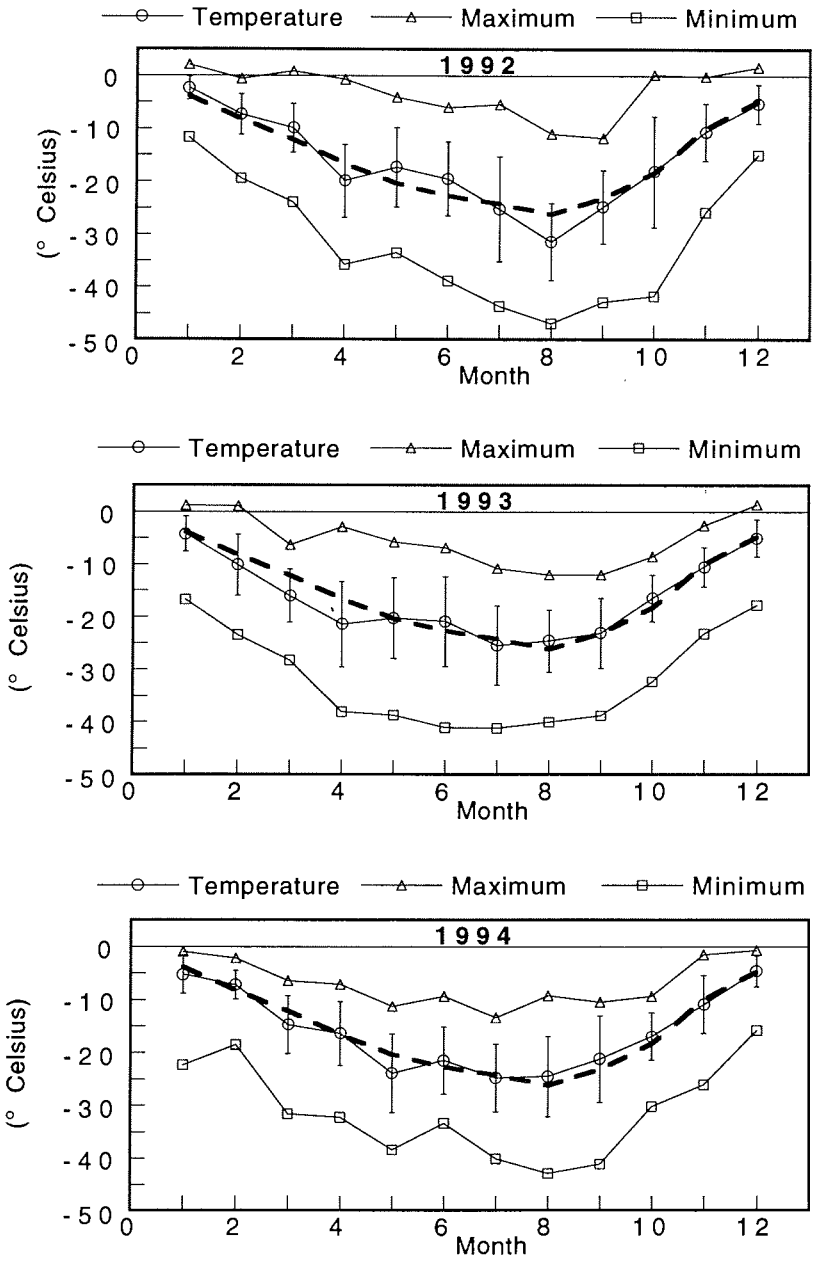

Figs. 5a-5c Monthly mean, maximum and minimum values of surface air temperatures. Mean temperature values are plotted with standard deviation with respect to the routine 3-hourly synoptic observations. The bold dashed line represents the 10 year averages from 1982 to 1992.

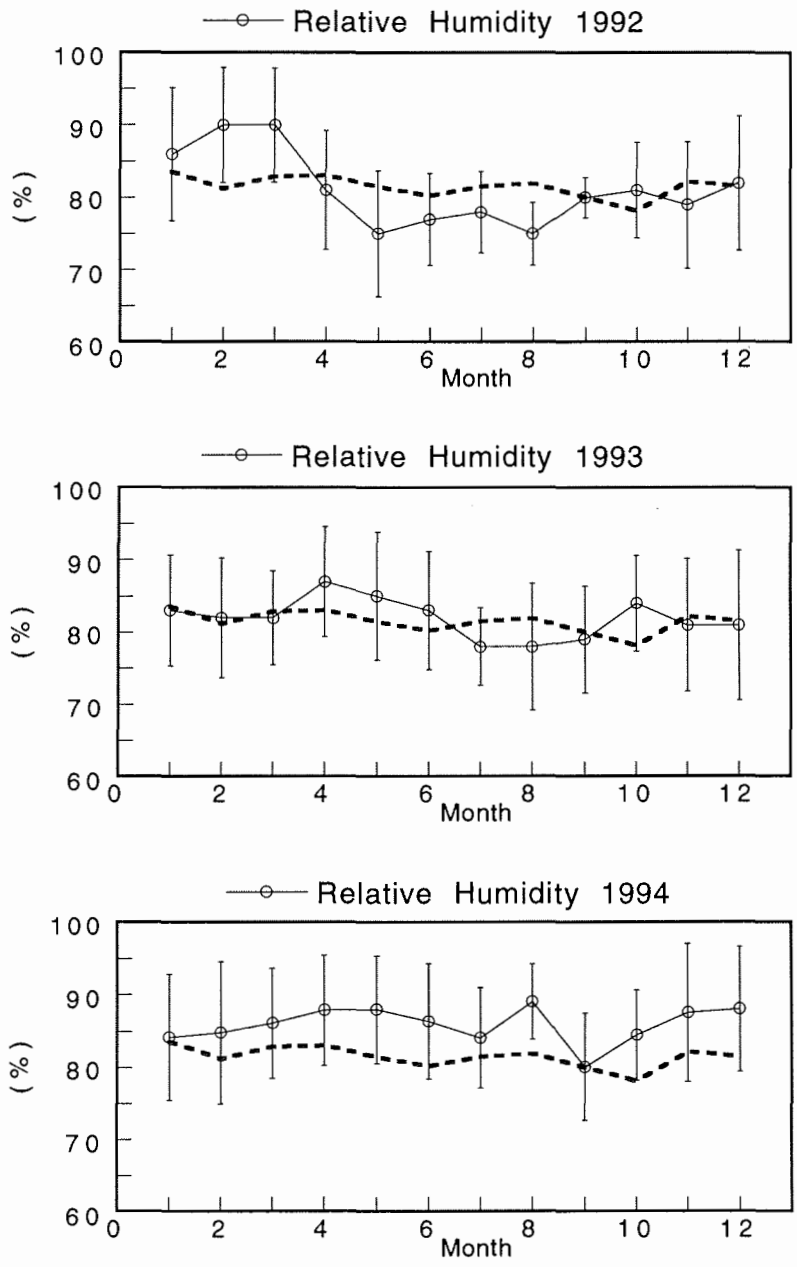

Figs. 6a-6c Monthly mean values of relative humidity. Mean values are plotted with standard deviation with respect to the routine 3-hourly synoptic observations. The bold dashed line represents the 10 year averages from 1982 to 1992.

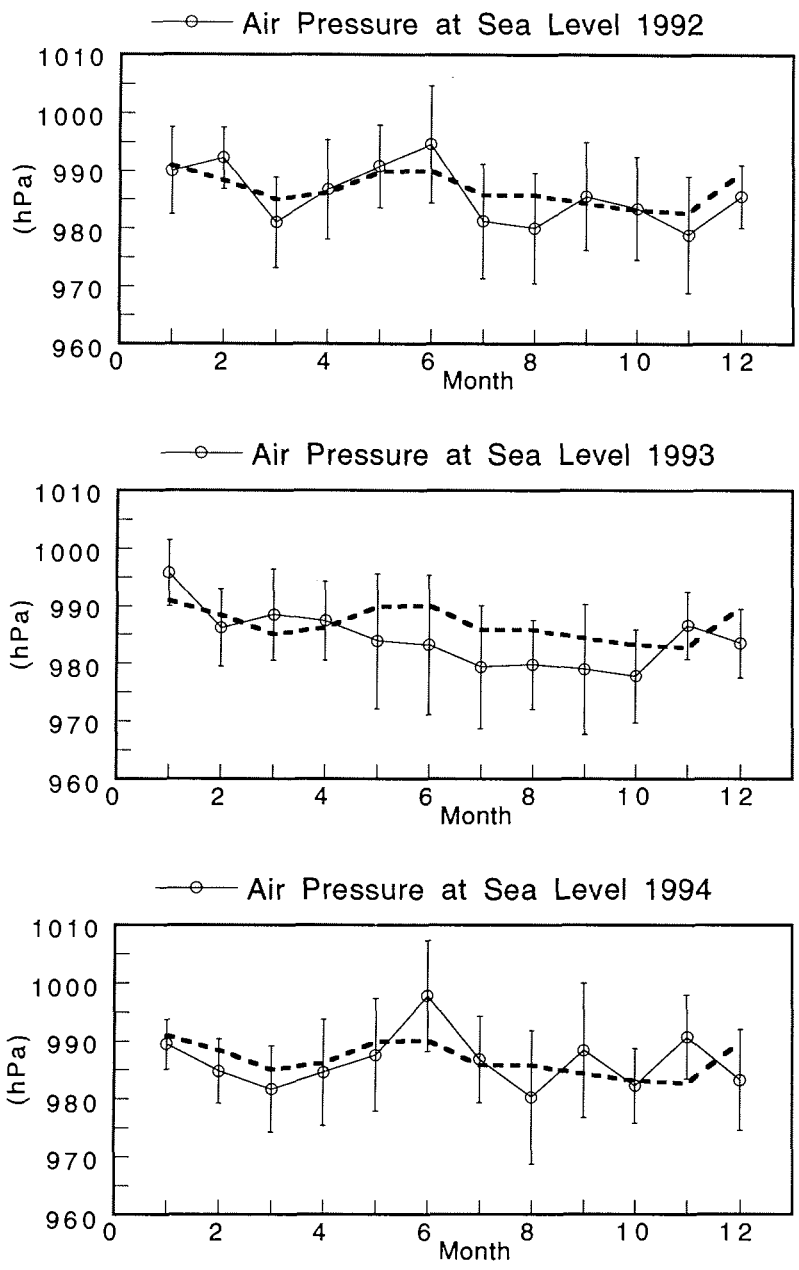

Figs. 7a-7c Monthly mean values of air pressure at sea level. Mean values are plotted with standard deviation with respect to the routine 3-hourly synoptic observations. The bold dashed line represents the 10 year averages from 1982 to 1992.

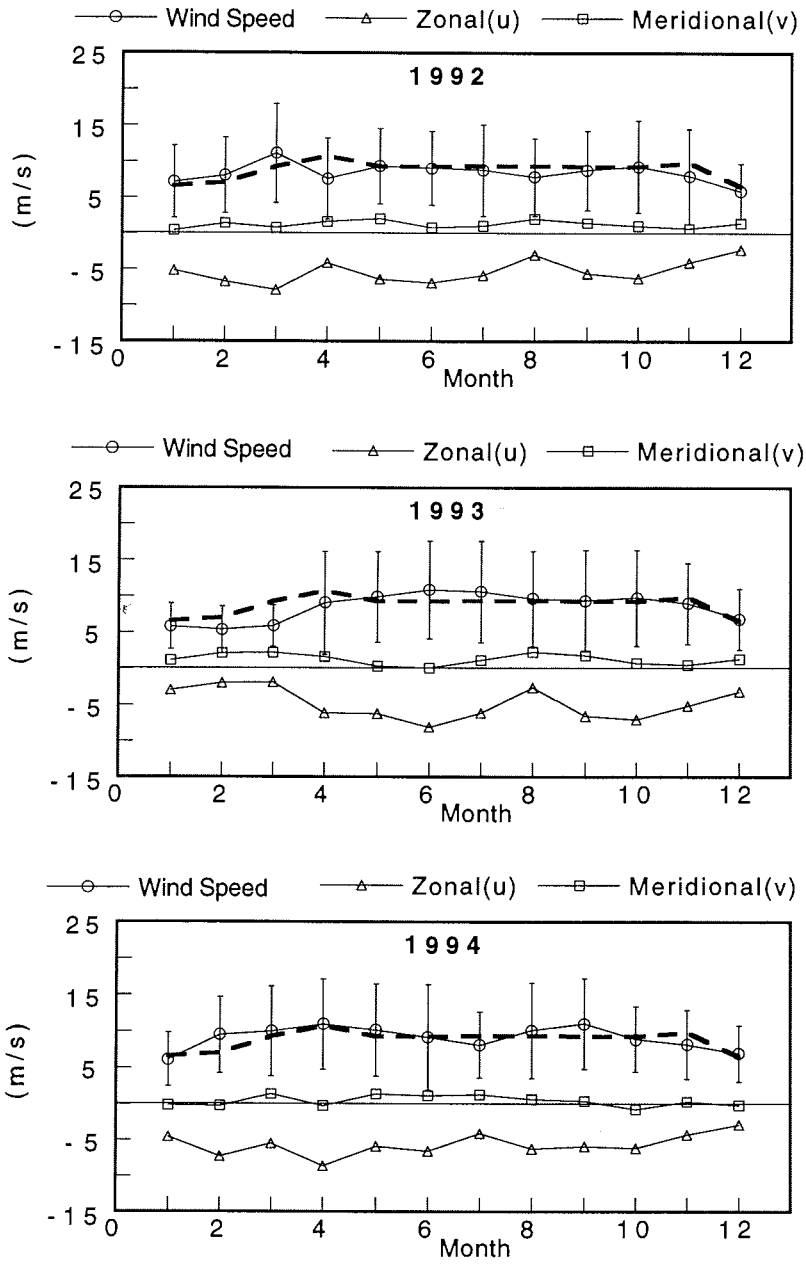

Figs. 8a-8c Monthly mean values of wind speed and wind components. Mean wind speeds are plotted with standard deviation with respect to the routine 3-hourly synoptic observations. The bold dashed line represents the 10 year averages from 1982 to 1992.

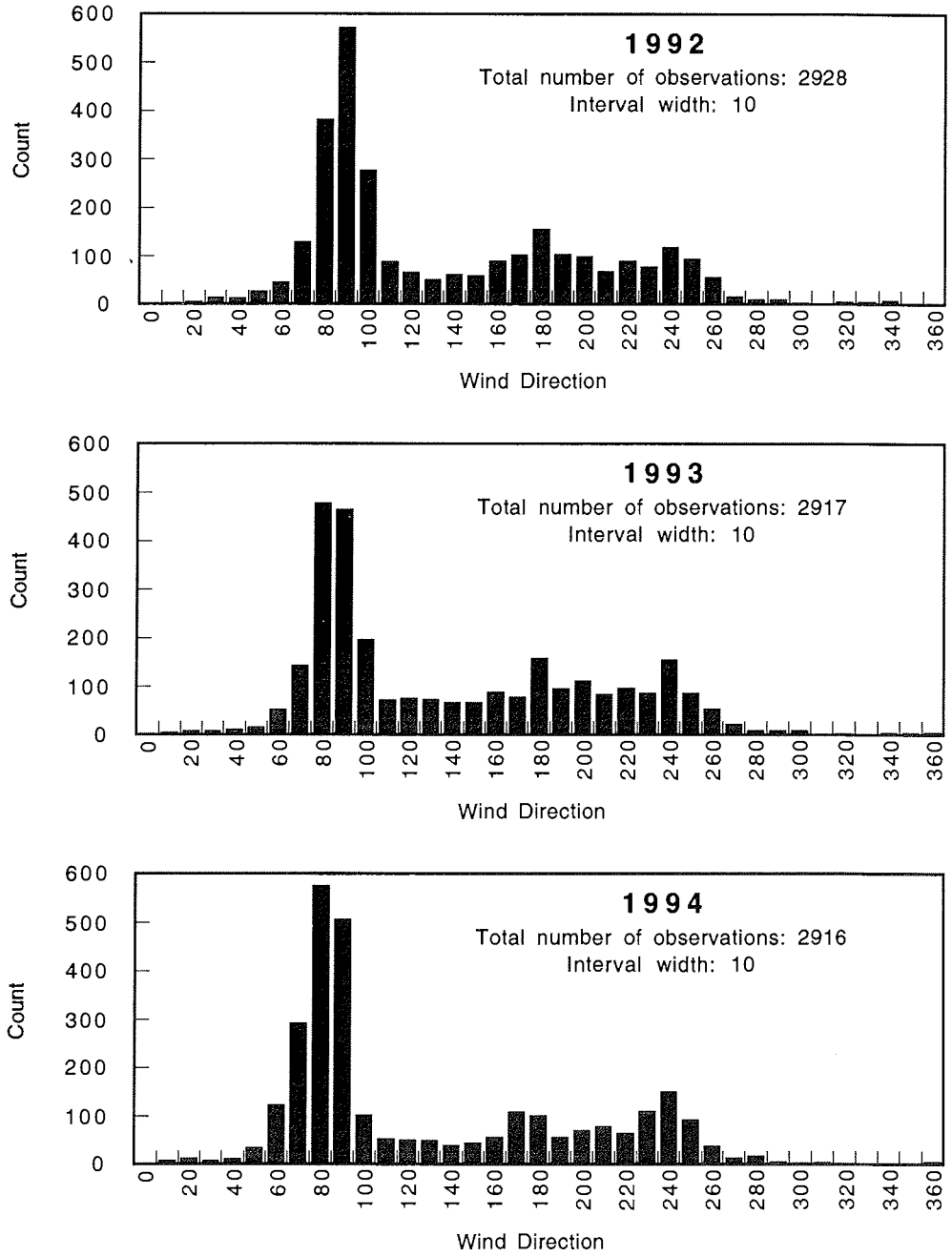

Figs. 9a-9c Frequency distributions of wind direction for all routine 3-hourly synoptic observations during one year.

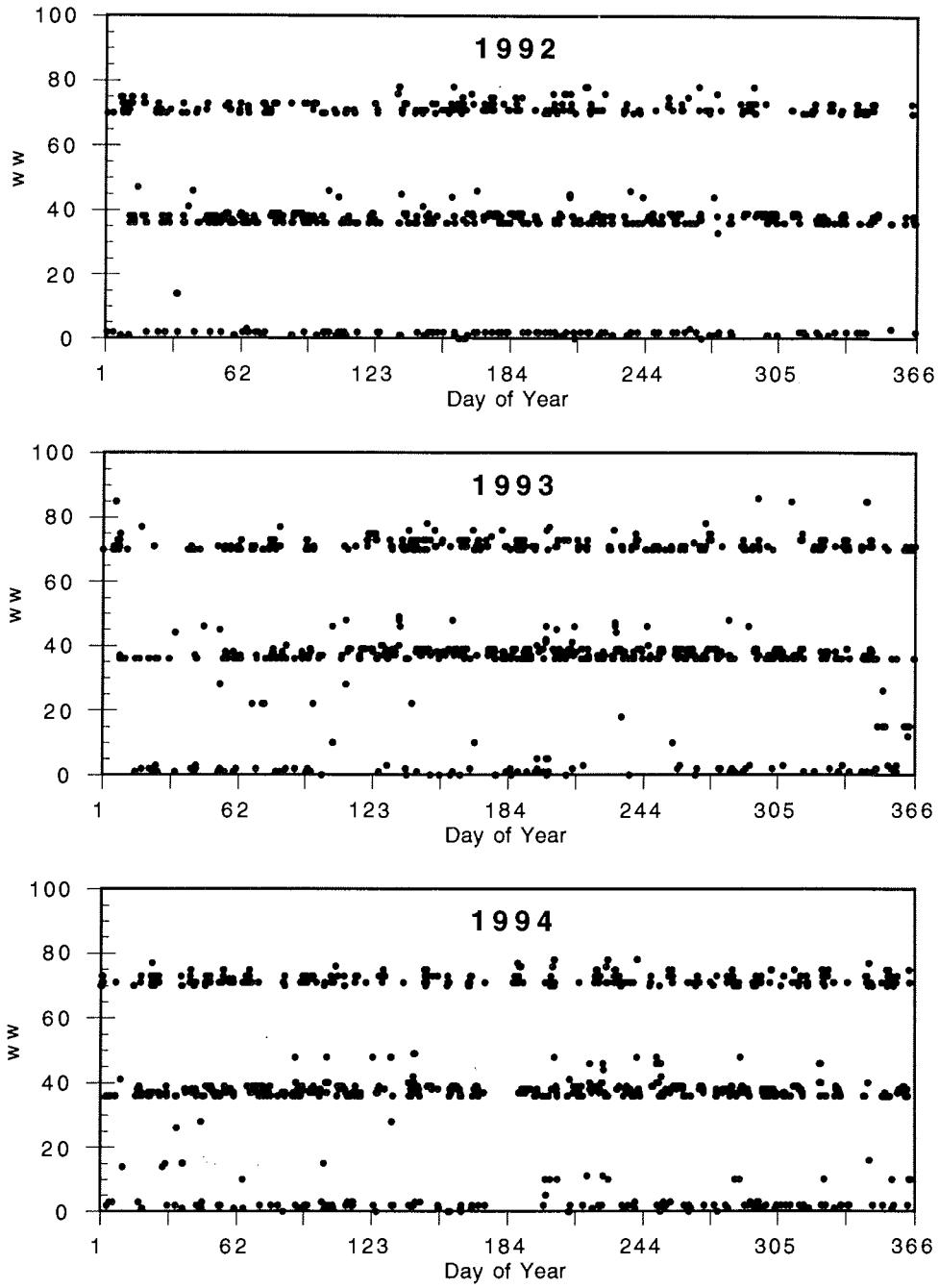

Figs. 10a-10c Annual course of present weather phenomena (ww) from the routine 3-hourly synoptic observations according to the FM12-code.

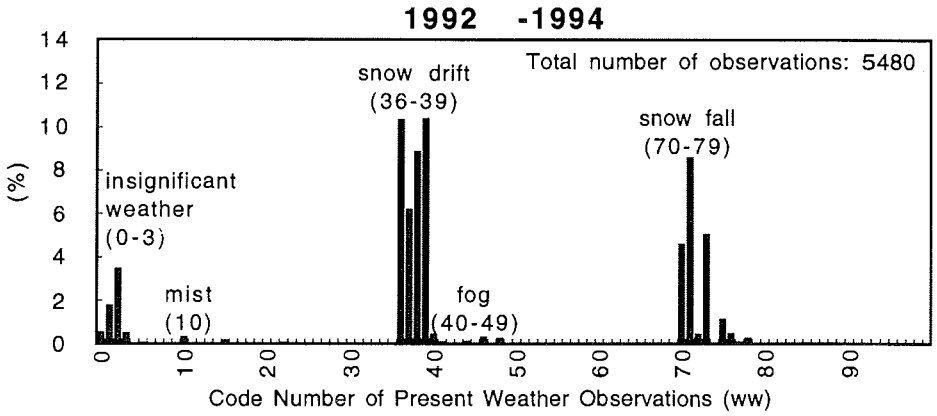

Fig. 11 Frequency distribution of present weather phenomenona (ww) from visual 3-hourly synoptic observations during 1992 - 1994 according to the FM12-code.

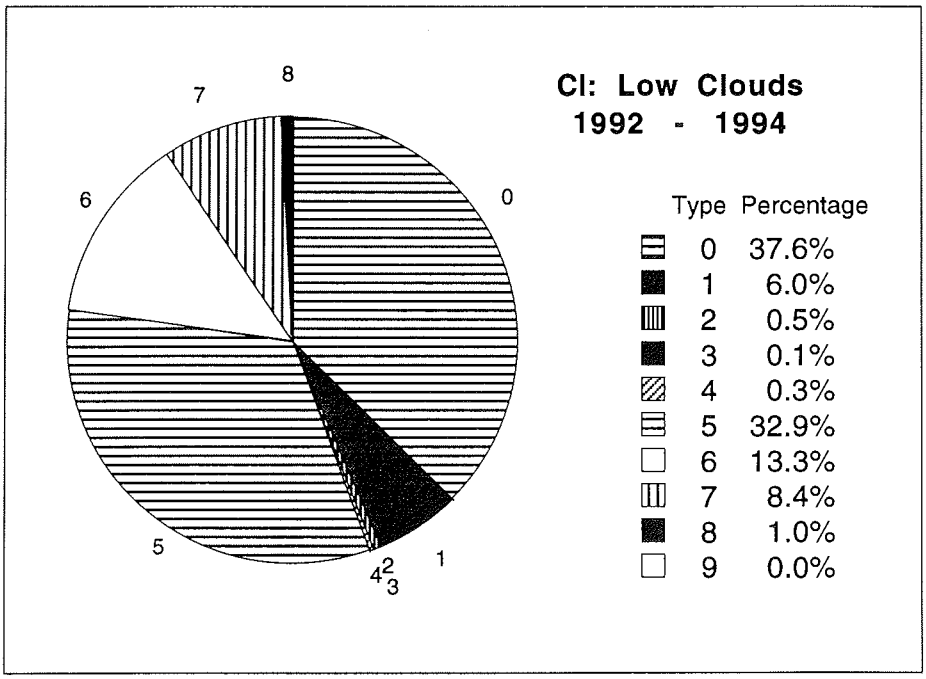

Fig. 12a Frequency distribution of low clouds from 3-hourly synoptic observations during 1992 - 1994 according to the FM12-code.

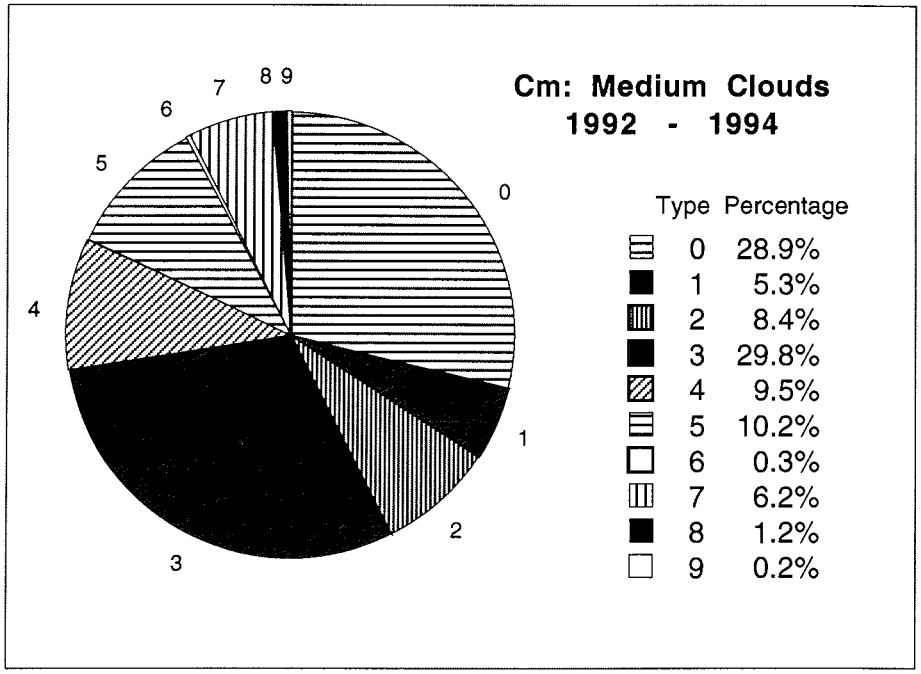

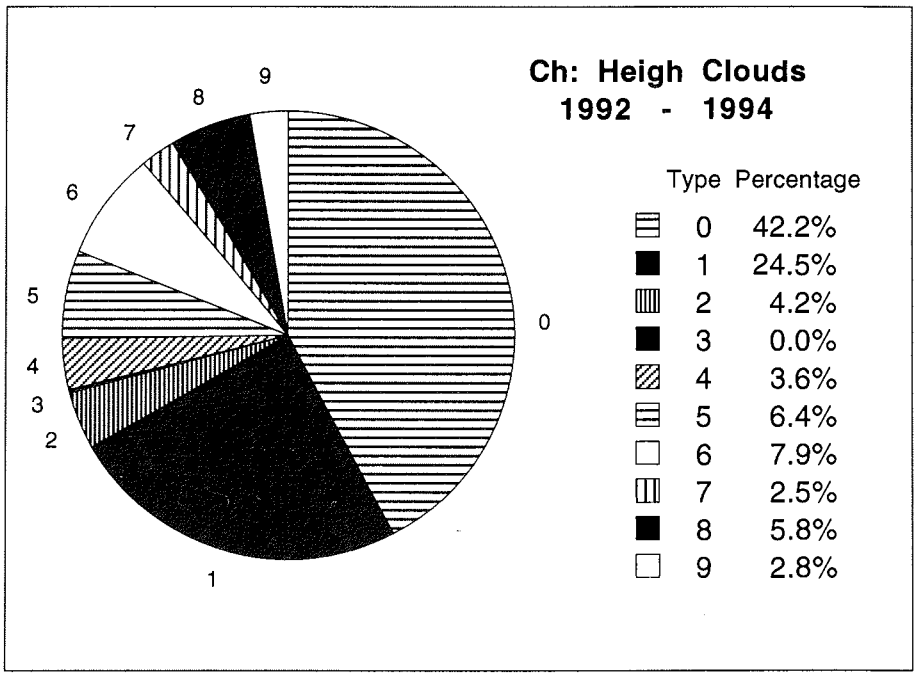

Figs. 12b-12c Frequency distributions of medium and heigh clouds from 3-hourly synoptic observations during 1992 - 1994 according to the FM12-code.

4.2) Upper Air Soundings

Radiosondes are launched once daily. In summertime the balloons usually reach heights between 30 and 37 km. In wintertime - when stratospheric temperatures drop below -80 °C - even specially treated balloons tend to burst at lower levels.

4.2.1) Temperatures
Figs. 13a-13c display time-height sections of the air temperature. Most obvious is the strong annual variation in the lower stratosphere with minimum values in July or August below -90°C.

Date	Min.Temp (°C)	Height (m) of Min.Temp.
24 Jul 1992	-91.6	22063
26 Jul 1993	-91.4	20750
10 Aug 1994	-94.7	23930

At the end of September sudden stratosperic warming starts first in layers above 25km height and proceeds slowly downwards.

4.2.2) Tropopause
The height of the tropopause is defined as the lowest level above which the temperature decrease with height is less than 0.2°C per 100m. This condition must be fulfilled over a range of at least 2000m. Figs. 20a-20c present the results according to this definition. During summer the tropopause is well pronounced. The tropopause and the temperature minimum coinside at a level around 9000m.

During polar night formally a tropopause can often be defined, but physically no distinct boundary between the troposphere and stratosphere exists. The heights of the temperature minimum is mostly well above the heights of the tropopause. Thus, the tropopause temperatures do not represent the minimum temperatures. In general, the tropopause rises during the winter period and the stratosphere is then characterized by small lapse rates (Figs. 26a-28l). The annual mean temperature at the tropopause lies at about -60°C.

4.2.3) Wind
Figs. 14a-17c display time-height sections of wind values. Easterly winds dominate in the lower troposphere up to a height of about 5000 m. Only during summer (December - March) weak easterlies

exist in all height levels. Between March and December the upper troposphere and the stratosphere are governed by westerlies, with increasing velocity with height. This phenomeon indicates that the polar vortex is well estabished in the upper atmosphere. The westerly wind maximum appears at the end of September at heights above 30km.

The meridional wind component is normally much weaker and show a small tendency to winds from south, see also Figs. 26a - 26l. Only around end of September strong meridional wind components exists in the stratosphere which are responsible for the sudden stratospheric warming during this season. At Neumayer southerly wind components indicate the breakdown of the stratospheric vortex in 1992, while in 1993 and 1994 a strong northerly stratospheric current during this time of the year was observed.

4.2.4) Ozone

Ozone soundings started at Neumayer Station in March 1992, about one month after the ozone sounding programme at the Georg-Forster Station (70°46´S, 11°41´E) was stopped. Figs. 18a-18c display time-height sections of the ozone concentration, while in Figs. 24a - 24c show the total ozone, as calculated by integration of the profiles. Data before March 1992 were taken from Georg-Forster Station.

During summer the maximum of the ozone concentration over Neumayer exists typically at height levels between 20 and 25 km. The total ozone varies around 300 Dobsen units. Until the beginning of September the height of the ozone maximum level decreases by about 5km, indicating a mean downward vertical displacement of the air mass within the polar vortex.

During September, when sun light hits the stratosphere again, the ozone layer vanishes quite suddenly and nearly completely. Instead of local ozone maxima, local ozone minima can be found at height levels between 16 and 21 km. The total ozone drops to about 150 Dobsen units with the lowest values in early October. This phenomenon is frequently referenced as ozone hole. At the end of November, when the polar vortex breakes down, warm air masses with higher ozone concentrations are advected towards the South Pole from lower latitudes. As an example an assessment of the ozone depletion in 1994 can be found in WMO (1995).

4.2.5) Humidity

The relative air humidity (Figs. 19a-19c, 26a - 28l) continuously decreases with height in the troposphere and is mostly close to zero in the stratosphere. This effect is partly caused by the fact that relative air humidity is defined with respect to the absolute water vapour pressure over a plain pure water surface which is always greater than the absolute water vapour pressure over ice. Thus, in a very cold atmospere, were no liquid water exists, the maximum relative air humidity must stay well below 100%.

Figs. 25a-25c present the total amount of water vapour in the vertical air column over a horizontal reference area (precipitable water, ppw). 1 cm ppw is equivalent to 1 g H_2O/cm^2. Only during summer the precipitable water content sometimes exceeds 1 g H_2O/cm^2.

4.2.6) Standard Pressure Levels

Figs. 22a-22c depict the height variation of different standard pressure levels. There are no marked variations below the 300 hpa level. The annual period above the 100hPa level reflects the strong stratospheric temperature cycle (see also Figs. 13a-13c).

The temperatures at standard pressure levels, see Figs. 23a-23c, show a rather low temporal variation at the beginning of each year. While the polar vortex is established, bigger temperature variations are observed. The strongest stratospheric temperature variations are measured during the breakdown of the stratospheric vortex, while the highest stratospheric temperatures occure directly after the breakdown.

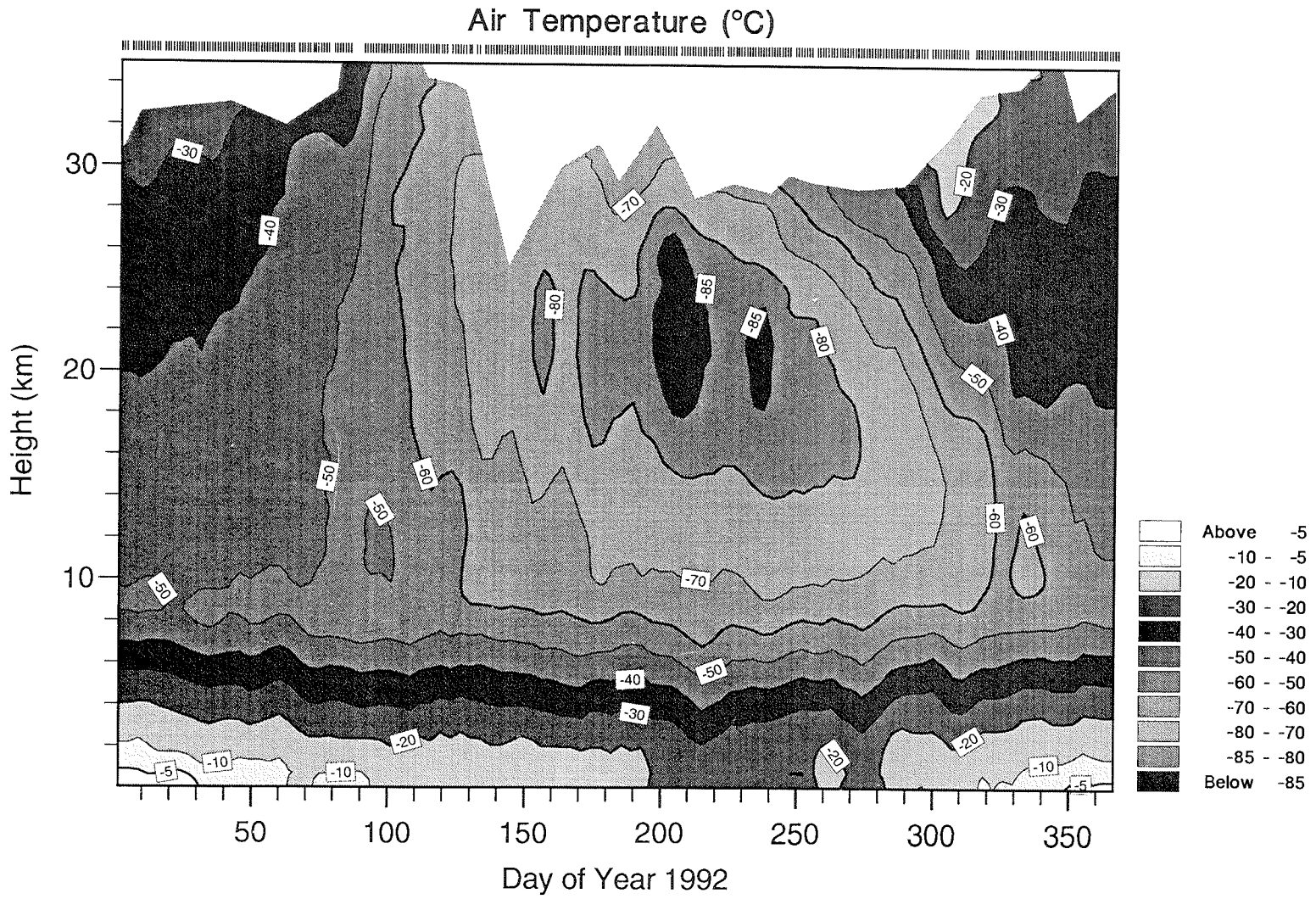

Fig. 13a Time - height section of temperature (°C) from daily radiosonde soundings 1992

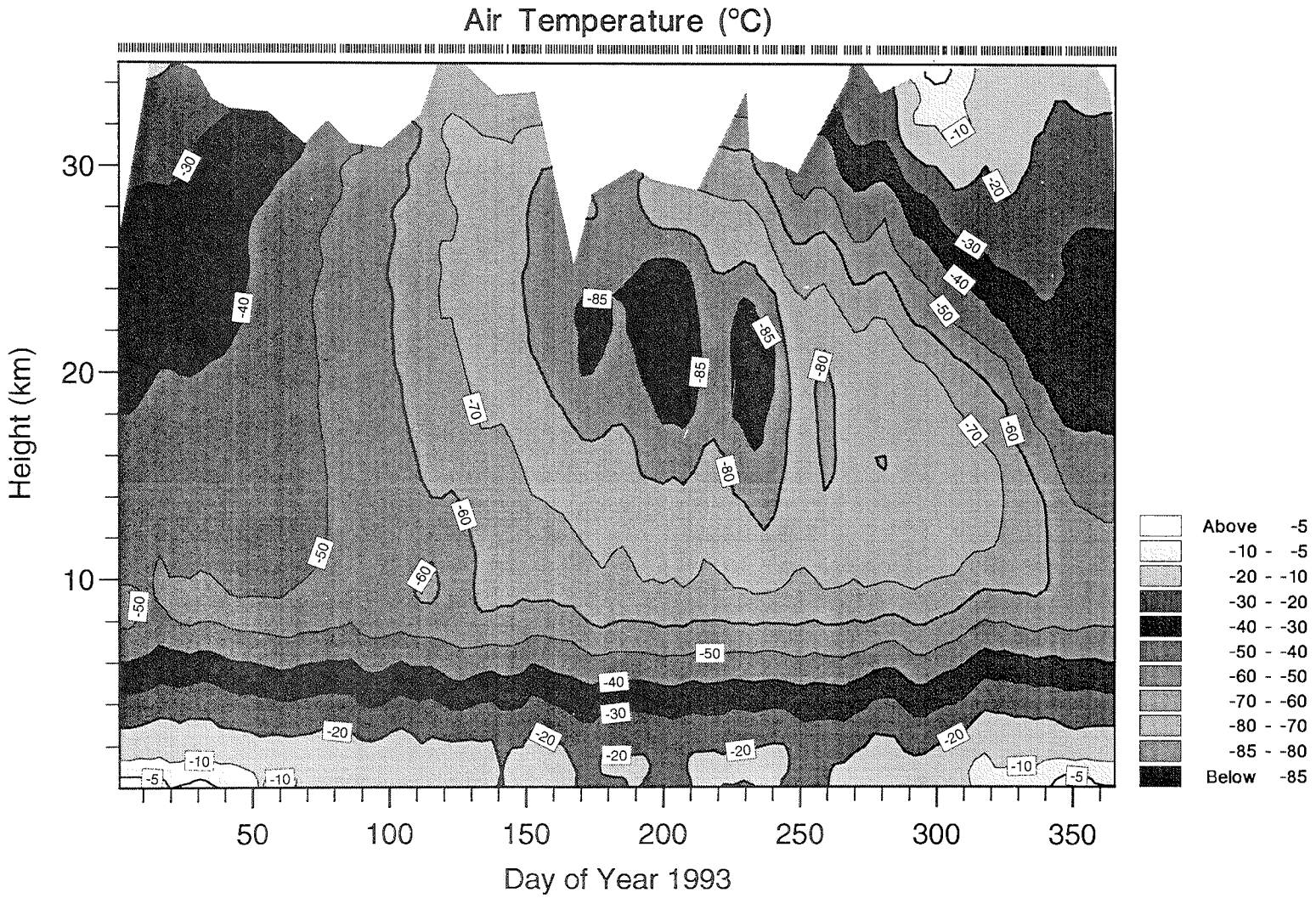

Fig. 13b Time - height section of temperature (°C) from daily radiosonde soundings 1993

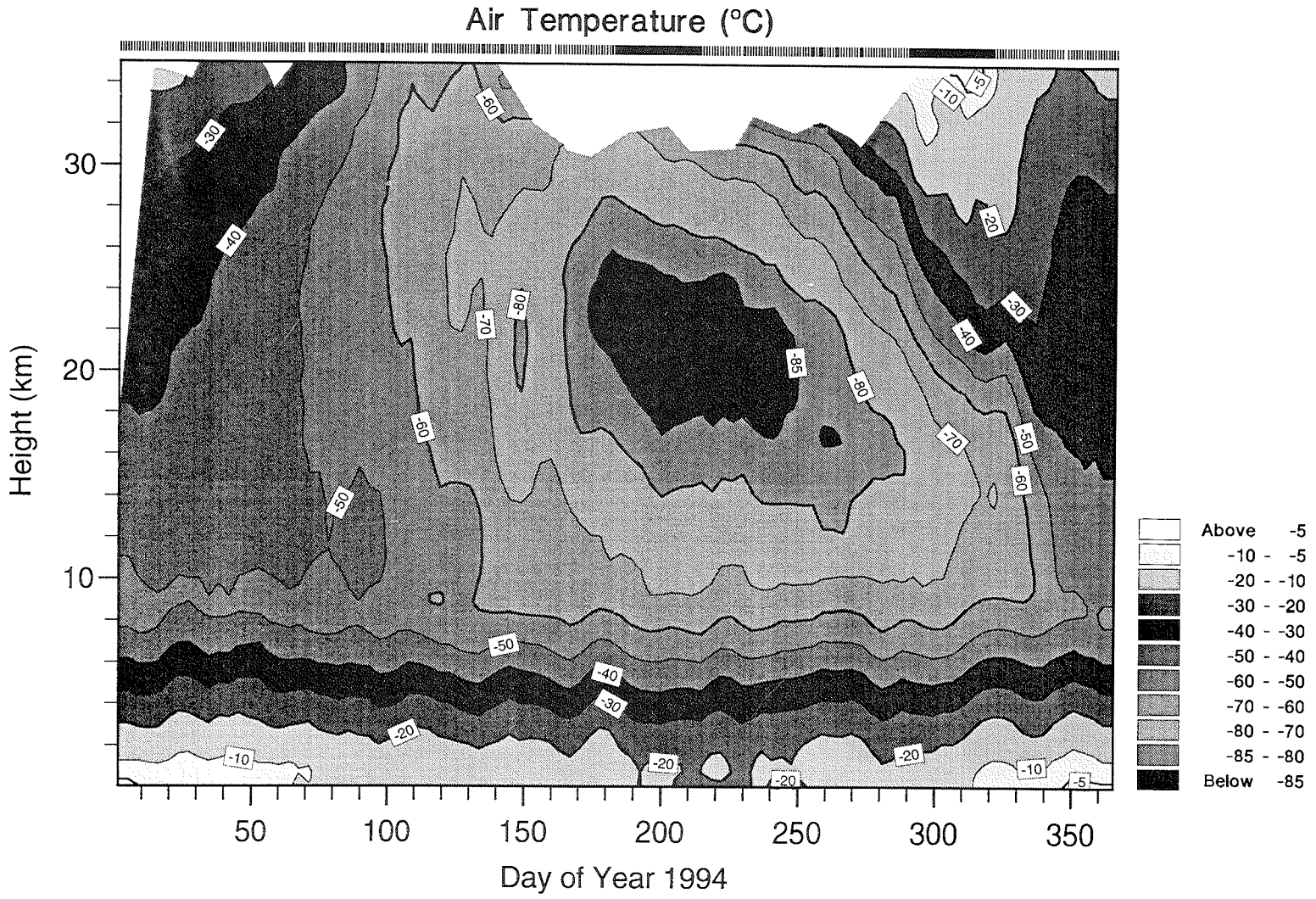

Fig. 13c Time - height section of temperature (°C) from daily radiosonde soundings 1994

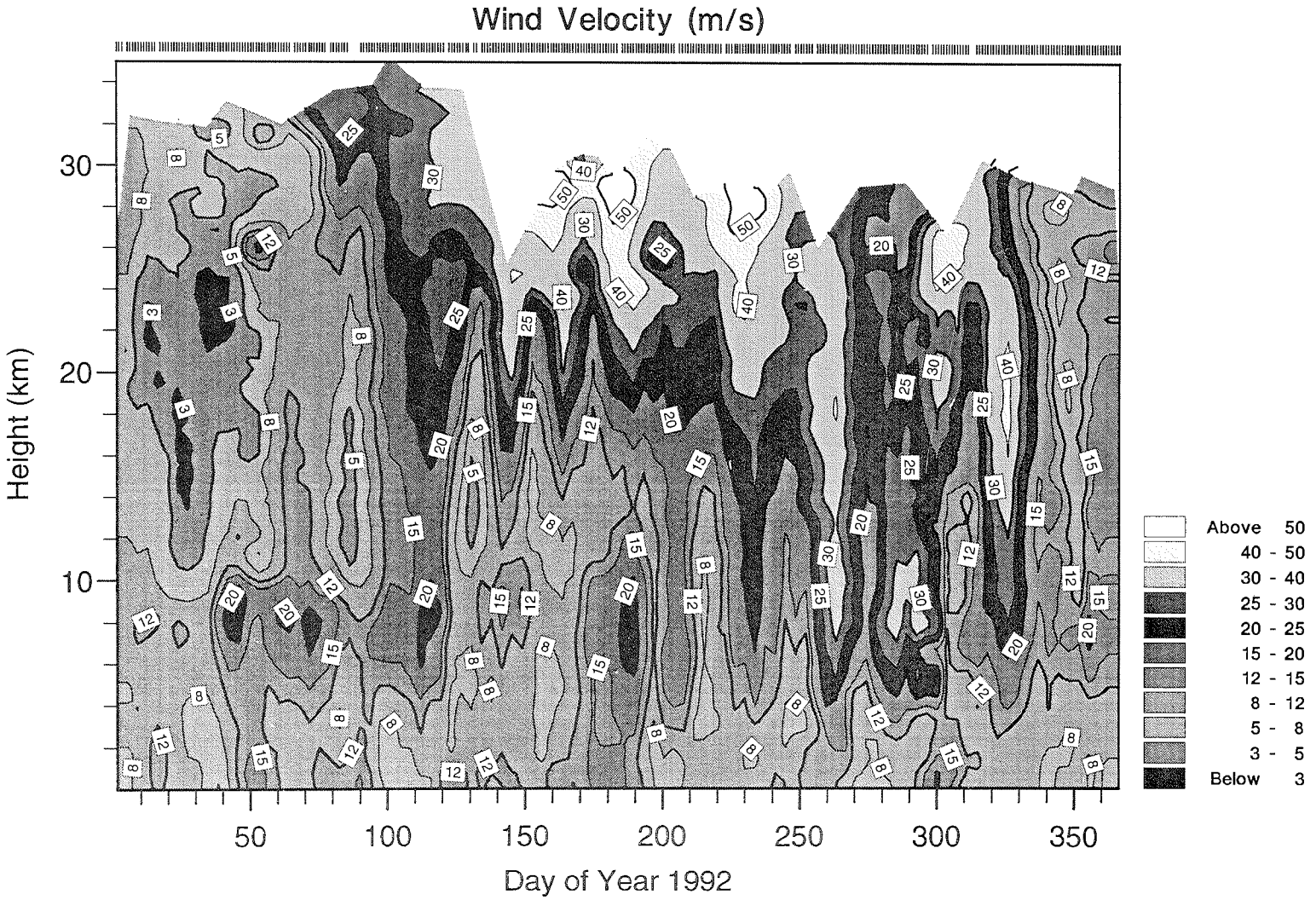

Fig. 14a Time - height section of wind velocity (m/s) from daily radiosonde soundings 1992

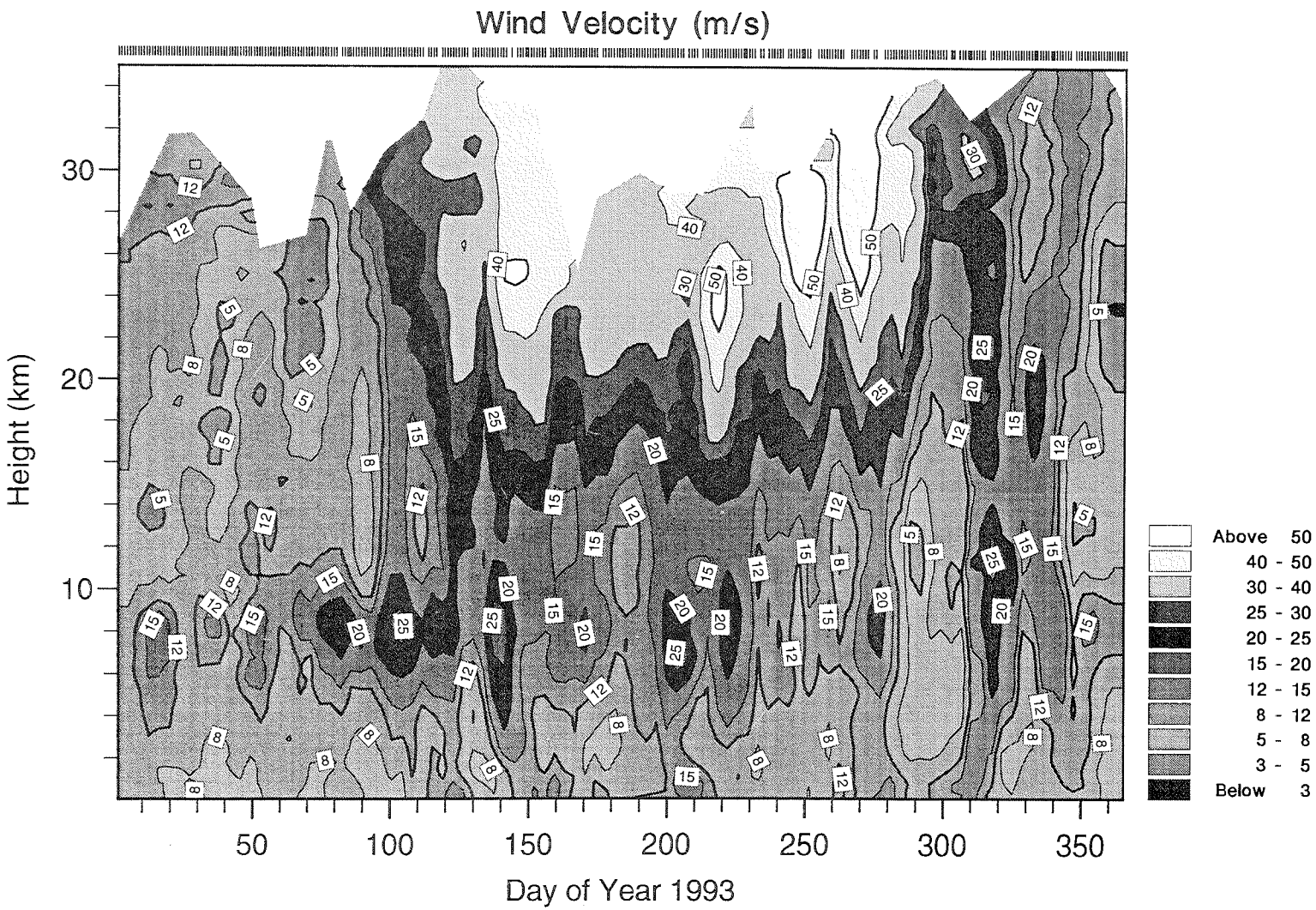

Fig. 14b Time - height section of wind velocity (m/s) from daily radiosonde soundings 1993

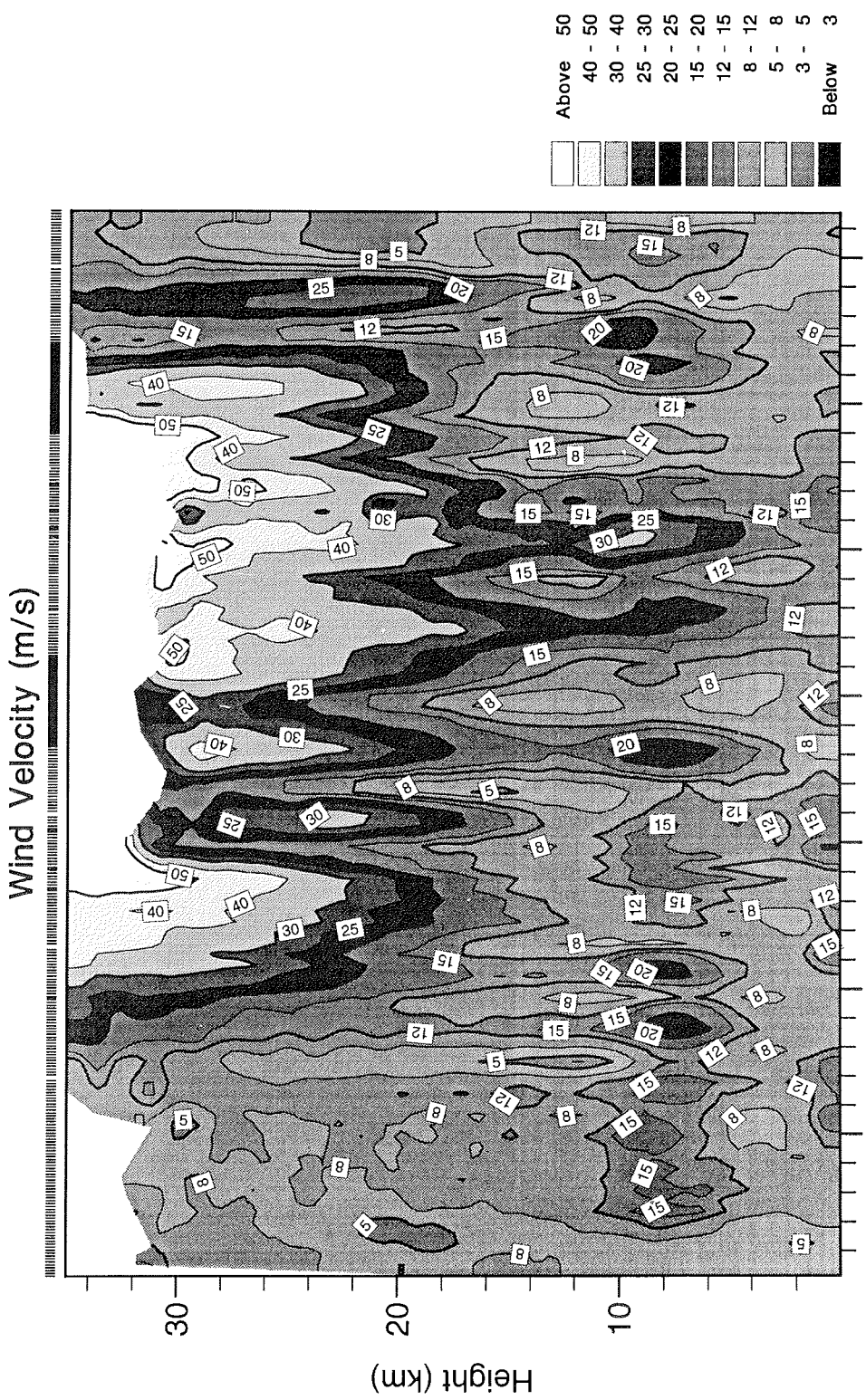

Fig. 14c Time - height section of wind velocity (m/s) from daily radiosonde soundings 1994

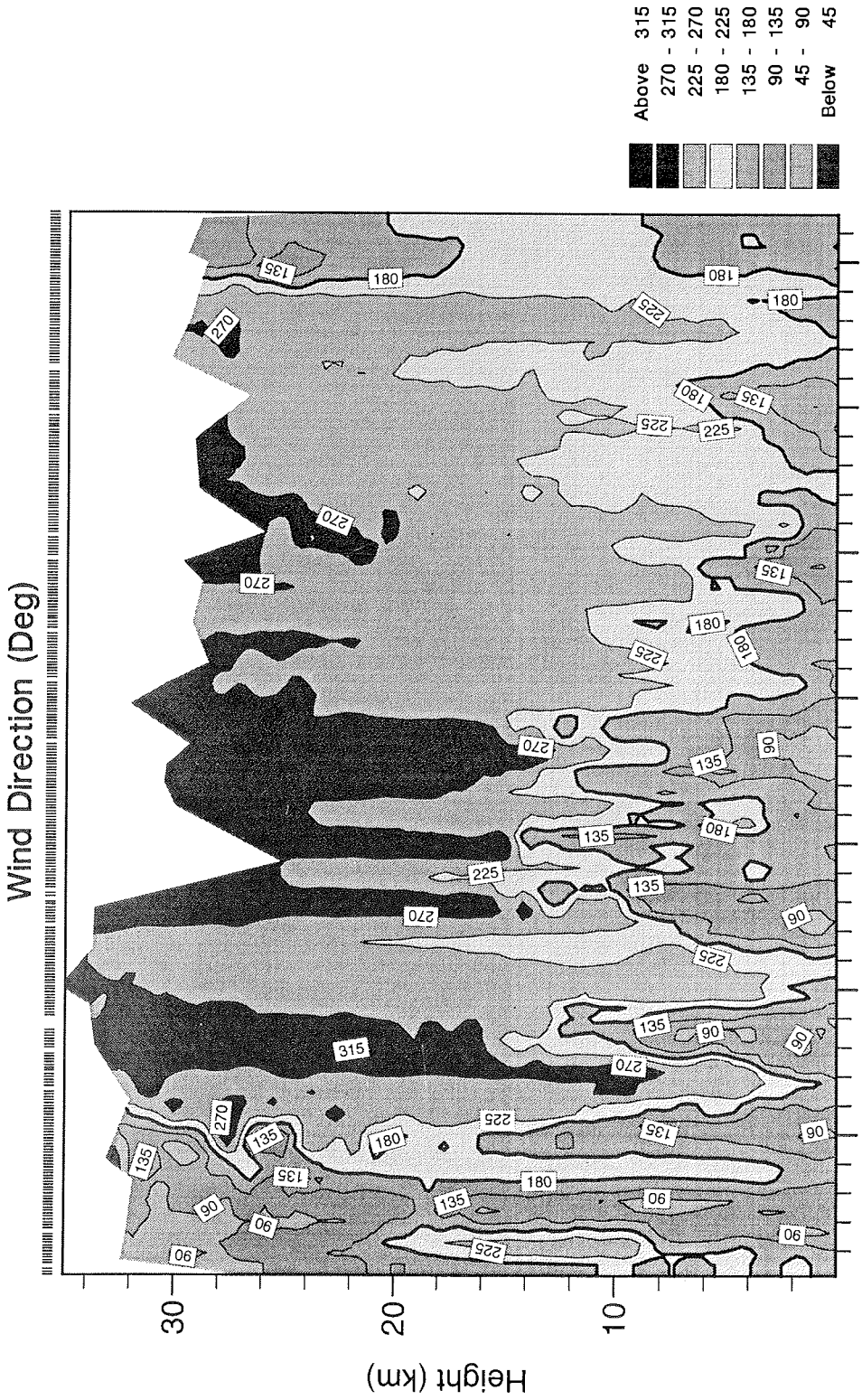

Fig. 15a Time - height section of wind direction (°) from daily radiosonde soundings 1992

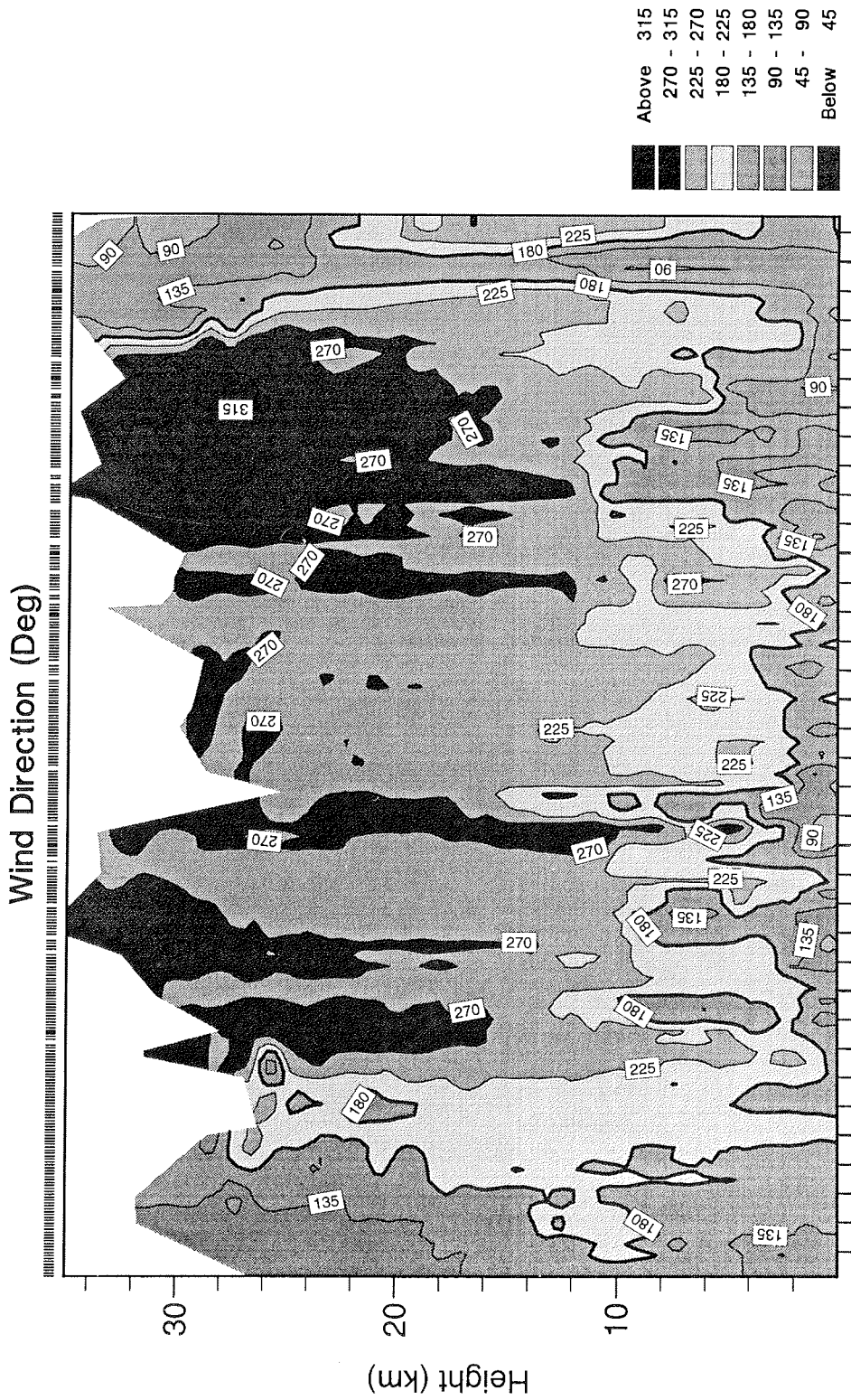

Fig. 15b Time - height section of wind direction (°) from daily radiosonde soundings 1993

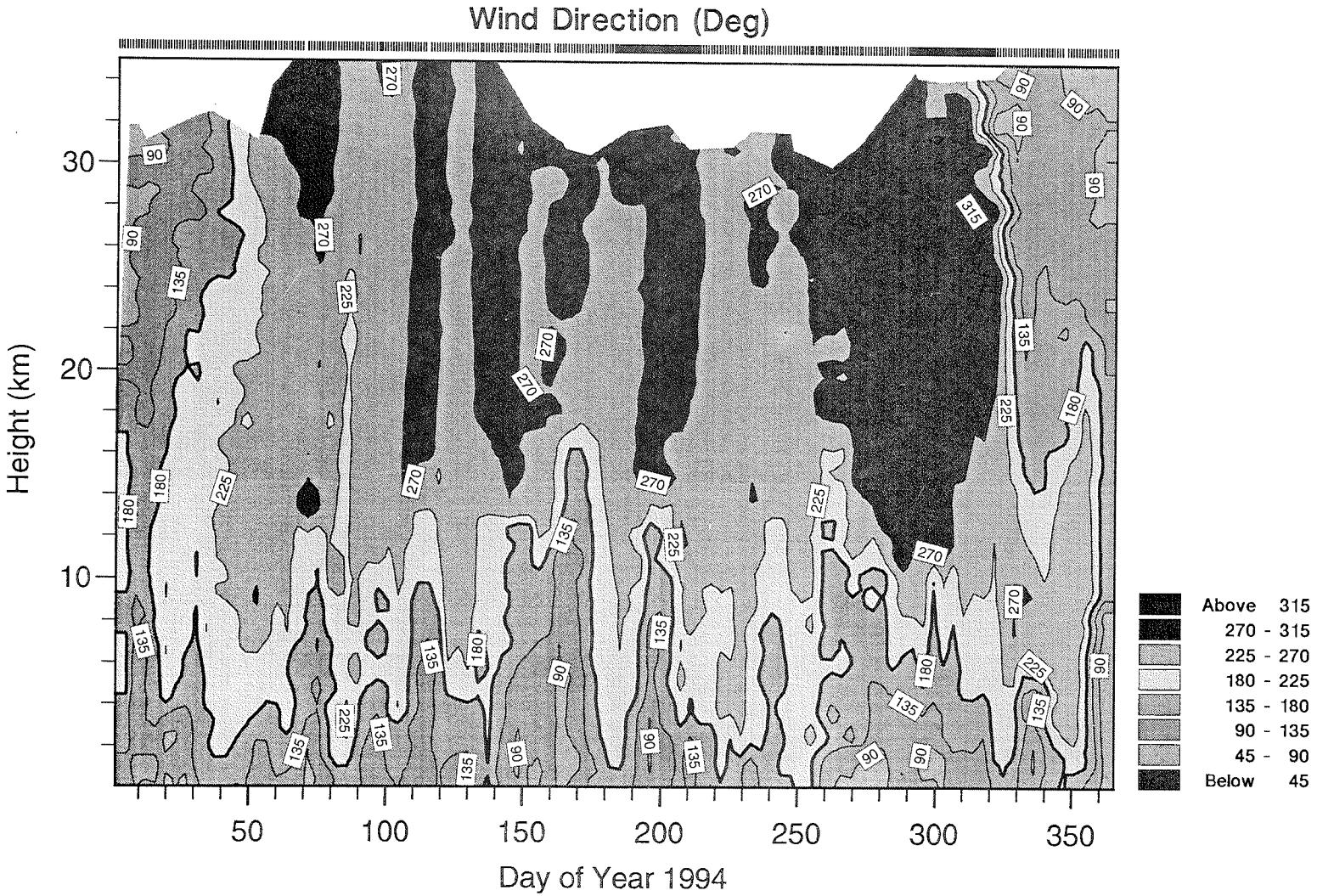

Fig. 15c Time - height section of wind direction (°) from daily radiosonde soundings 1994

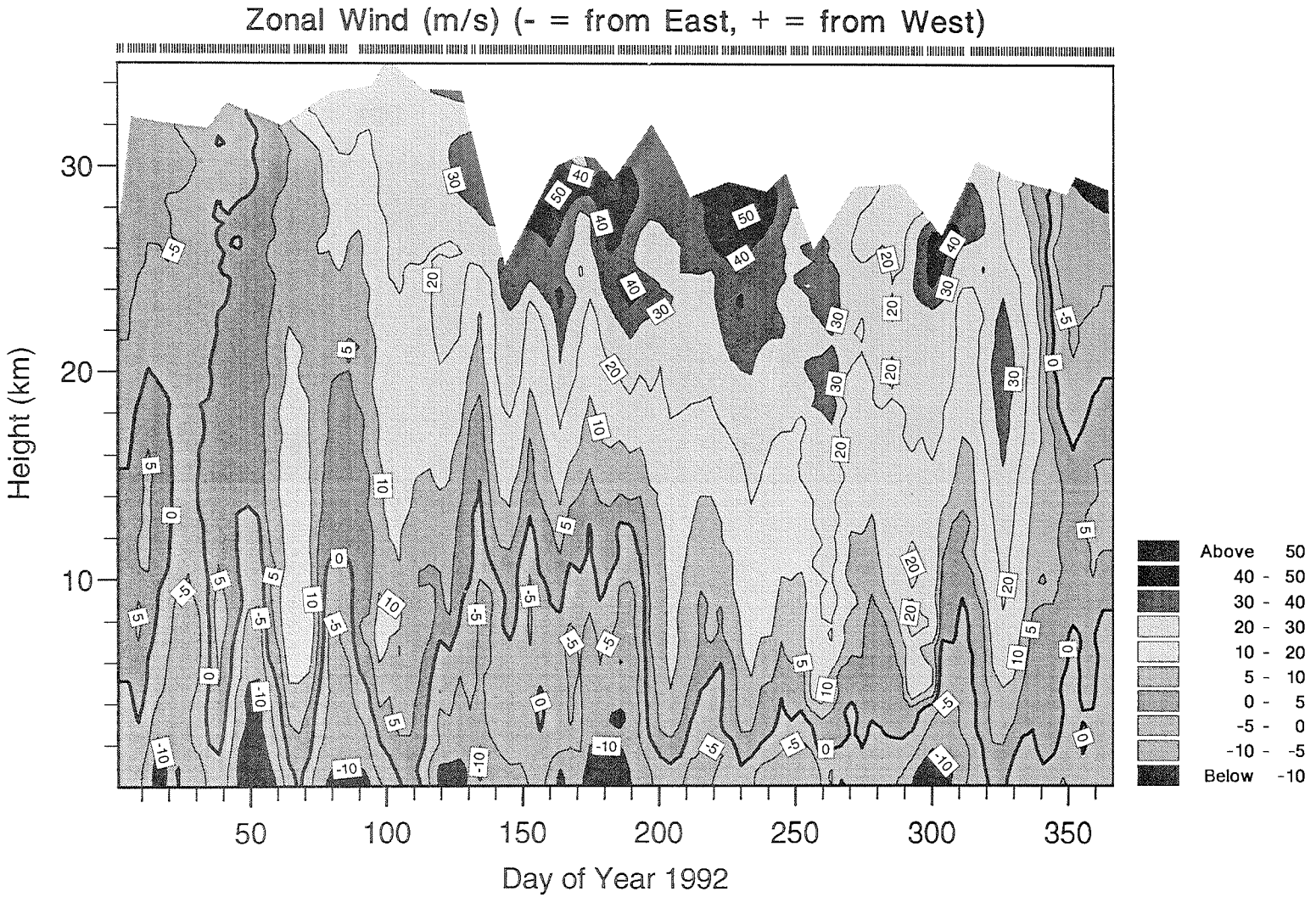

Fig. 16a Time - height section of zonal wind (m/s) from daily radiosonde soundings 1992 (- = from East, + = from West)

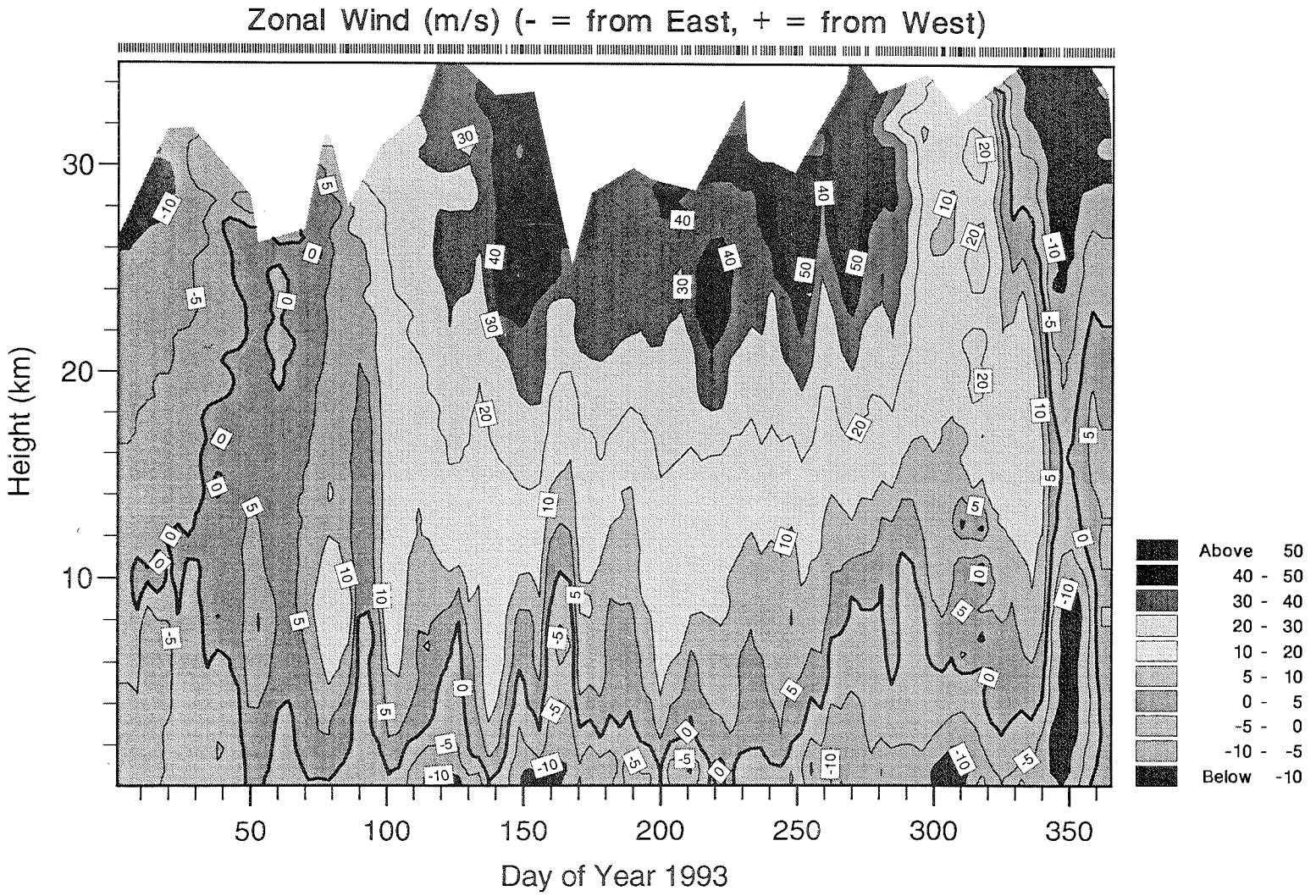

Fig. 16b Time - height section of zonal wind (m/s) from daily radiosonde soundings 1993 (- = from East, + = from West)

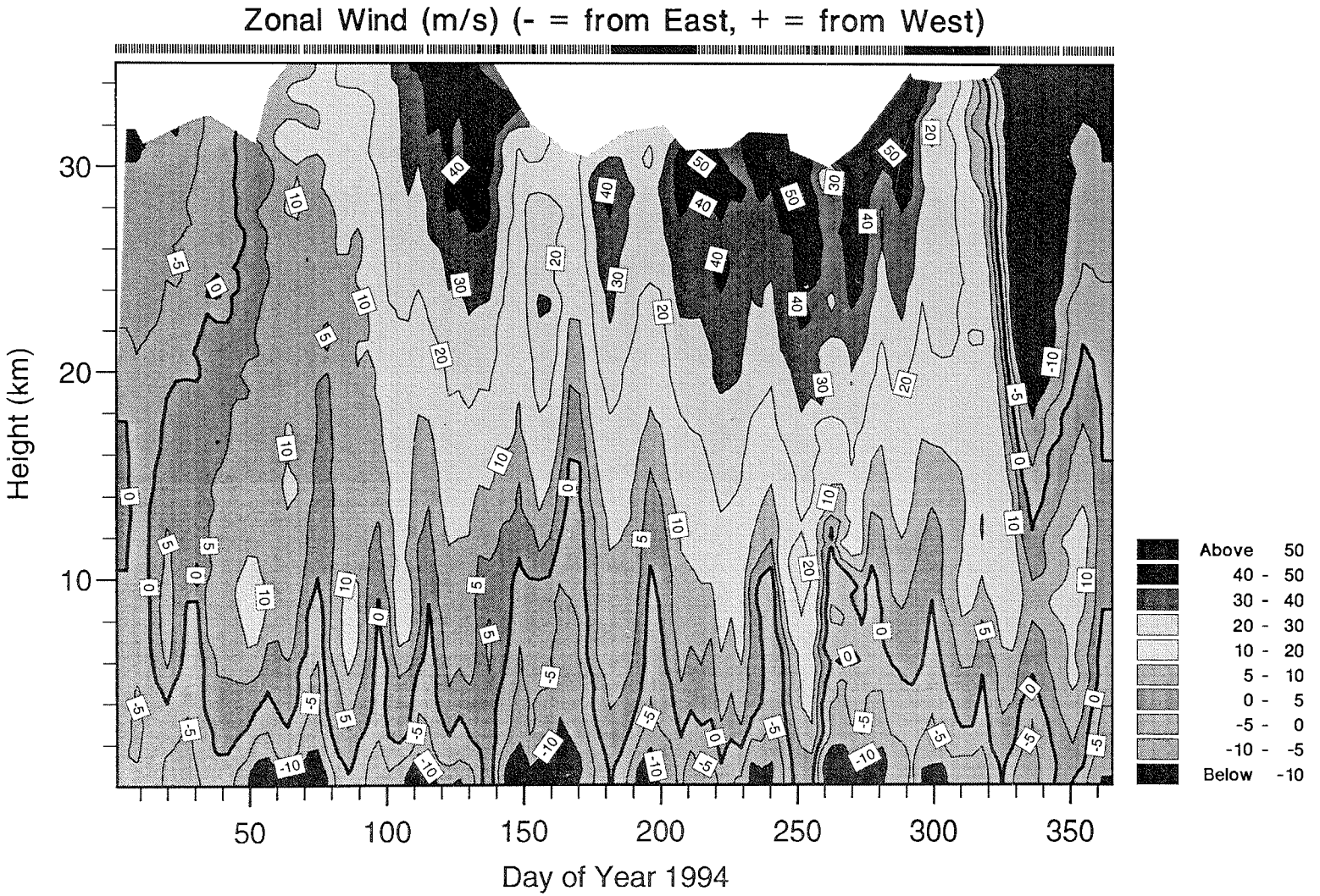

Fig. 16c Time - height section of zonal wind (m/s) from daily radiosonde soundings 1994 (- = from East, + = from West)

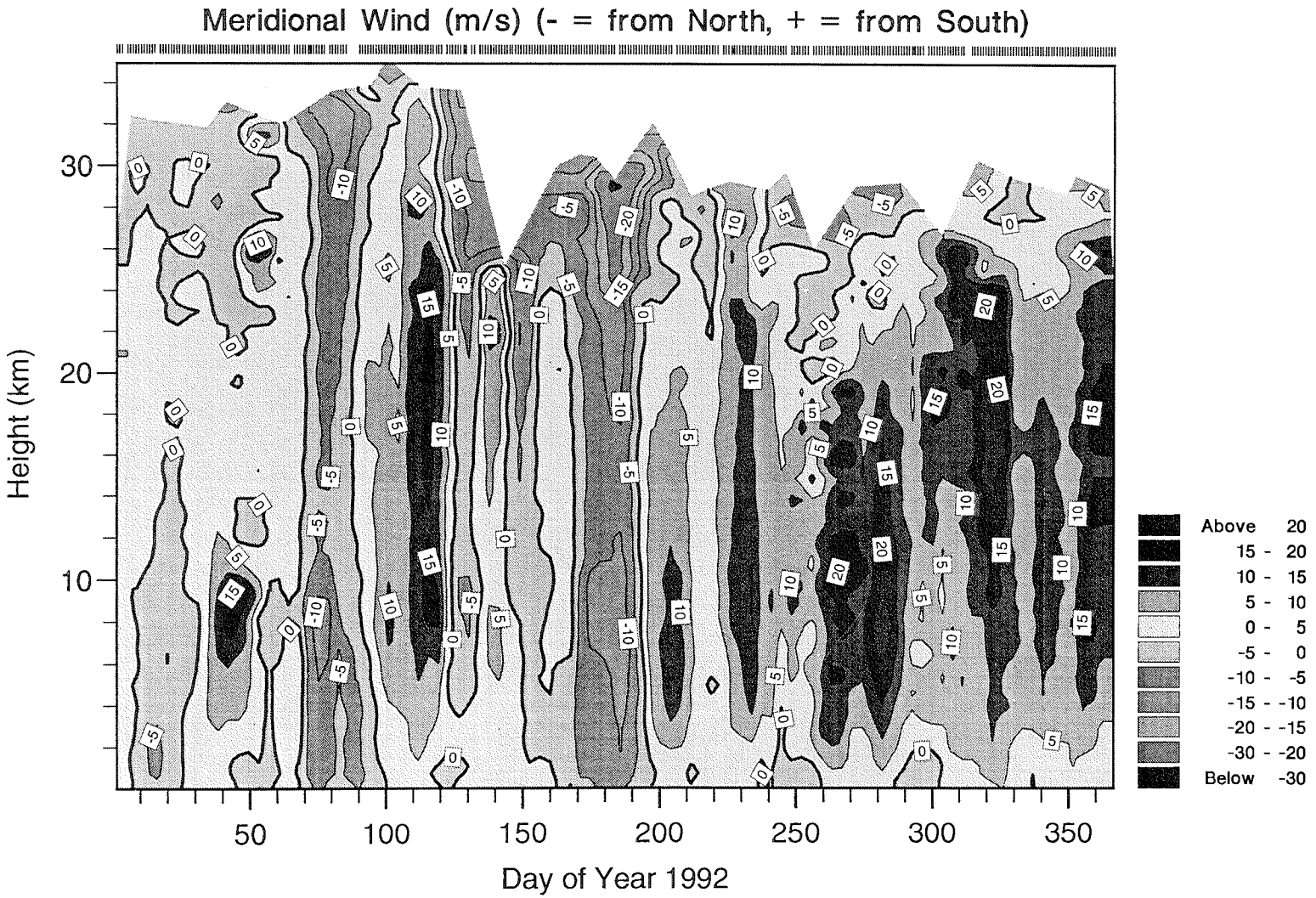

Fig. 17a Time - height section of meridional wind (m/s) from daily radiosonde soundings 1992 (- = from North, + = from South)

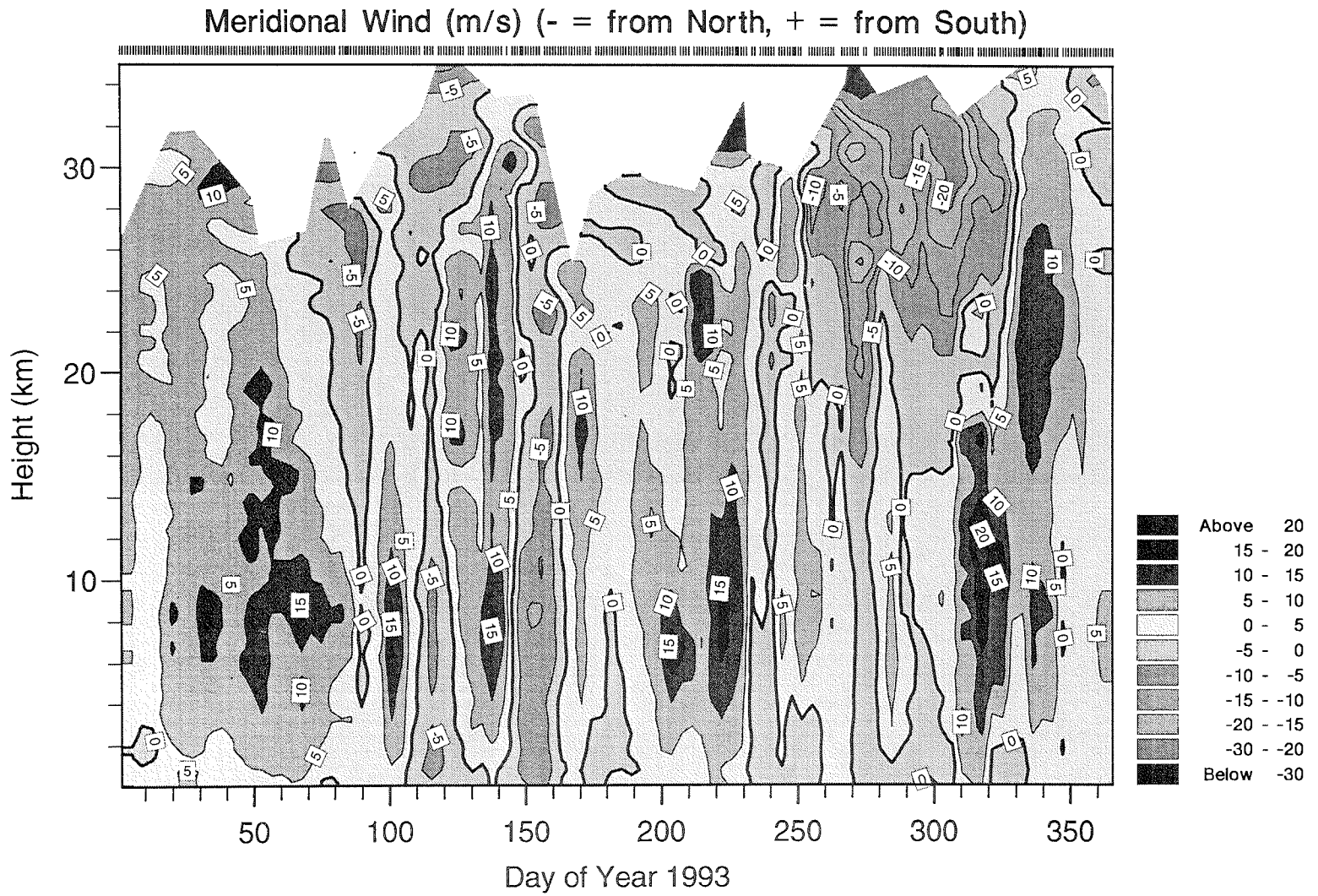

Fig. 17b Time - height section of meridional wind (m/s) from daily radiosonde soundings 1993 (- = from North, + = from South)

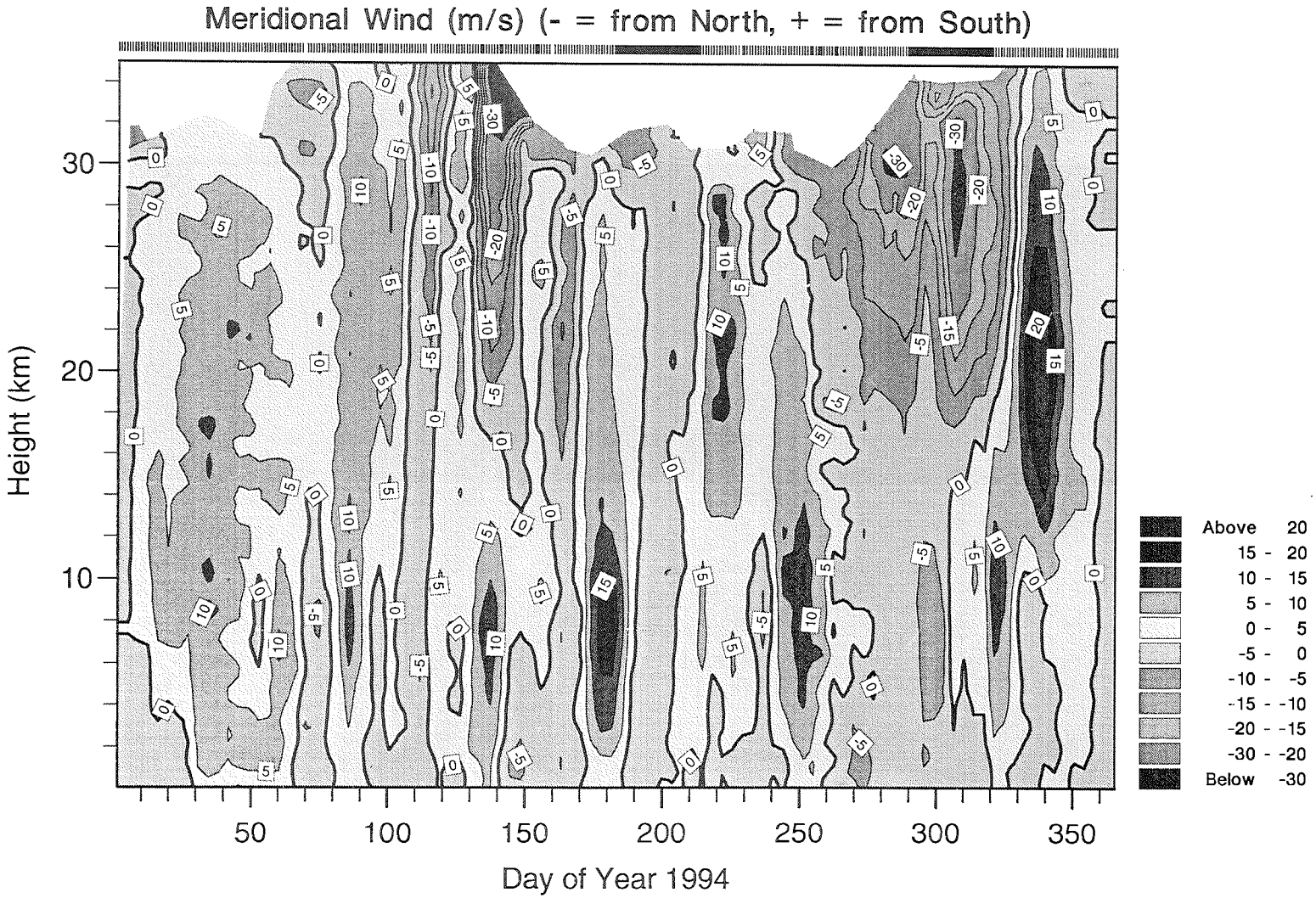

Fig. 17c Time - height section of meridional wind (m/s) from daily radiosonde soundings 1994 (- = from North, + = from South)

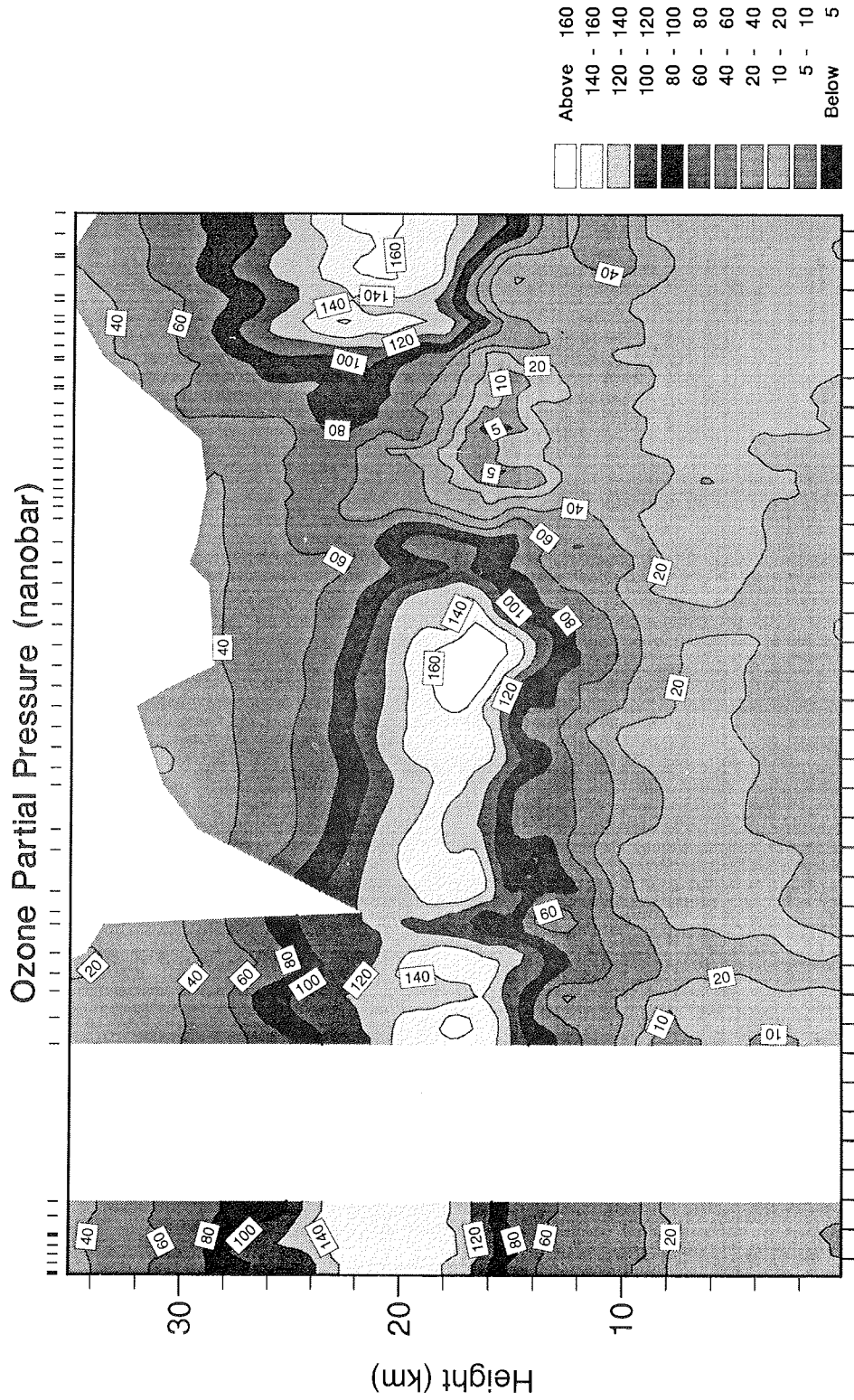

Fig. 18a Time - height section of ozone partial pressure (nanobar) from daily radiosonde soundings 1992

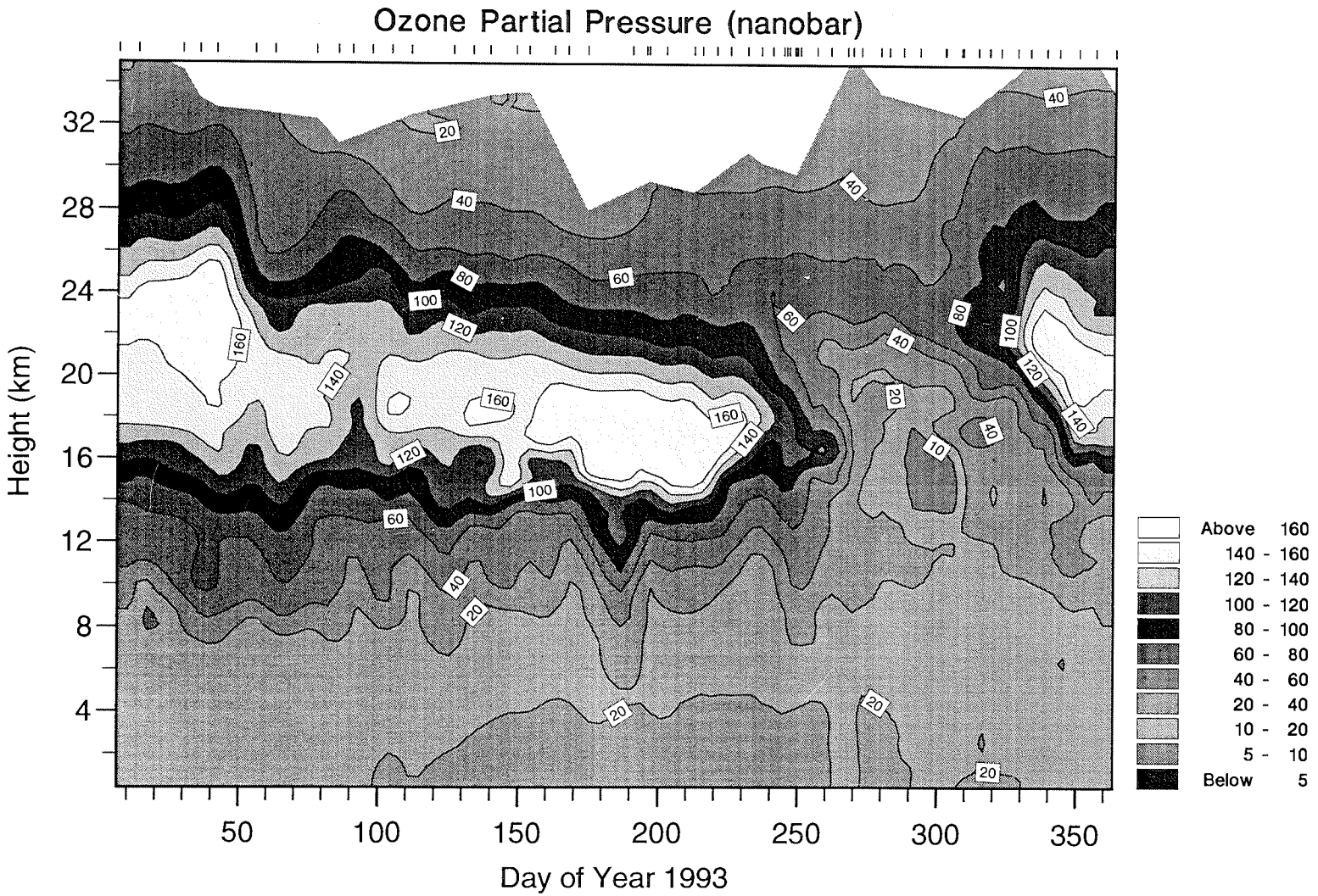

Fig. 18b Time - height section of ozone partial pressure (nanobar) from daily radiosonde soundings 1993

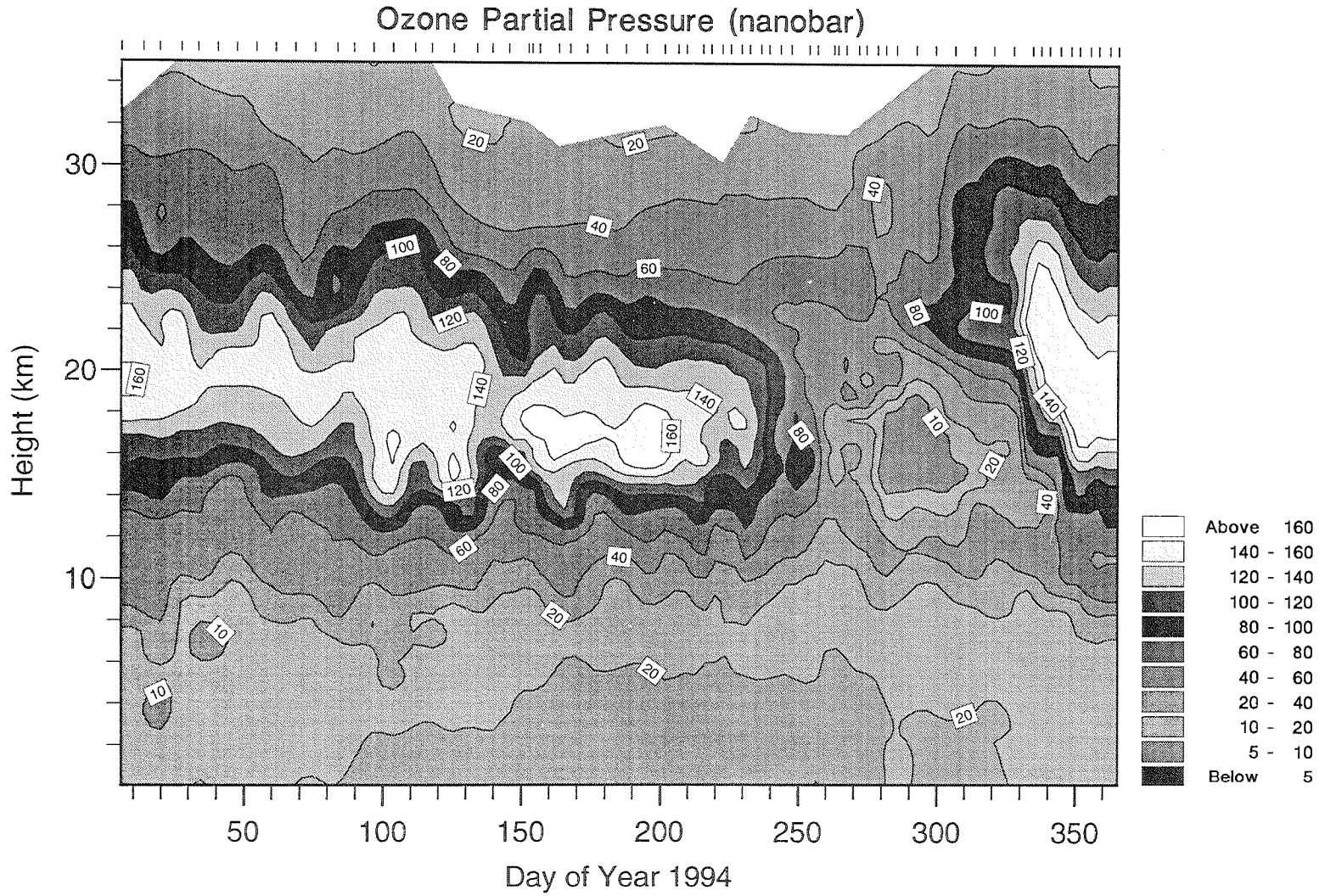

Fig. 18c Time - height section of ozone partial pressure (nanobar) from daily radiosonde soundings 1994

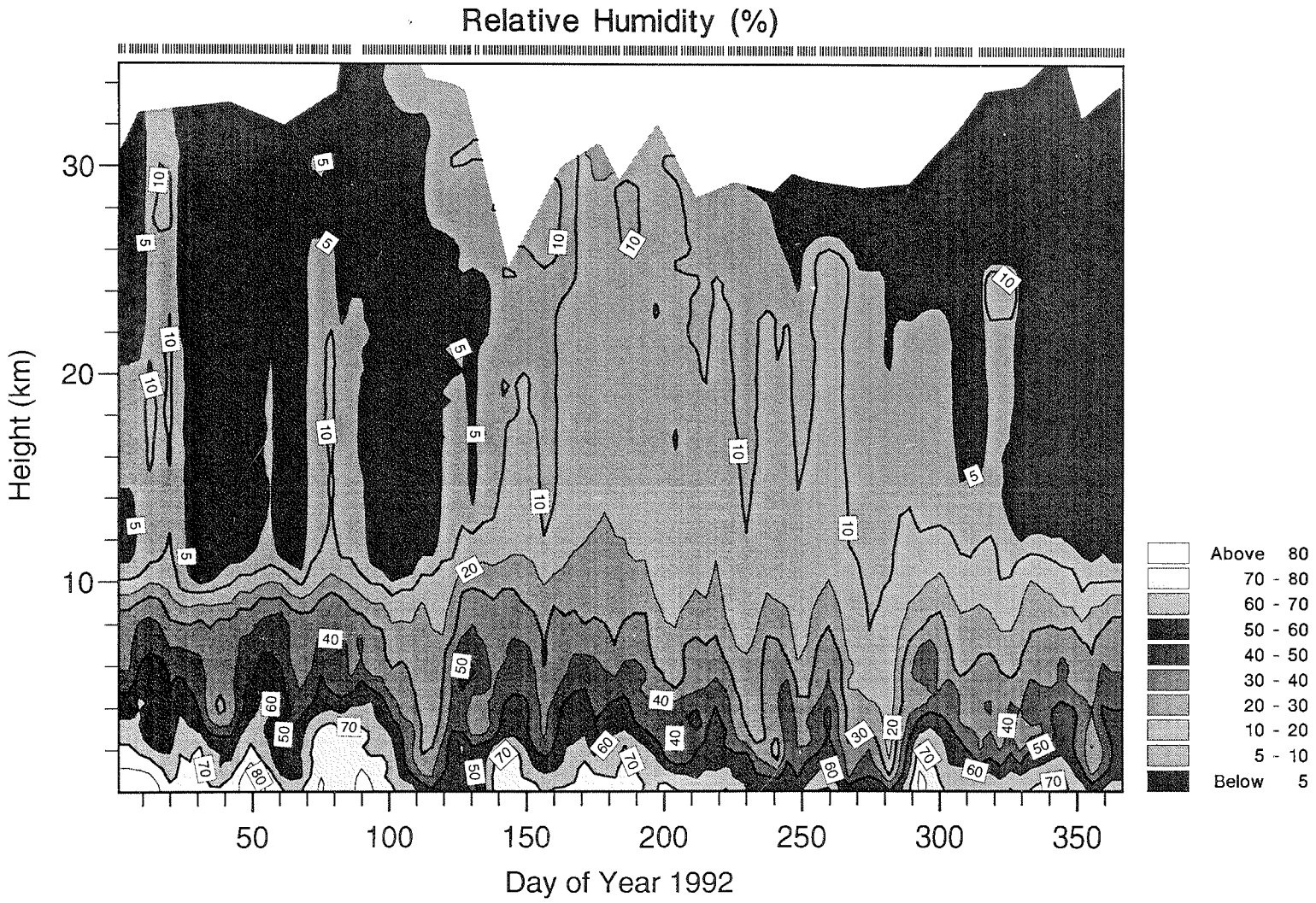

Fig. 19a Time - height section of relative humidity (%) from daily radiosonde soundings 1992

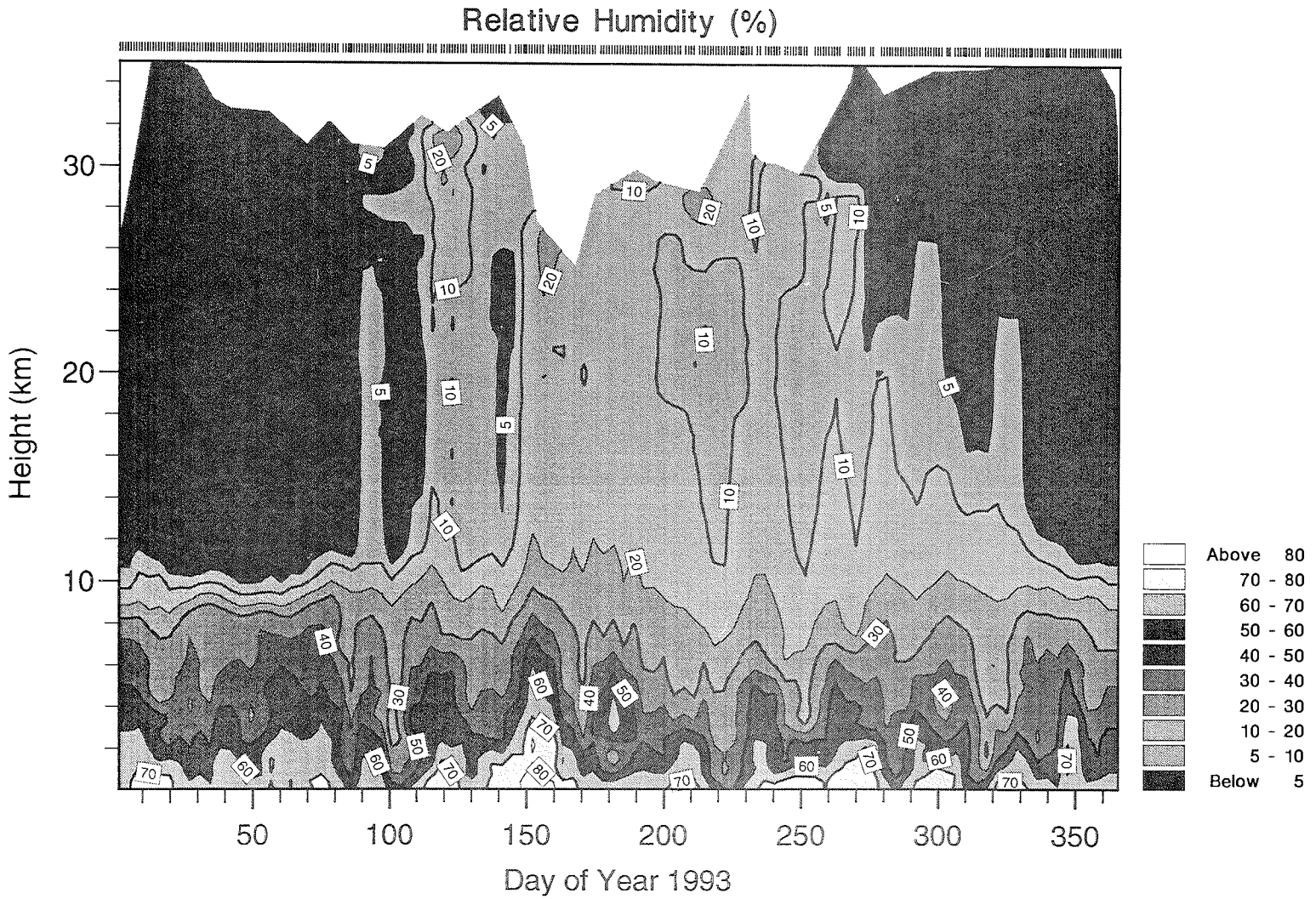

Fig. 19b Time - height section of relative humidity (%) from daily radiosonde soundings 1993

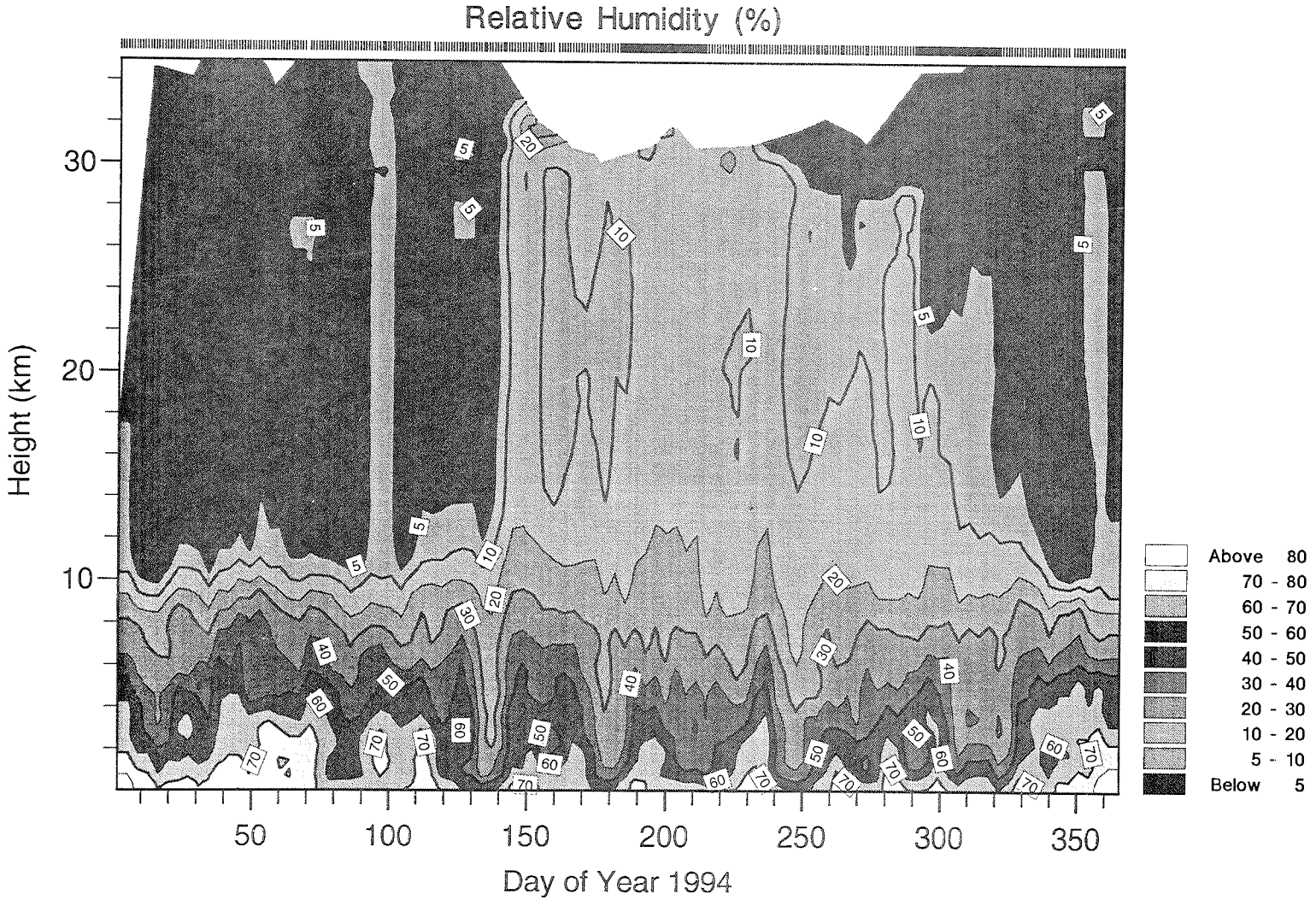

Fig. 19c Time - height section of relative humidity (%) from daily radiosonde soundings 1994

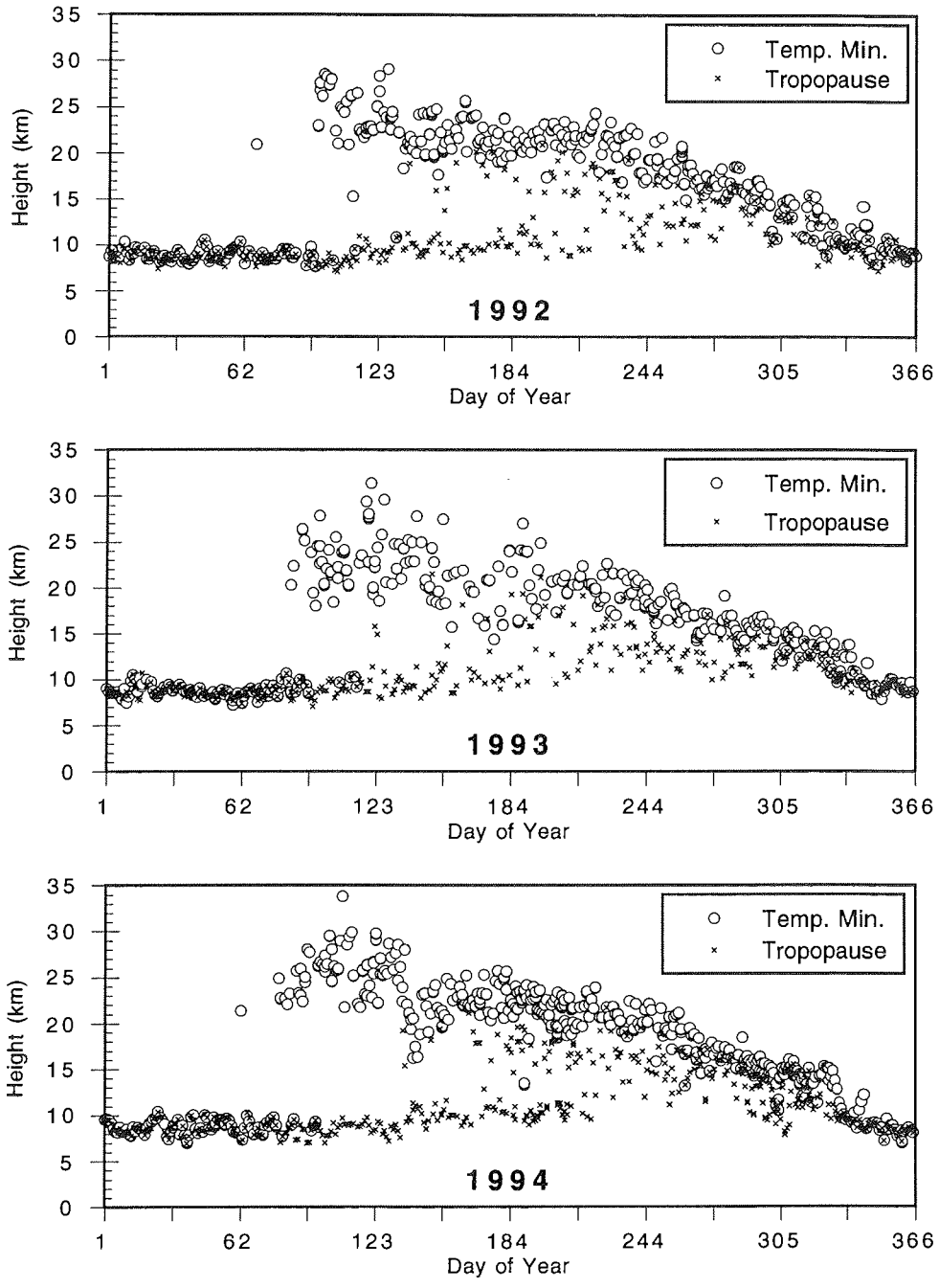

Figs. 20a- 20c Heights of tropopause and heights of temperature minimum, calculated from daily radiosonde data for the years 1992 - 1994.

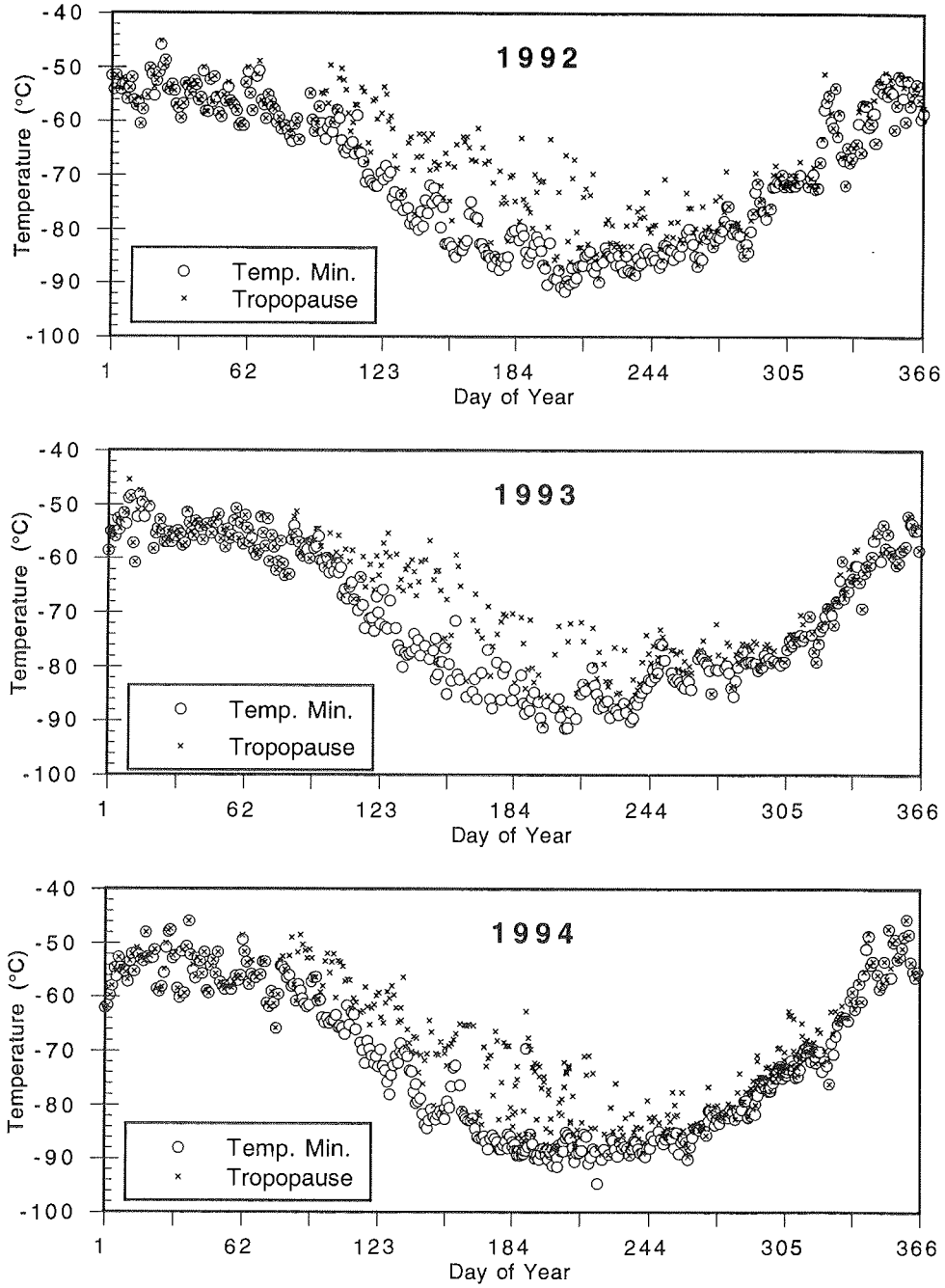

Figs. 21a-21c Temperatures of tropopause and temperature minima calculated from daily radiosonde data of the years 1992 - 1994.

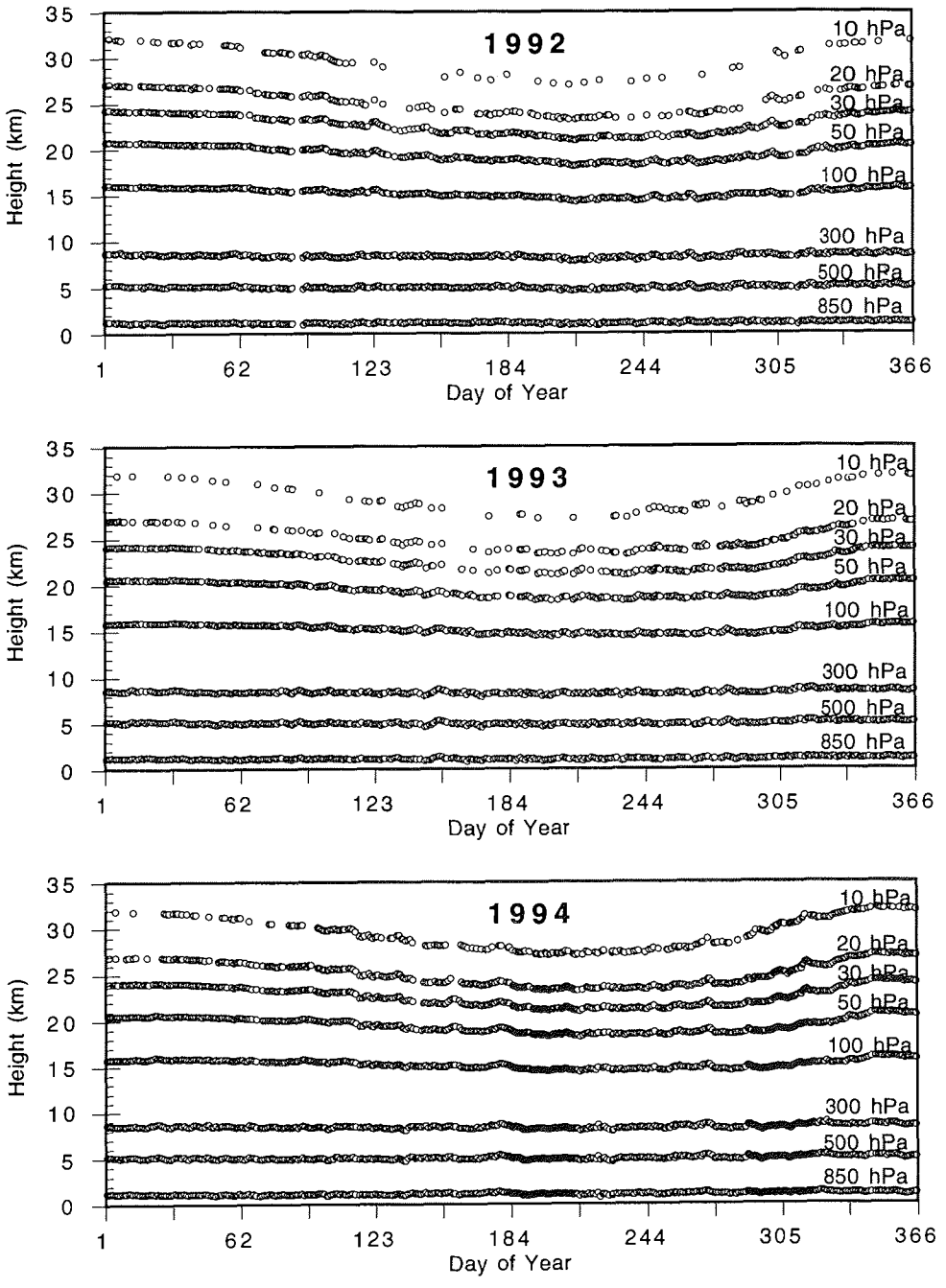

Figs. 22a-22c Heights of different standard pressure levels from daily radiosonde data of the years 1992 - 1994.

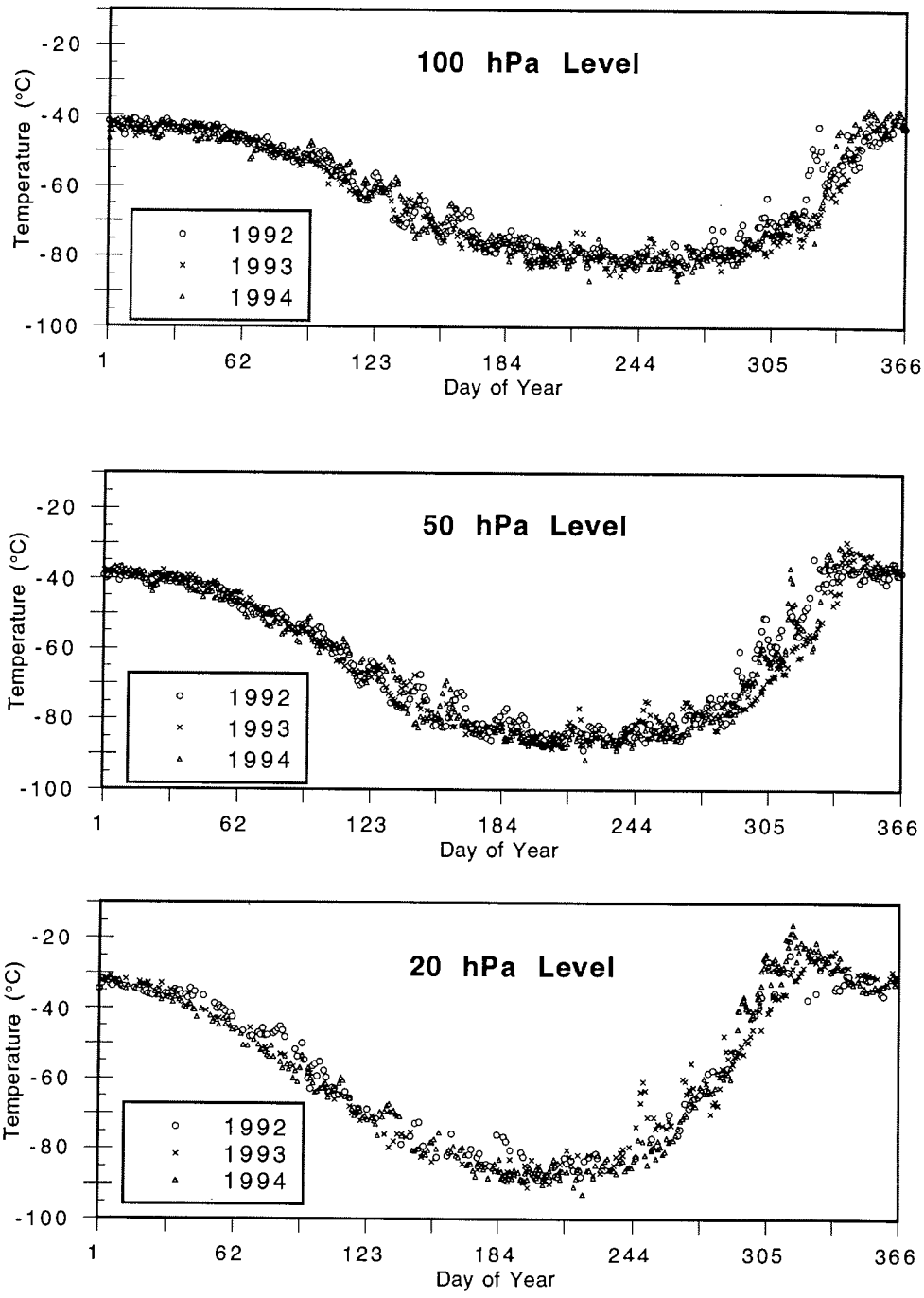

Figs. 23a-23c Temperatures at mean pressure levels calculated from daily radiosonde data of the years 1992 - 1994.

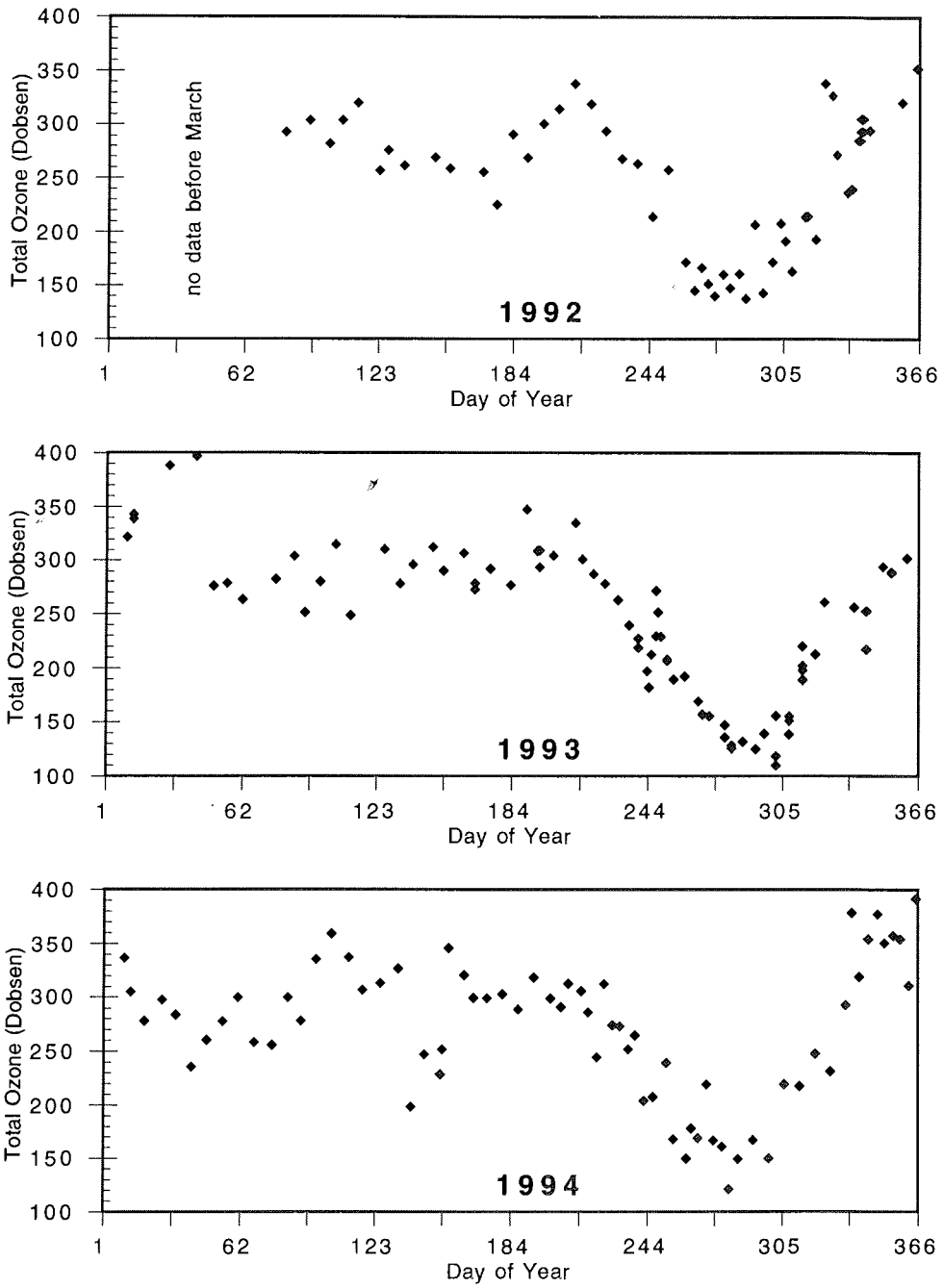

Figs. 24a-24c Total ozone calculated from radiosonde data of the years 1992 - 1994.

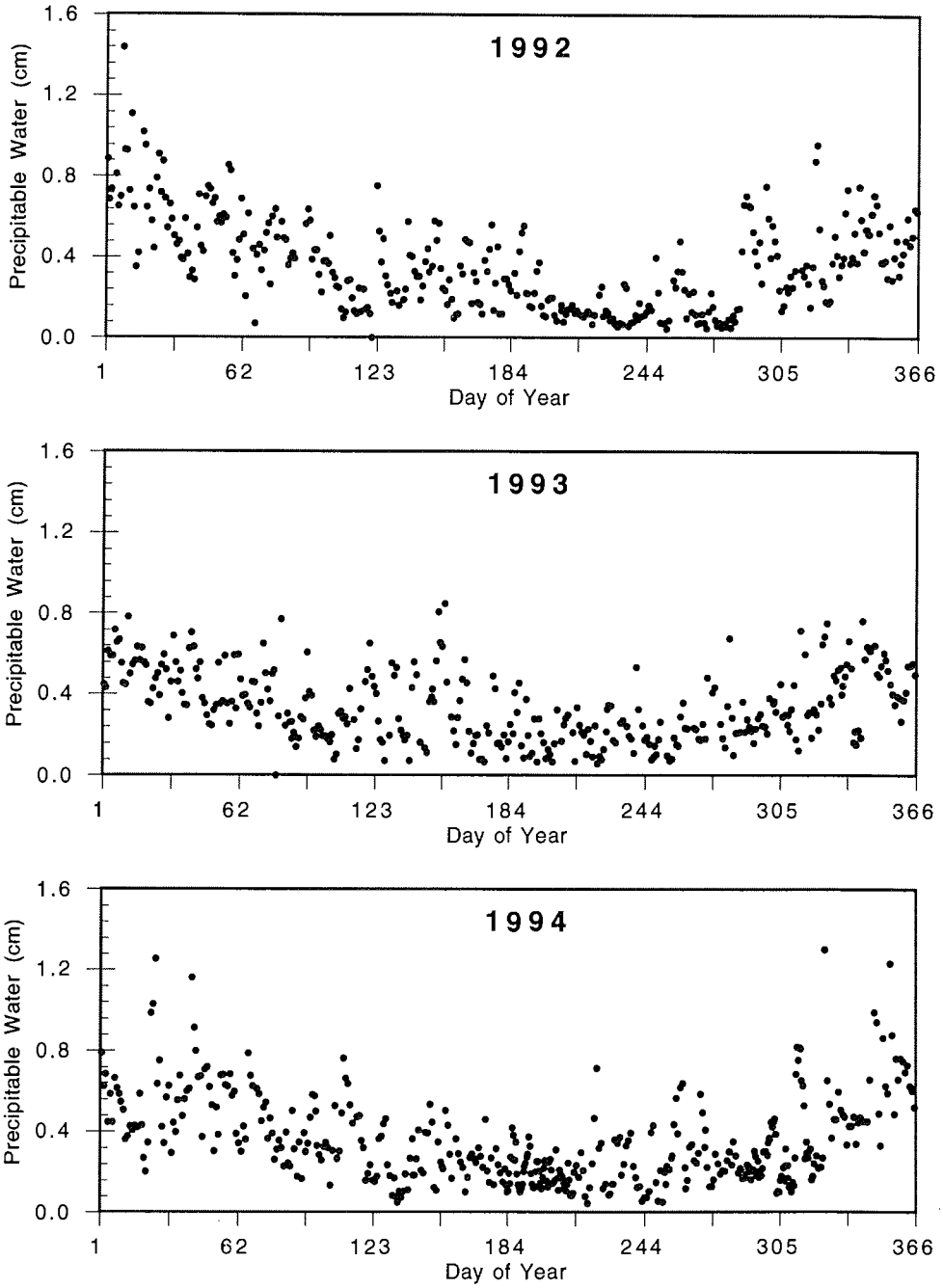

Figs. 25a-25c Precipitable water (content of water vapour in a vertical column) from daily radiosonde data of the years 1992 - 1994.

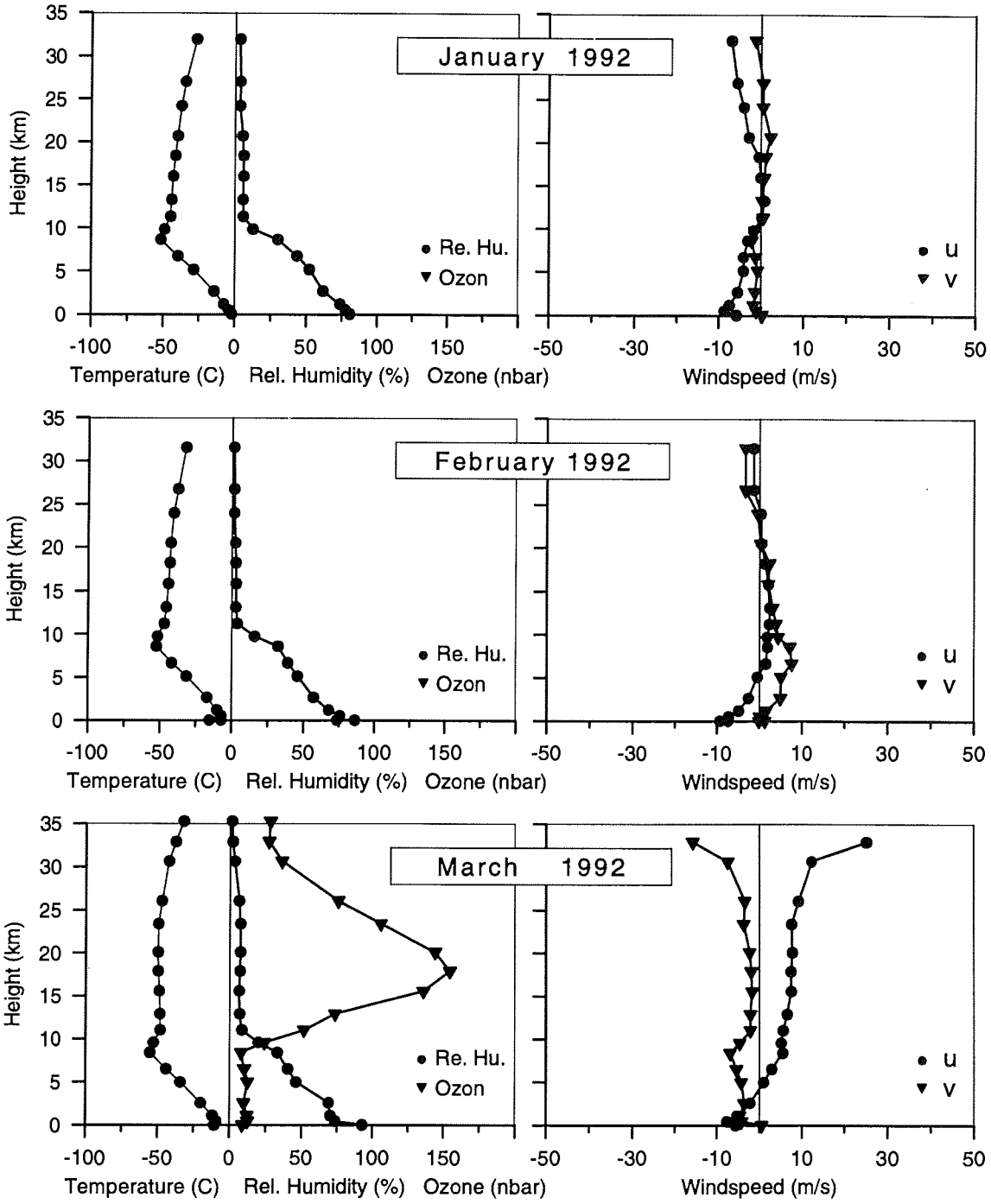

Figs. 26a-26c Mean monthly profiles of temperature, relative humidity, zonal (u) and meridional (v) wind component.

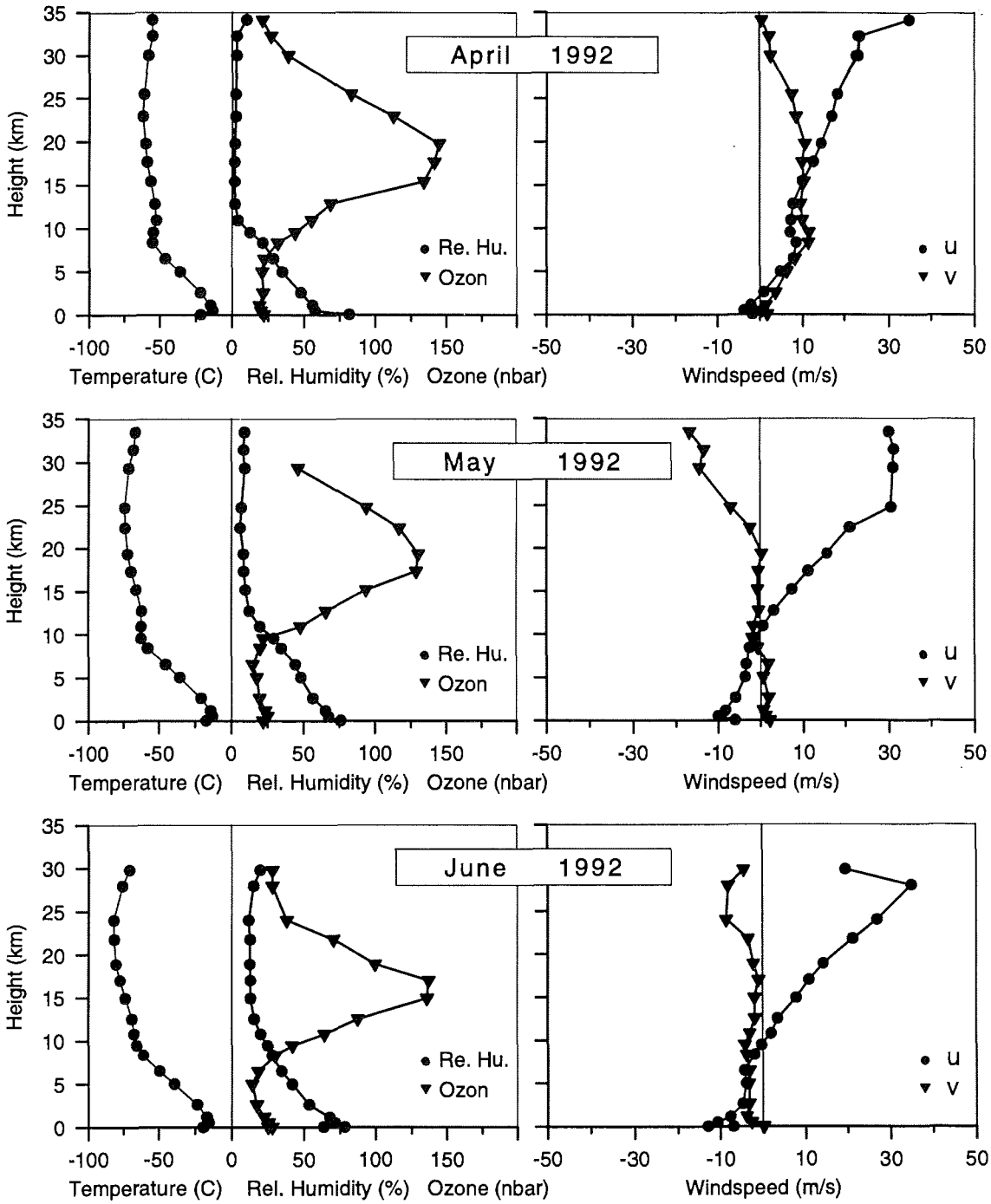

Figs. 26d-26f Mean monthly profiles of temperature, relative humidity, zonal (u) and meridional (v) wind component.

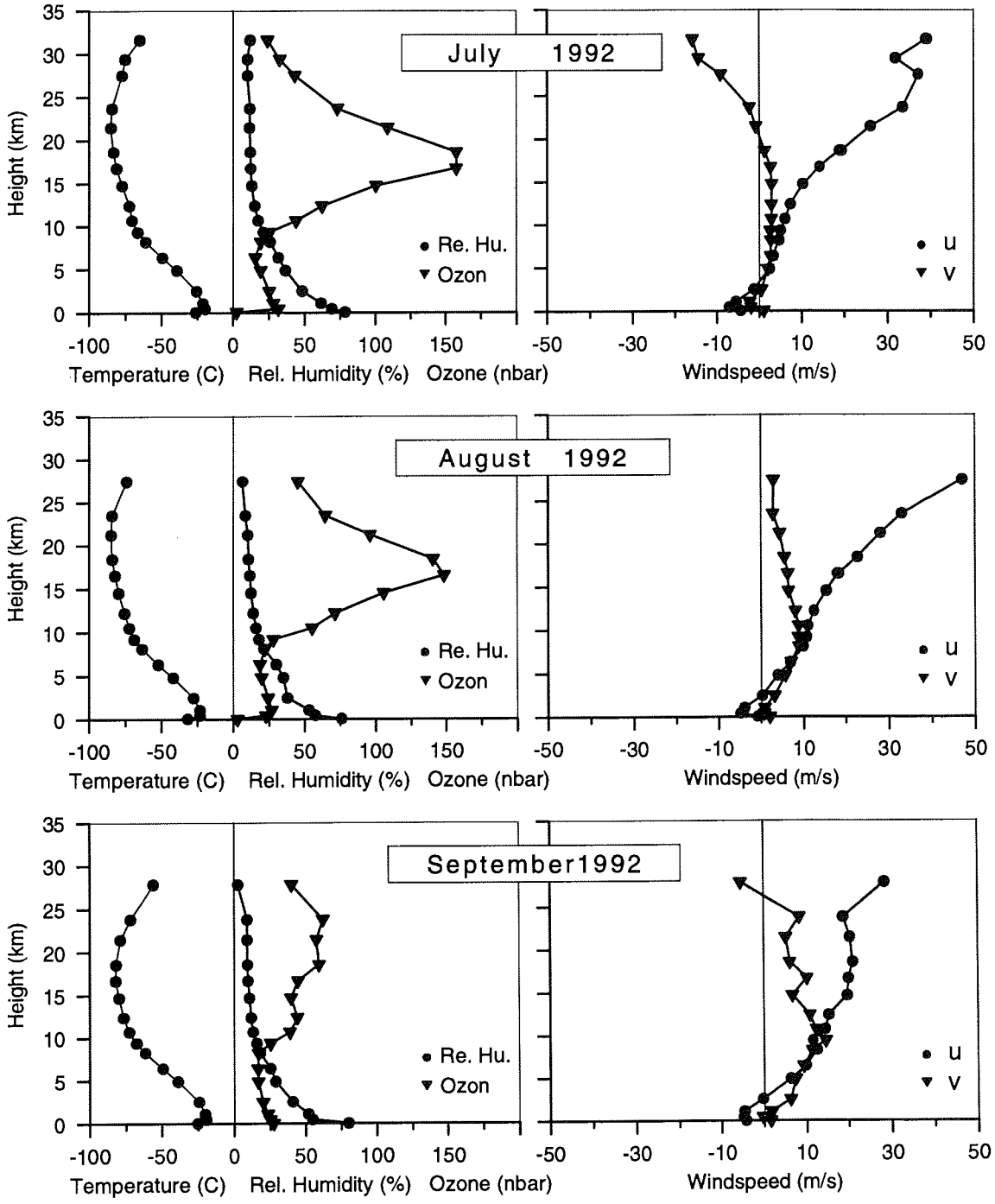

Figs. 26g-26i Mean monthly profiles of temperature, relative humidity, zonal (u) and meridional (v) wind component.

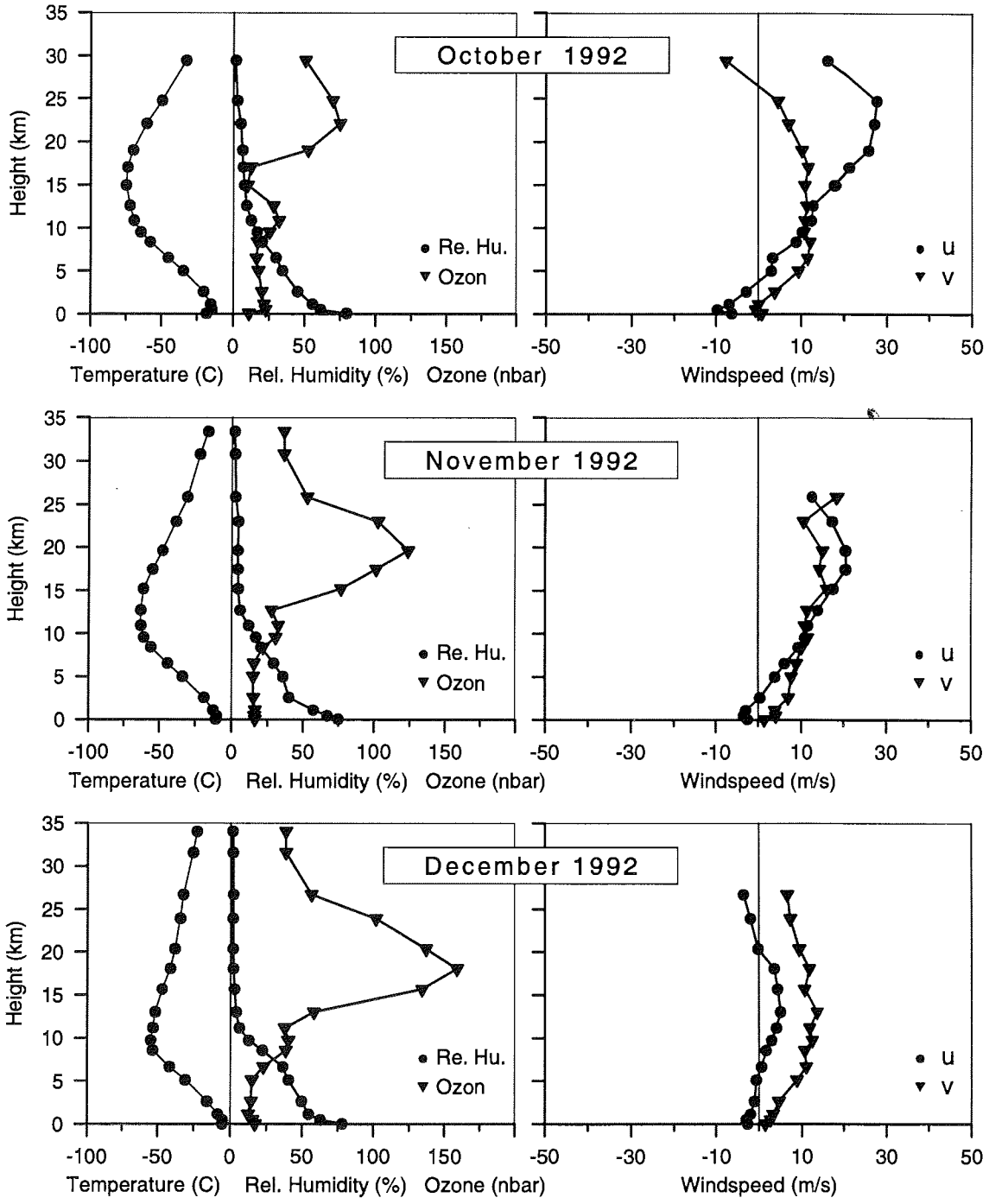

Figs. 26j-26l Mean monthly profiles of temperature, relative humidity, zonal (u) and meridional (v) wind component.

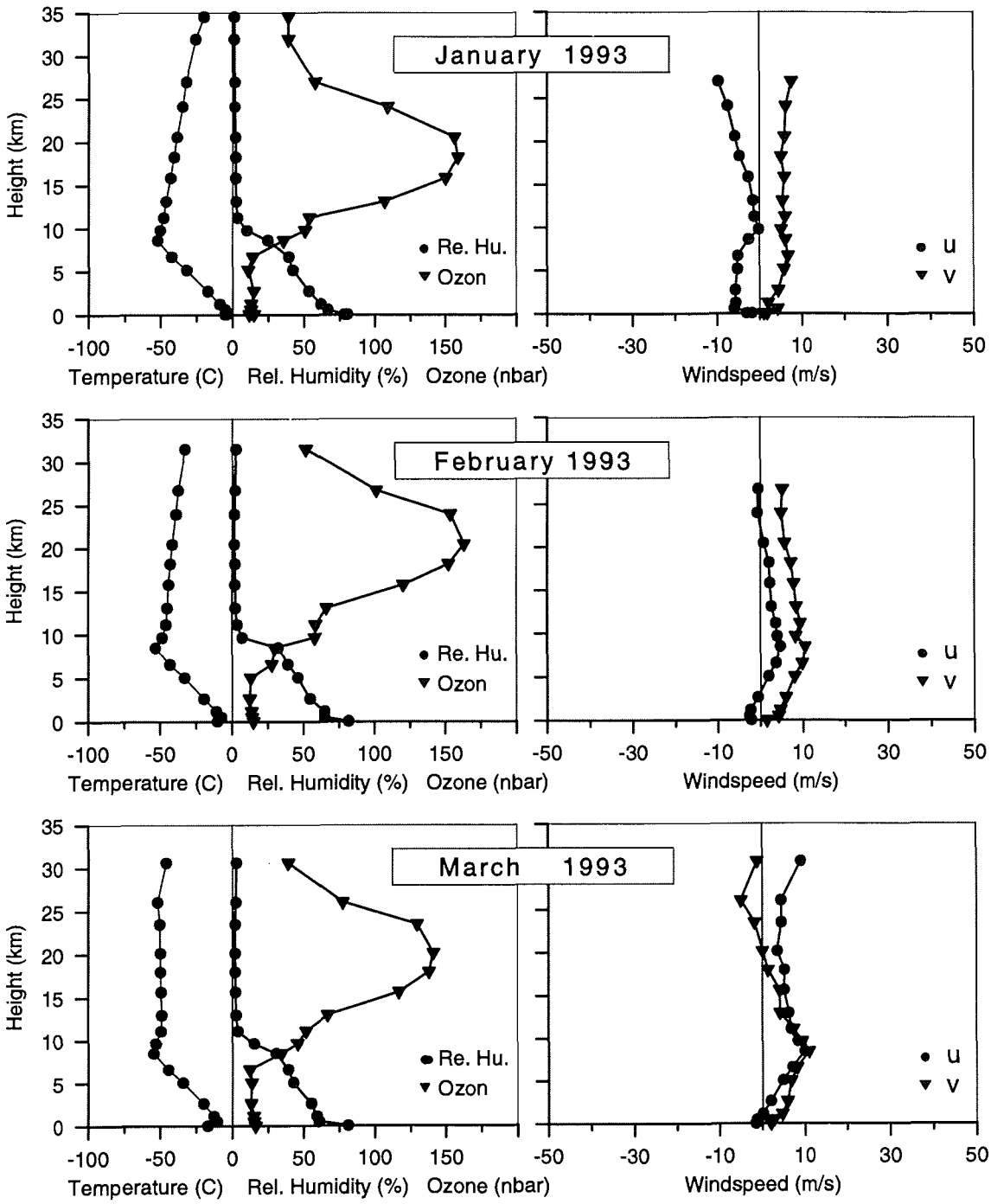

Figs. 27a-27c Mean monthly profiles of temperature, relative humidity, zonal (u) and meridional (v) wind component.

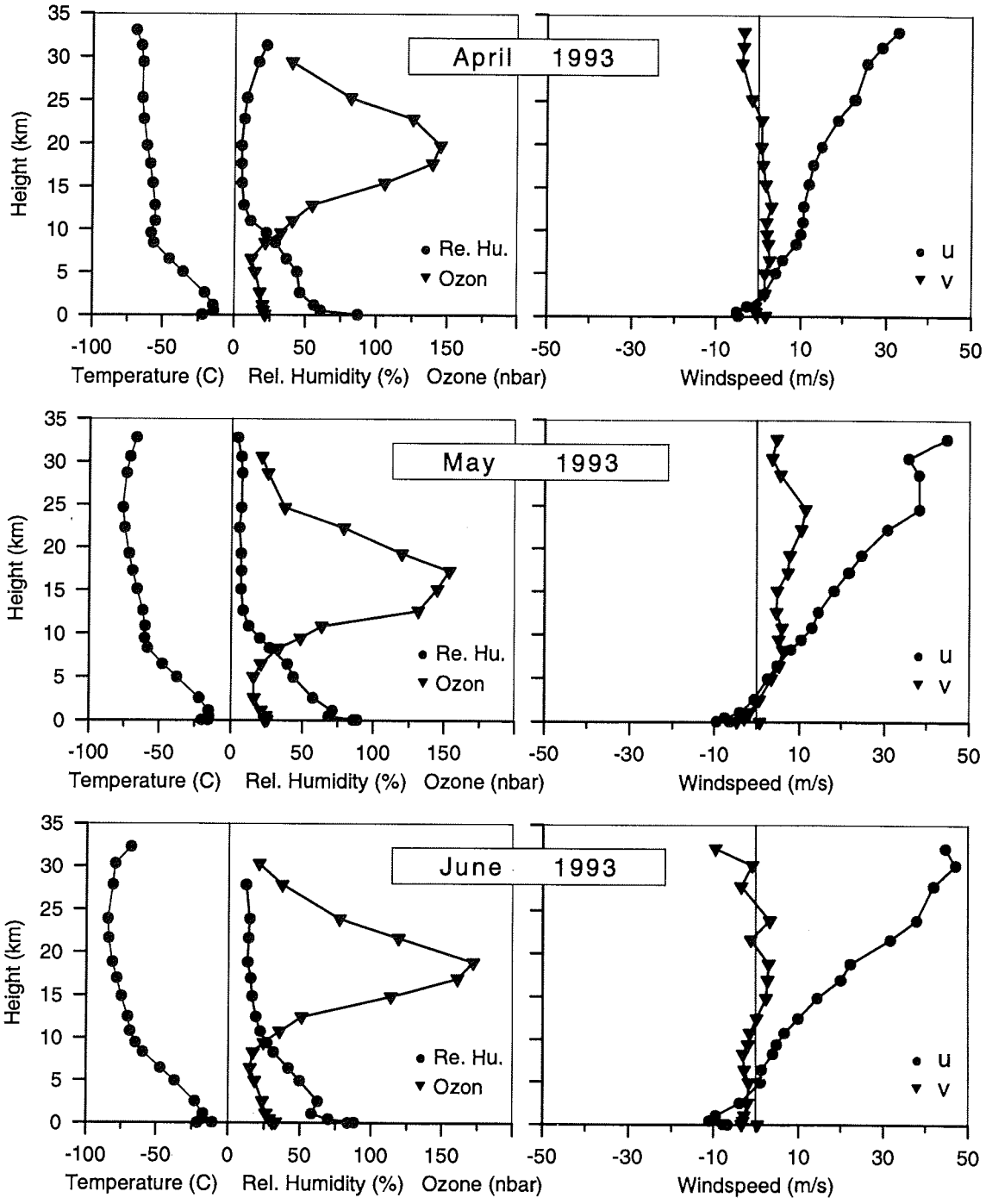

Figs. 27d-27f Mean monthly profiles of temperature, relative humidity, zonal (u) and meridional (v) wind component.

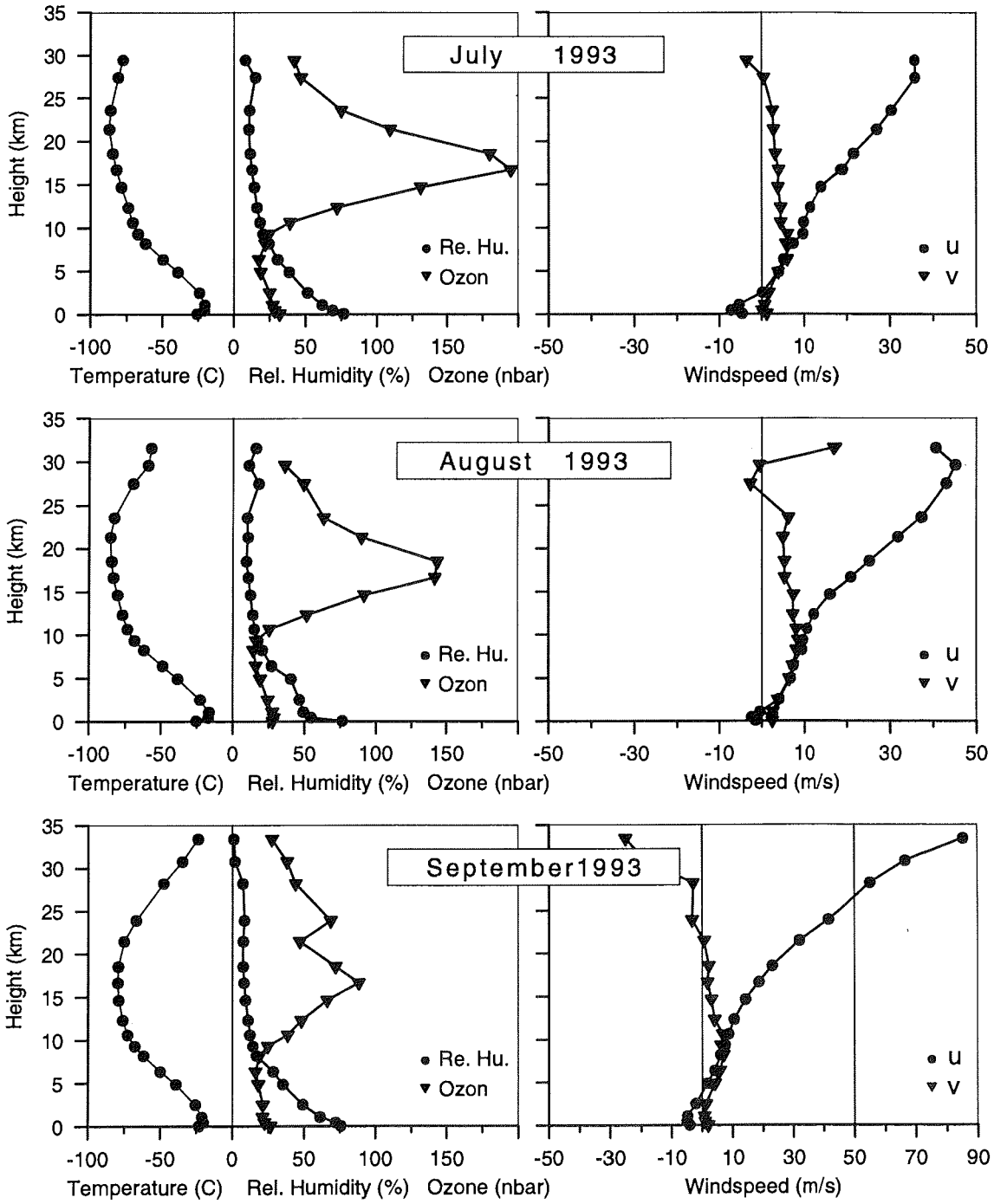

Figs. 27g-27i Mean monthly profiles of temperature, relative humidity, zonal (u) and meridional (v) wind component.

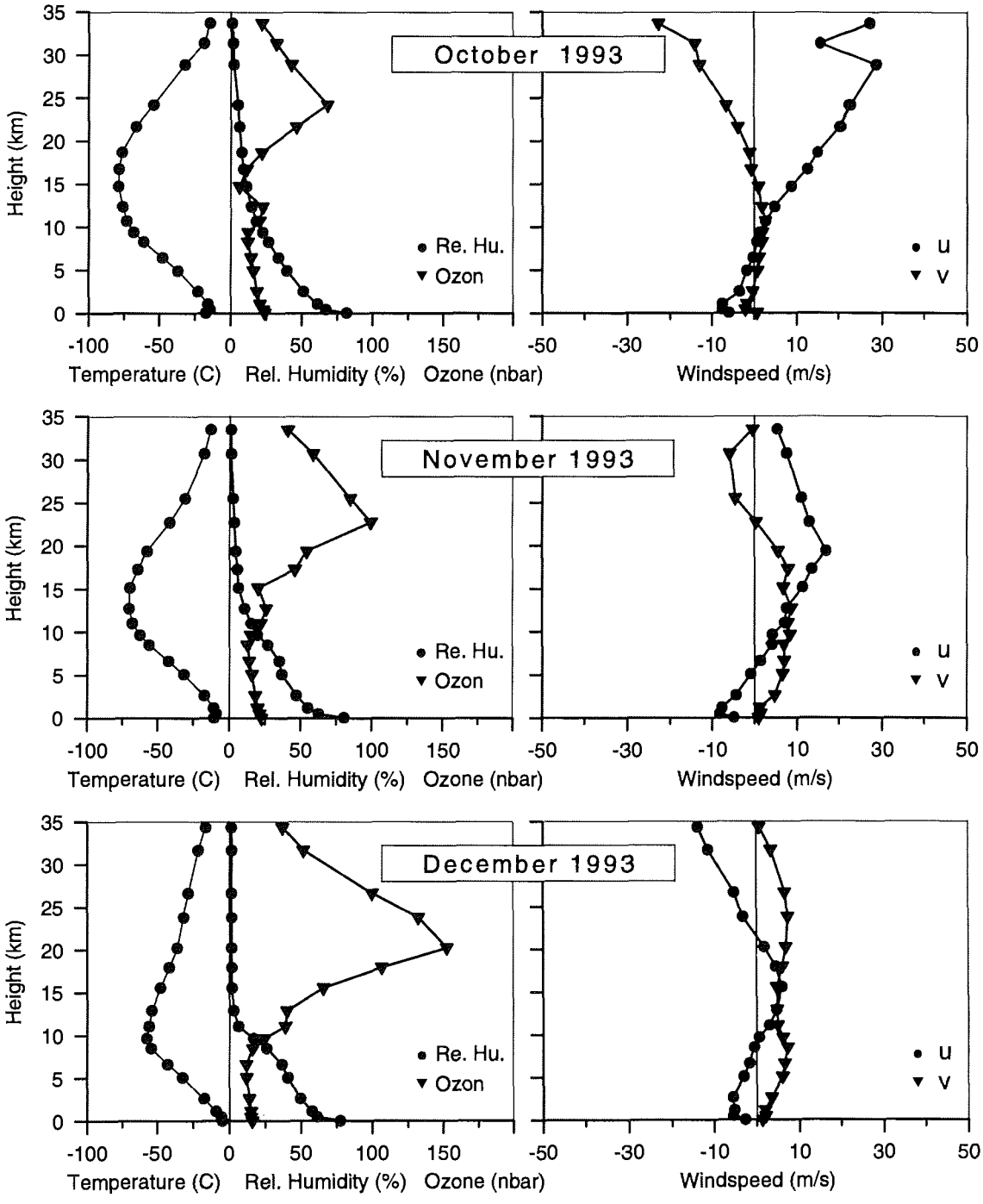

Figs. 27j-27l Mean monthly profiles of temperature, relative humidity, zonal (u) and meridional (v) wind component.

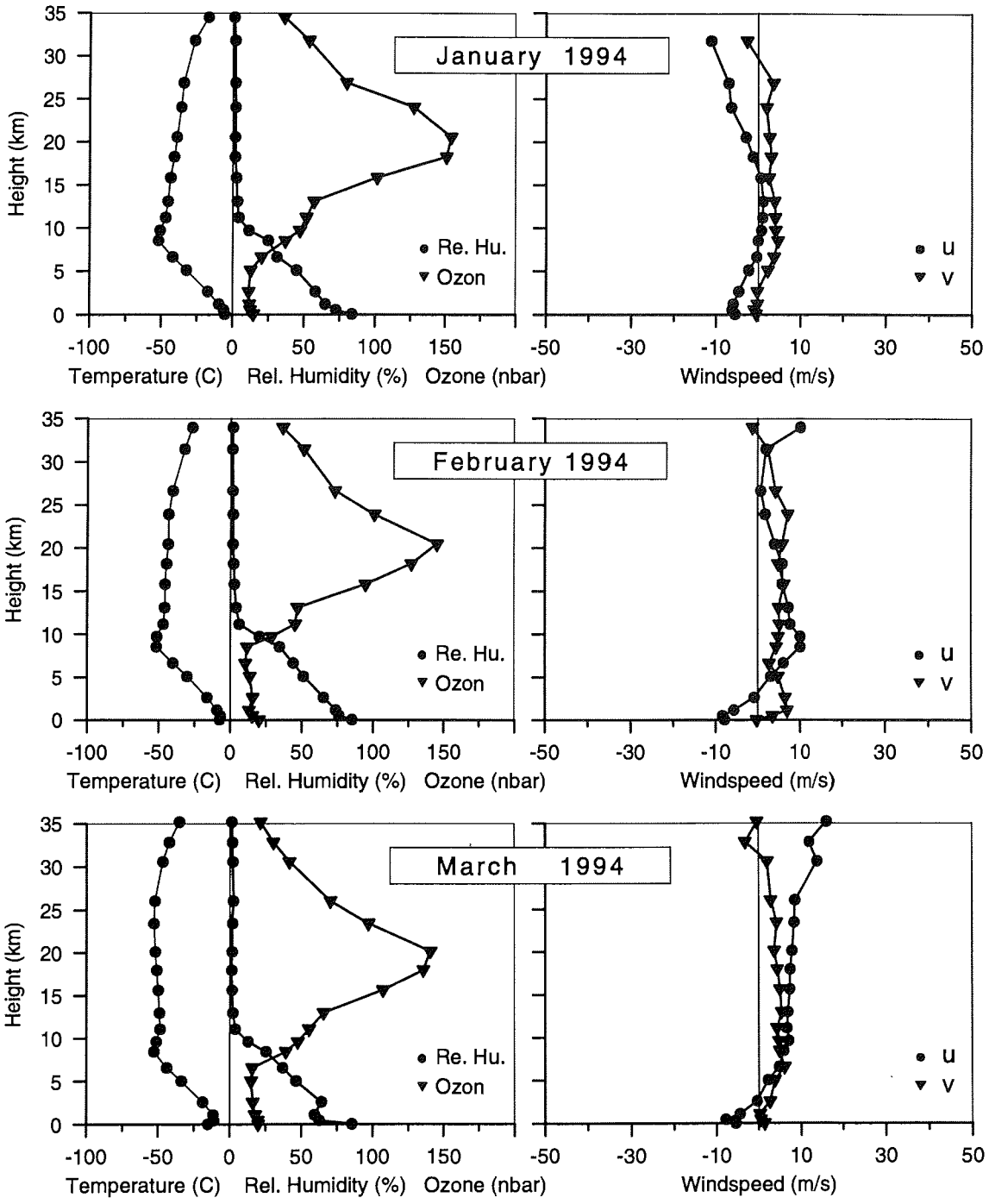

Figs. 28a-28c Mean monthly profiles of temperature, relative humidity, zonal (u) and meridional (v) wind component.

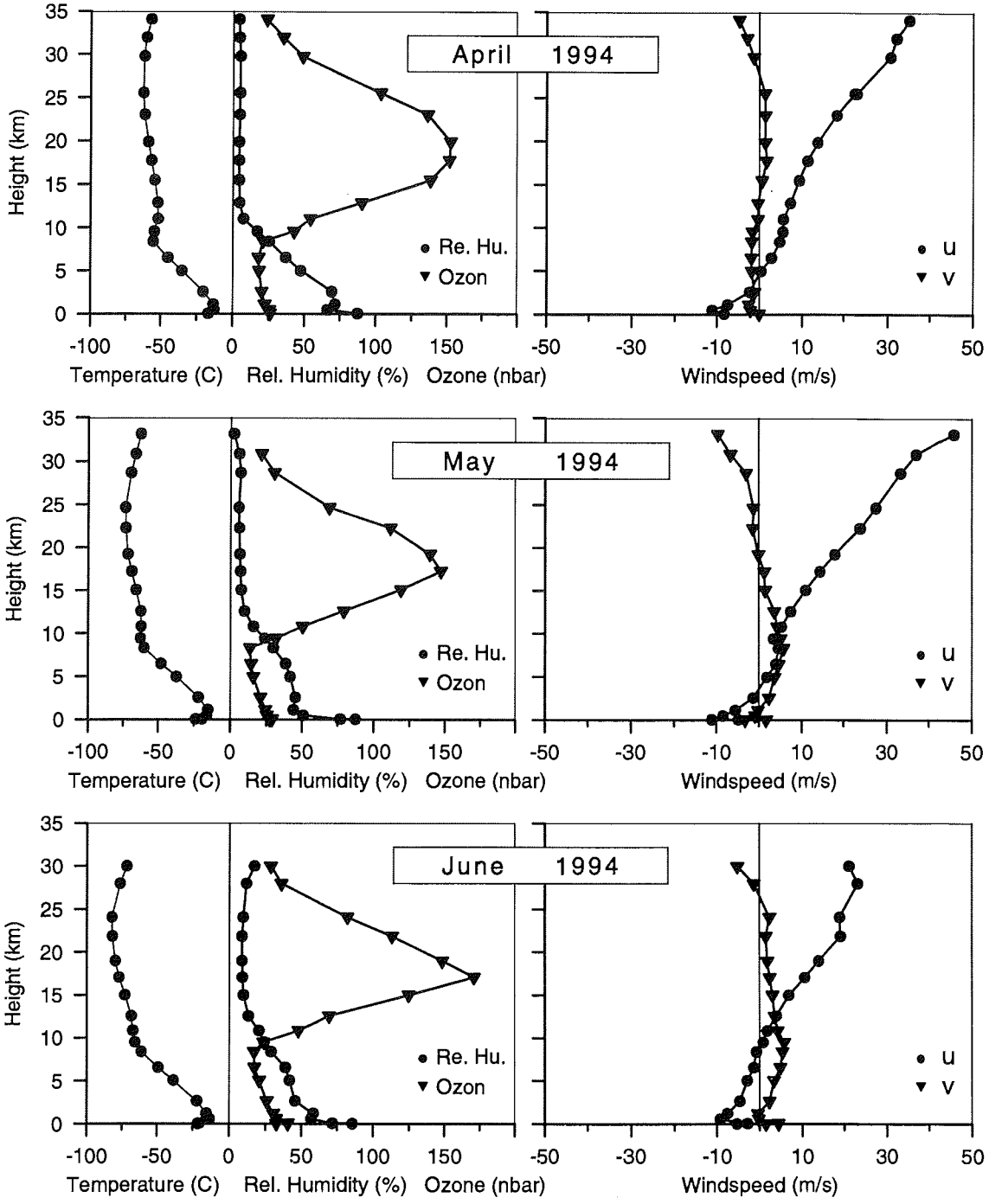

Figs. 28d-28f Mean monthly profiles of temperature, relative humidity, zonal (u) and meridional (v) wind component.

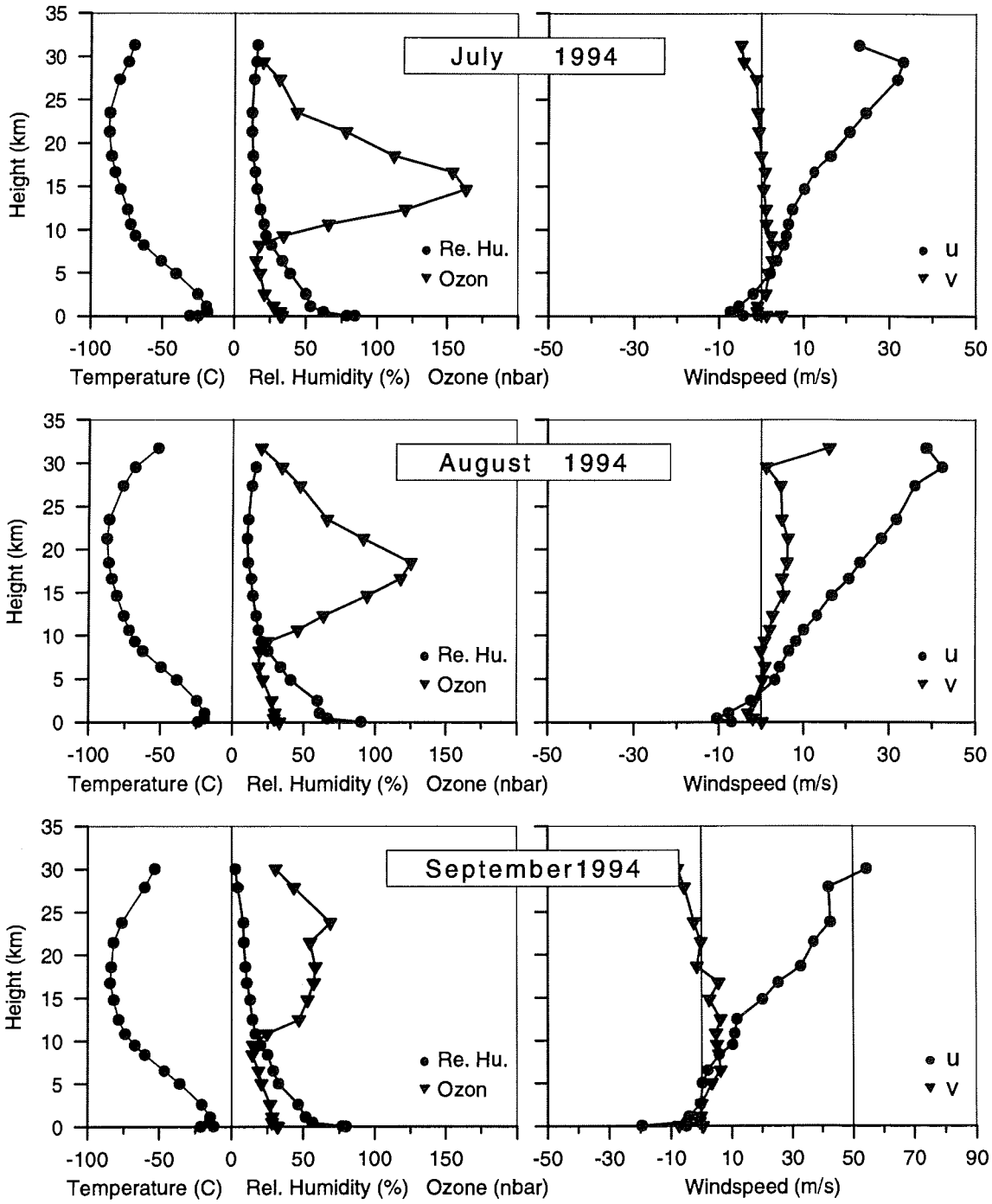

Figs. 28g-28i Mean monthly profiles of temperature, relative humidity, zonal (u) and meridional (v) wind component.

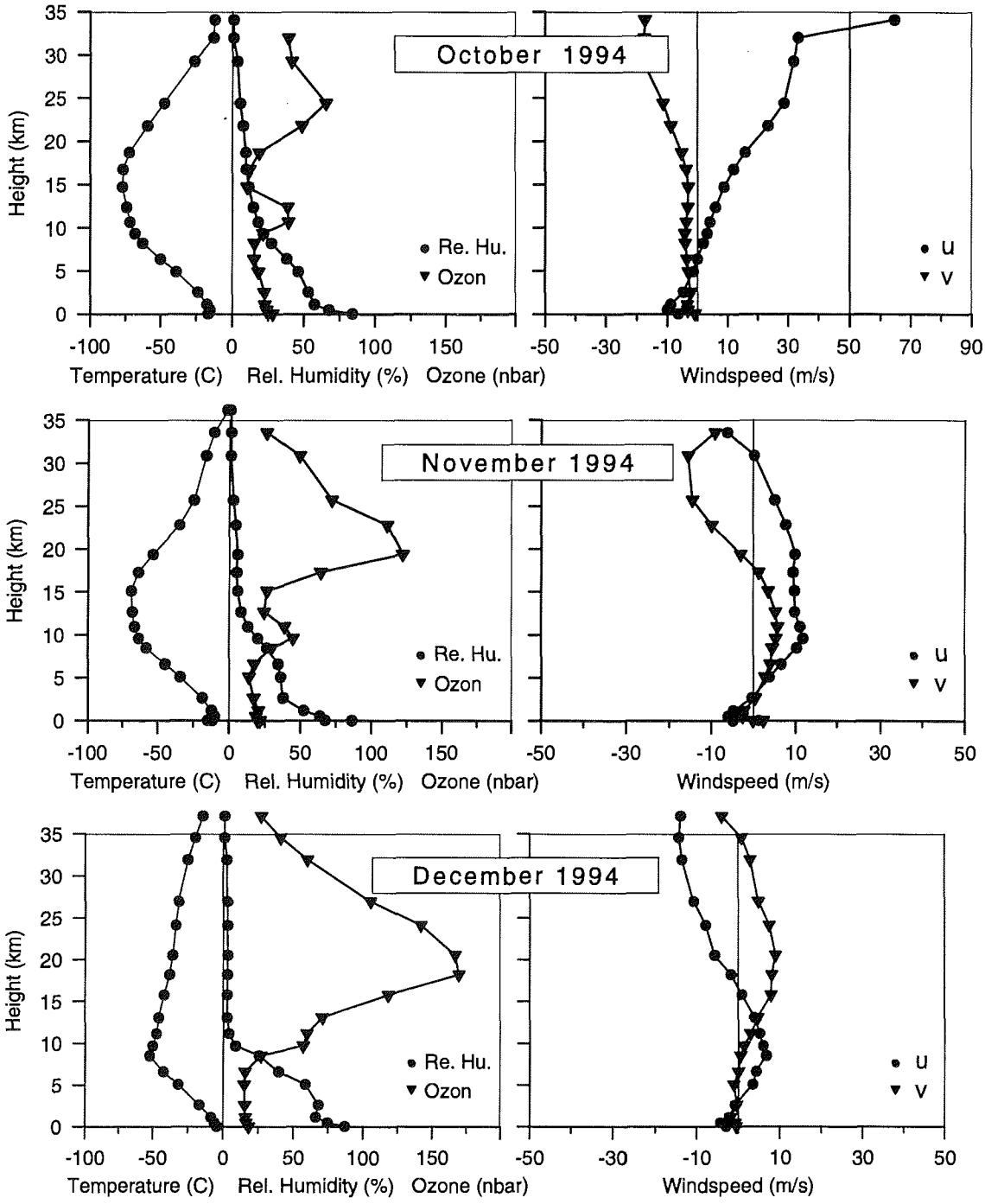

Figs. 28j-28l Mean monthly profiles of temperature, relative humidity, zonal (u) and meridional (v) wind component.

4.3) Radiation Measurements

The radiation measurements at Neumayer take place in the framework of the global "**B**aseline **S**urface **R**adiation **N**etwork" **BSRN**, (WMO, 1991). The objective of the BSRN is to provide the highest possible quality, high sampling rate observations of short and long-wave surface radiation fluxes with co-located surface and upper-air meteorological data at a small number of selected stations in contrasting climatic zones. The uniform and consistent measurements throughout the network are used

- to monitor the background (least influenced by immediate human activities which are regionally concentrated) short-wave and long-wave radiative components and their changes with the best methods currently available,
- to provide data for the calibration of satellite-based estimates of the surface radiative fluxes and
- to produce high quality observational data to be used for validating the theoretical computations of radiative fluxes by models.

4.3.1) Error Discussion

The accuracy of the calibration of modern pyranometer is about 2%. Due to high albedo values at Neumayer many errors occur rather similarly in both, the global solar radiation K⇓ and in the reflected solar radiation K⇑. Thus in the net short-wave radiation K^* a great deal of these influences is compensated.

The calibration uncertainties of the pyrgeometer can be devided into two parts:

- The instrument temperature can be determined to an accuracy of better than 1°C, leading to errors of the radiation fluxes of less than 3 W/m^2.
- The long-wave sensitivity of the thermopile can be calibrated to an accuracy of 10%. Fortunately, at Neumayer Station the downward long-wave thermopile output is mostly below ±100 W/m^2. Thus the maximum error is approximately 10 W/m^2. The upward long-wave thermopile output seldom exceeds ±10 W/m^2, with an error of less than 1 W/m^2.

The sensitivity of pyrgeometers with respect to short-wave radiation is not exactly zero. Evidently about 2-3% of the short-wave radiation penetrates the dome and increases the thermopile output. For this reason it is recommended to use pyrgeometers in

combination with shadow disks to exclude effects at least of the direct short-wave radiation. Because of the frequent blizzards at Neumayer only stable shadow rings could be used. However, due to the extremly high albedo, the downward and upward diffus part of the short-wave radiation is so large, that the pyrgeometer were not shaded at all.

This leads to errors for instantaneous measurements of both long-wave components of about 20-30 W/m^2 at noon during summer. For daily averaged summer values the effect counts for about 10-15 W/m^2. For annual averages it drops to 2-3 W/m^2. Due to the high albedo the long-wave balances are nearly not concerned at any averaging intervall. While the sun is below the horizon, this error do not exist.

The short-wave influence upon the long-wave measurements can be corrected by using the simultaneoulsy measured short-wave fluxes. However, within this report, no correction of this kind has been performed.

4.3.2. Time Series based on 5 Minute Averages

As an example of a time series based on 5 minute averages Figs. 29 - 34 show values of the 19th of January 1994. In the morning the total cloud amount is between 7 and 8 octa Statocumulus and Altostratus with bases between 60 and 3000 meter. In the afternoon, the sky is totally free of clouds, see Fig. 29.

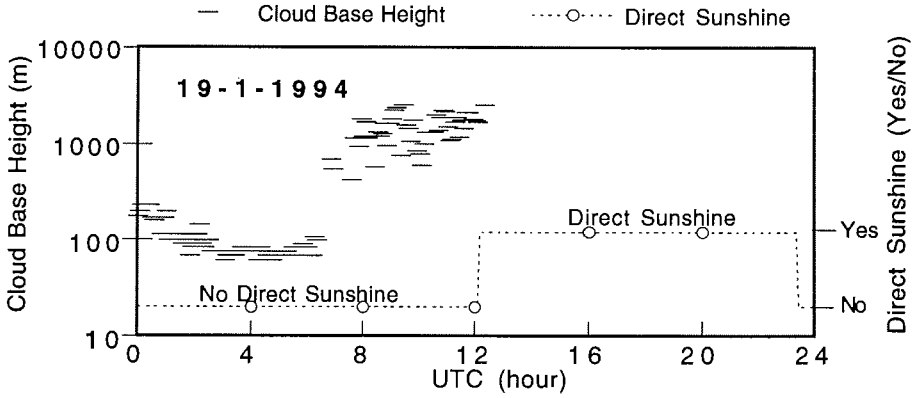

Fig. 29 Cloud base height and direct sunshine for the 19th of January 1994 based on 5 minute averages.

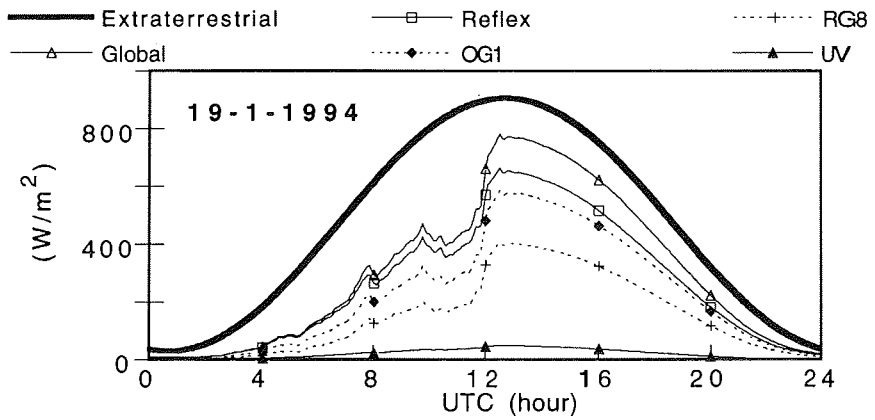

Fig. 30 Radiation values at the 19th of January 1994 based on 5 minute averages.

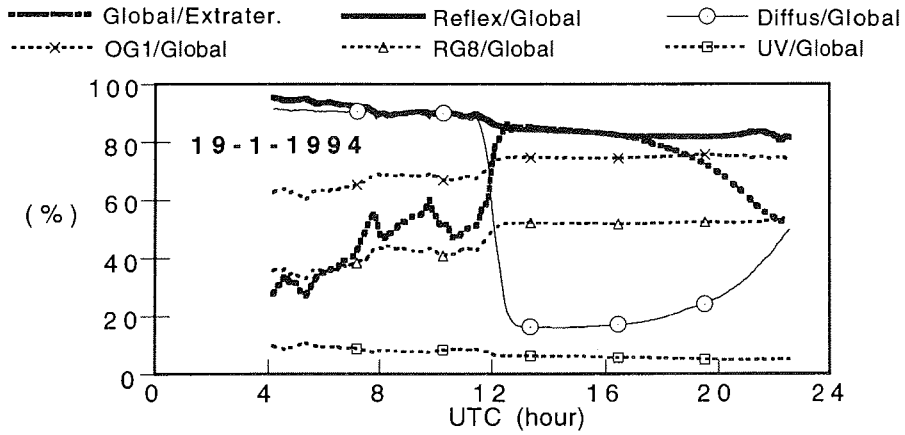

Fig. 31 Relationships between various radiation components for the 19th of January 1994 based on 5 minute averages.

During the cloudy period, about 50% of the extraterrestrial insolation reaches the ground as diffuse radiation (Fig. 30 and Fig. 31). During the cloudless period about 80% of the extraterrestrial insolation penetrates to the Earth´s surface near noon. This ratio shrinks in the afternoon towards sunset.

In the morning, the albedo (Reflex/Global in Fig. 31) is about 90%, which is typical for a surface covered by freshly fallen snow. About noon the strong sun radiation altered the snow surface and the albedo dercreases to values around 80%.

The spectral composition of the global radiation depends to a certain extent on clouds, as also shown in Fig. 31. While the percentage of the global radiation (305 - 2800nm) within the OG1 (530 -2800nm) and RG8 regime (695 - 2800nm) increase with

decreasing cloud amount, the percentage of the UV regime (300 - 370nm) shows an opposite behavior.

Under obscured conditions the upward long-wave radiation gets nearly compensated by the downward long-wave radiation (Fig. 32). In other words: The so-called atmospheric emissivity $\varepsilon_A = L\Downarrow / L\Uparrow$ is close to one, if the sky is covered completety by low clouds (König-Langlo and Augstein, 1994).

The emissivity of the snow $\varepsilon = L\Uparrow / (\sigma T_0^4)$ with σ = Stefan-Boltzmann constant and T_0 = snow surface temperature can also be taken as close to one. Thus, before noon, both long-wave fluxes with values about 300 W/m^2 correspond to temperatures of the snow surface and the subcloud atmosphere shortly below freezing, which is typical for cloudy mid-summer days at Neumayer (Fig. 34).

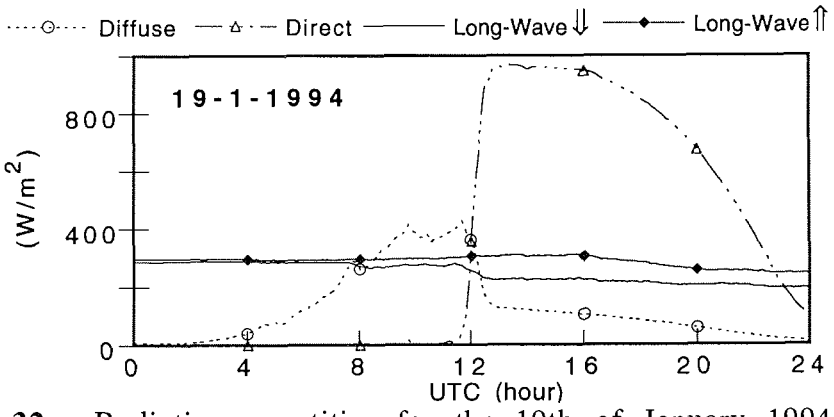

Fig. 32 Radiation quantities for the 19th of January 1994 based on 5 minute averages.

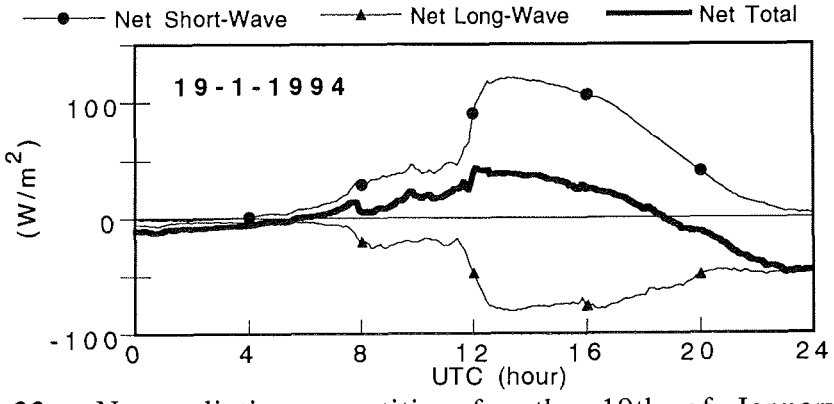

Fig. 33 Net radiation quantities for the 19th of January 1994 based on 5 minute averages.

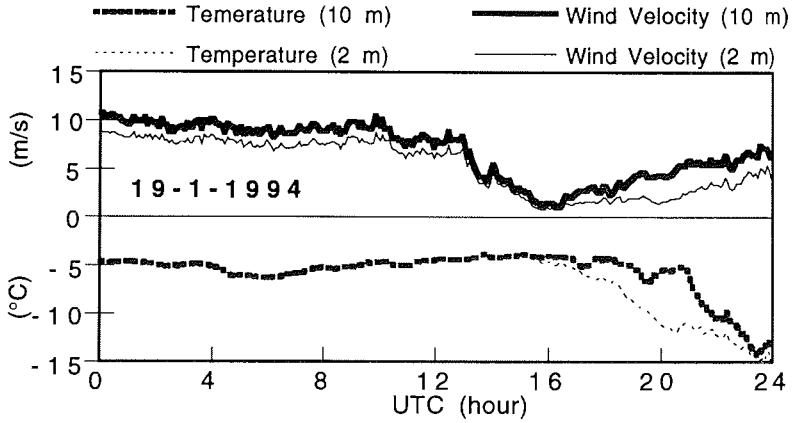

Fig. 34 Temperature and wind velocity at 2 and 10m height for the 19th of January 1994 based on 5 minute averages.

In the afternoon, directy after the clouds have vanished completely, the downward long-wave radiation drops from values around 300 W/m^2 to 220 W/m^2 (Fig. 32). The upward long-wave radiation decreases less drastically with a time lag of several hours. Thus the net long-wave energy losses at the surface are largest directly after the clouds have disappeared (-80 W/m^2), see Fig. 33. After 20 UTC, when the net short-wave energy gains decreases, the net total radiation becomes negative and the atmospheric boundary layer begins to cool in the lowest layer first (Fig. 34). This cooling also decreases the snow surface temperature and subsequently the upward long-wave radiation and the net long-wave energy losses.

The net short-wave radiation and the net long-wave radiation show both a strong dependence of clouds but in opposite directions (Fig. 33). Thus the dependence of the net total radiation on clouds is rather low. Only while the sun elevation is relatively high, the net total radiation increases with decreasing cloud coverages. In all other cases the cloud forcing on the net total radiation is zero or positive.

4.3.3. Time Series based on Daily Averages

Fig. 35 shows the variation of the global radiation and the extraterrestrial insolation for the years 1992, 1993 and 1994 based on daily averages. Depending on cloudiness between 50 and 80% of the potential short-wave input penetrates the atmosphere.

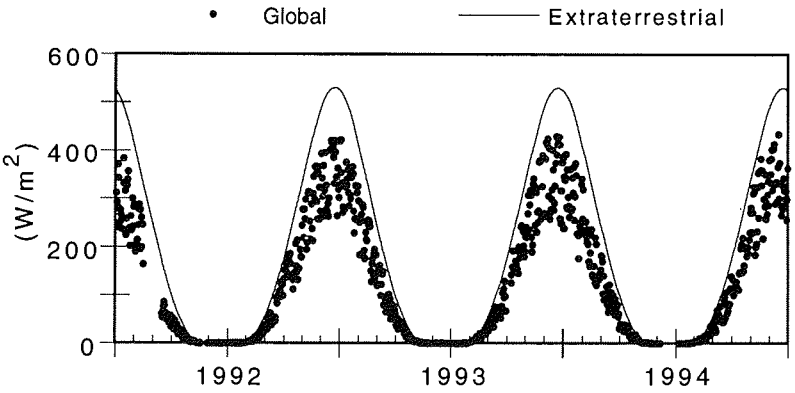

Fig. 35 Global radiation and the extraterrestrial insolation for the years 1992, 1993 and 1994 based on daily averages.

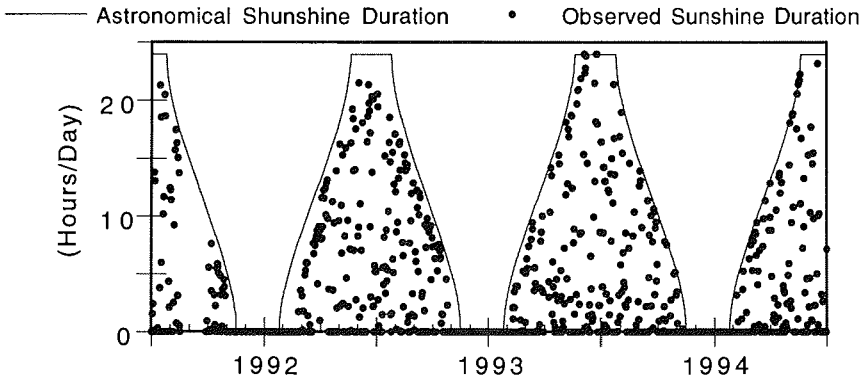

Fig. 36 Observed and astronomical sunshine duration for the years 1992, 1993 and 1994 based on daily averages.

Occasionally the observed sunshine duration, see Fig. 36 reaches nearly the astronomical value but days without direct sunshine also exists at all seasons.

During a few summer days the snow surface at Neumayer gains up to about 80 W/m^2 by the net short-wave radiation, see Fig. 37. Even these rather small short-wave energy gains at the snow surface do not start remarkable heating or melting processes, since they are mostly compensated by the net long-wave radiation losses (Fig. 37). This compensation mechanism is responsible for the rather smooth net total radiation balance during summer. Details of this compensation mechanism are demonstated in Fig. 39.

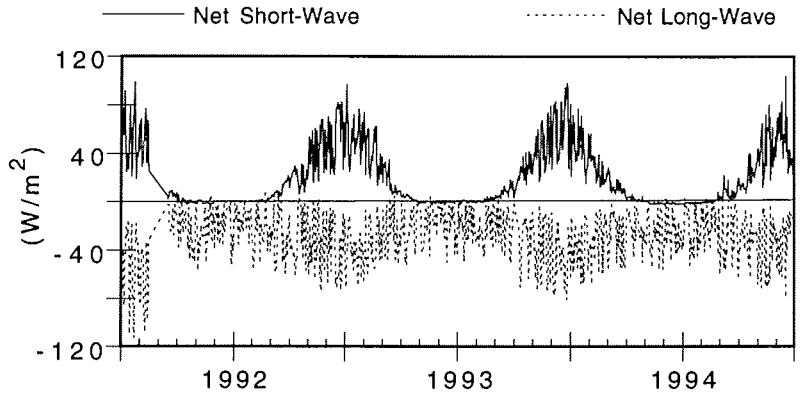

Fig. 37 Net short-wave and net long-wave radiation for the years 1992, 1993 and 1994 based on daily averages.

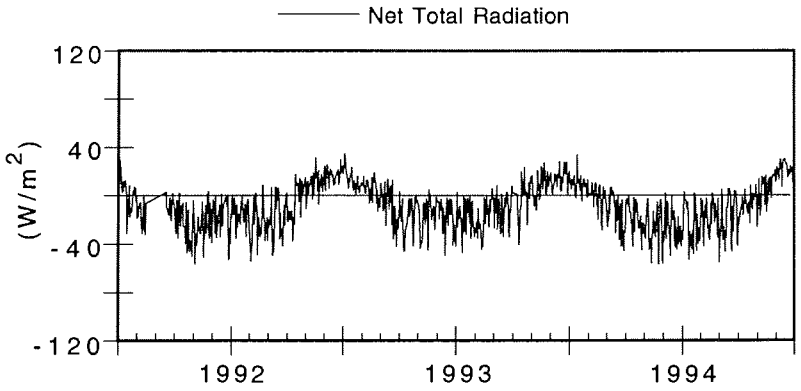

Fig. 38 Net total radiation for the years 1992, 1993 and 1994 based on daily averages.

Positive daily averaged net total radiation balances with maximum values above 10 W/m^2 occur only between November and February, see Fig. 38. During the rest of the year negative net total radiation balances dominate. They seldom fall below -50 W/m^2.

Occasionally slight positive net total radiation balances can be observed even during the polar night. Typically, these situations reflect conditions with surface inversions in conjunction with low-level stratus clouds.

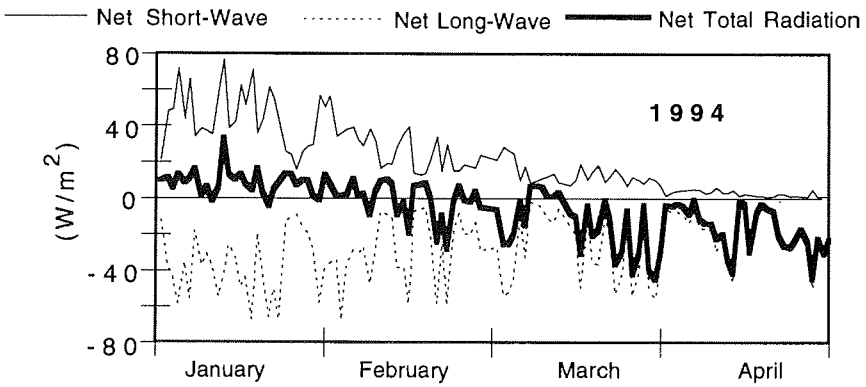

Fig. 39 Net short-wave, net long-wave and the net total radiation for January - April 1994 based on daily averages.

4.3.4. Relations Between Radiation Components

Fig. 40 shows the surface albedo values as calculated from daily averages of the reflected and global solar radiation for all cases when the global radiation exceeds 50 W/m^2. The extrem values of the albedo (below 75% and above 95%) may be caused by sastrugies (snow ondulations) below the measuring site.

For the Neumayer Station the average albedo is determined as 84% which is in close agreement with Schwerdtfeger's (1984) value (85%) for Antarctic ice shelf stations. Values above 90% are common after snow fall while an albedo around 75% is typical for the seldom cases with minor melting processes.

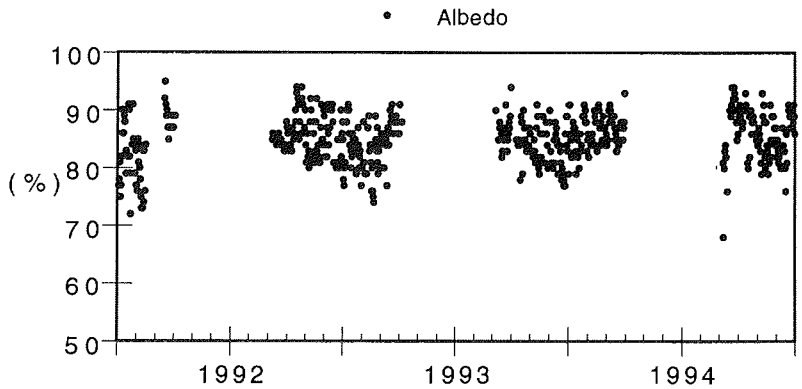

Fig. 40 Variation of the albedo for the years 1992, 1993 and 1994 based on daily averages. No values are displayed during polar night.

The diffuse part of the global radiation varies between 15% and 100% with a mean value of 65% and a median value shlighty above 70%, see Fig. 41.

Within the spectral range of the OG1 broadband filter (530 -2800nm) about 70% of the global radiation reaches the ground. The fraction of the global radiation within the RG8 regime (695 - 2800nm) amounts to 50%, while 5 - 10% of the global radiation falls into the UV range (300 - 370nm).

Variations of the spectral composition of the global radiation are due to clouds, the sun elevation, atmospheric tracer gases and aerosols.

The UV-measurements (TUVR, Eppley, 300 - 370nm) cover primarily the UV-A range (320 - 400nm) and include only parts of the ozone dependent UV-B radiation (280 - 320nm). Thus, the UV-measurements performed at Neumayer show only a rather small dependence on the total atmospheric ozone column density. Improved UV-measurements, covering the whole UV-B range with a high spectral resolution, will be performed at Neumayer in future.

During austral autumn, when 300 dobsen units are typical, 4.0% of the extraterrestrial insolation where measured by the TUVR, while this percentage increase slightly to 4.7% during austral spring, when the total ozone above Neumayer drobs below 200 dobsen.

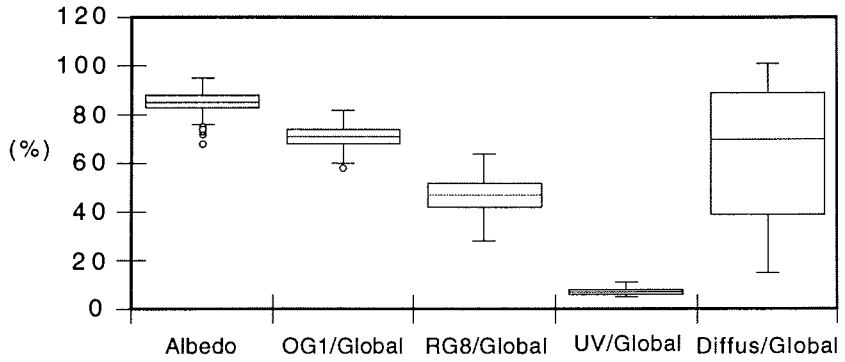

Fig. 41 Percentage of relations between different radiation components for the years 1992, 1993 and 1994 based on daily averages. Each box marks the limit of ± 25% of each variable. The horizontal lines within the boxes show the median values, the error bars represent the minima and maxima. Outliers are indicated by circles.

The upward long-wave radiation can be satisfactorily estimated on the basis of the Stefan-Boltzmann law by using the air temperature at 2 meters height and assuming a black body for the snow surface.

The downward long-wave radiation may be parameterized similarly with the aid of effective atmospheric emissitities ε_A ranging from 0.7 to 1.0, see Fig. 42.

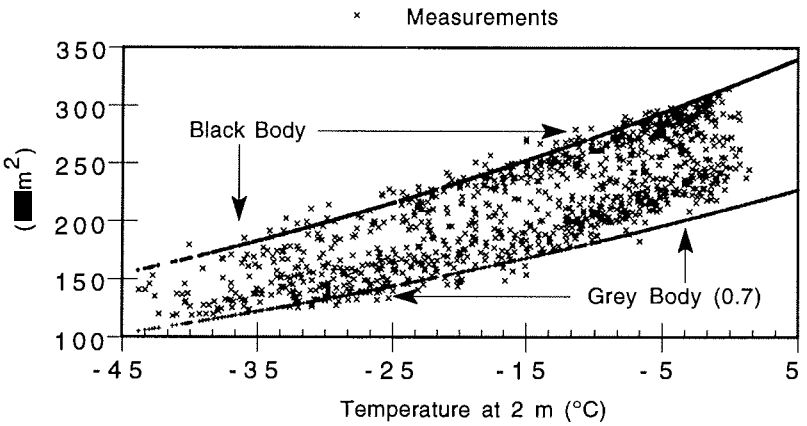

Fig. 42 Downward long-wave radiation versus air temperature at 2 meters height for the years 1992, 1993 and 1994 based on 5 minute averages for all cases with visual synoptic cloud observations.

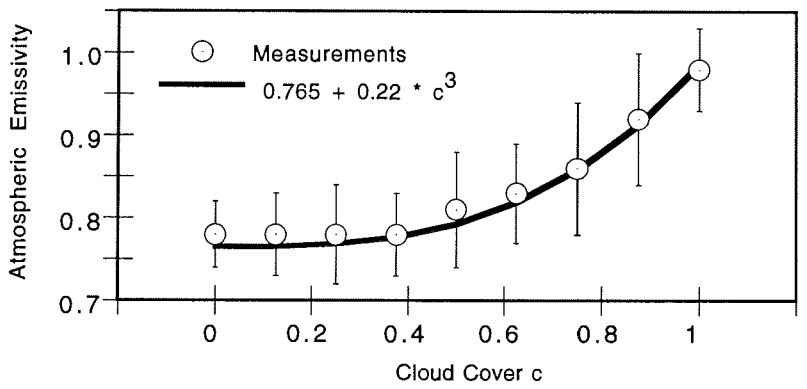

Fig. 43 Mean atmospheric emissivities versus total cloud cover $0 \leq c \leq 1$ for the years 1992, 1993 and 1994 based on 5 minute averages for all cases with visual synoptic cloud observations. The error bars represent the standard deviation, the bold line represents the cubic fit indicated in the Figure.

The atmospheric emissitity ε_A varies primarily with cloud cover as portrayed im Fig. 43. Due to the low temperatures at Neumayer , the water vapour pressure at the ground is unsignificant and need not to be taken into account explicitly (König-Langlo and Augstein, 1994).

Values exeeding the black body curve in Fig. 42 reflect conditions with a strong surface inversion in conjunction with low-level stratus clouds. Then the air temperature at 2 meters height is too low to represent the long-wave emission of the lower atmosphere. Such situations are generally short lived since they produce a positive surface radiation balance which leads to a rapid decrease of the surface inversion.

4.3.5. Aerosol Optical Depth

The Antarctic region is hardly contaminated by anthropogenic aerosols. Aerosols have only a small impact on the optical depth of the Antarctic atmosphere. Measurements taken since 1950 at Antarctic coastal stations suggest that during periods without volcanic activity, the aerosol optical depth of the Antarctic atmosphere is approximately constant ($\delta_a < 0.03$) and that there is no trend in the Antarctic aerosol concentration.

Since 1992 measurements of the spectral optical depth have been performed routinely, covering the period of the Cerro Hudson and Pinatubo aerosol loading of the stratosphere.

Data of the daily mean optical depth for two different wavelengths (500 and 1000nm) are presented in Fig. 44. The optical depths at these two wavelengths are calculated by linear interpolation of the photometer data between the central wavelengths. The derived values are controlled by the Ångström fit. The 500nm wavelength is recommended by WMO, while the 1000nm value represents the Ångström parameter Beta.

Significant effects of the volcanic aerosols on the southern polar stratosphere is obvious in both wavelengths by negative trends from January 1992 to December of 1994. The aerosol optical depth in August/September 1992 is higher than the measured optical depth in February 1992 (especially for 1000nm). Between April and July 1992 additional meridional transport of Pinatubo aerosol from equatorial to middle and higher latitudes of the southern hemisphere occurs (Trepte et al., 1994). This leads to an increase in the measured aerosol optical depth after the return of sunlight in August 1992.

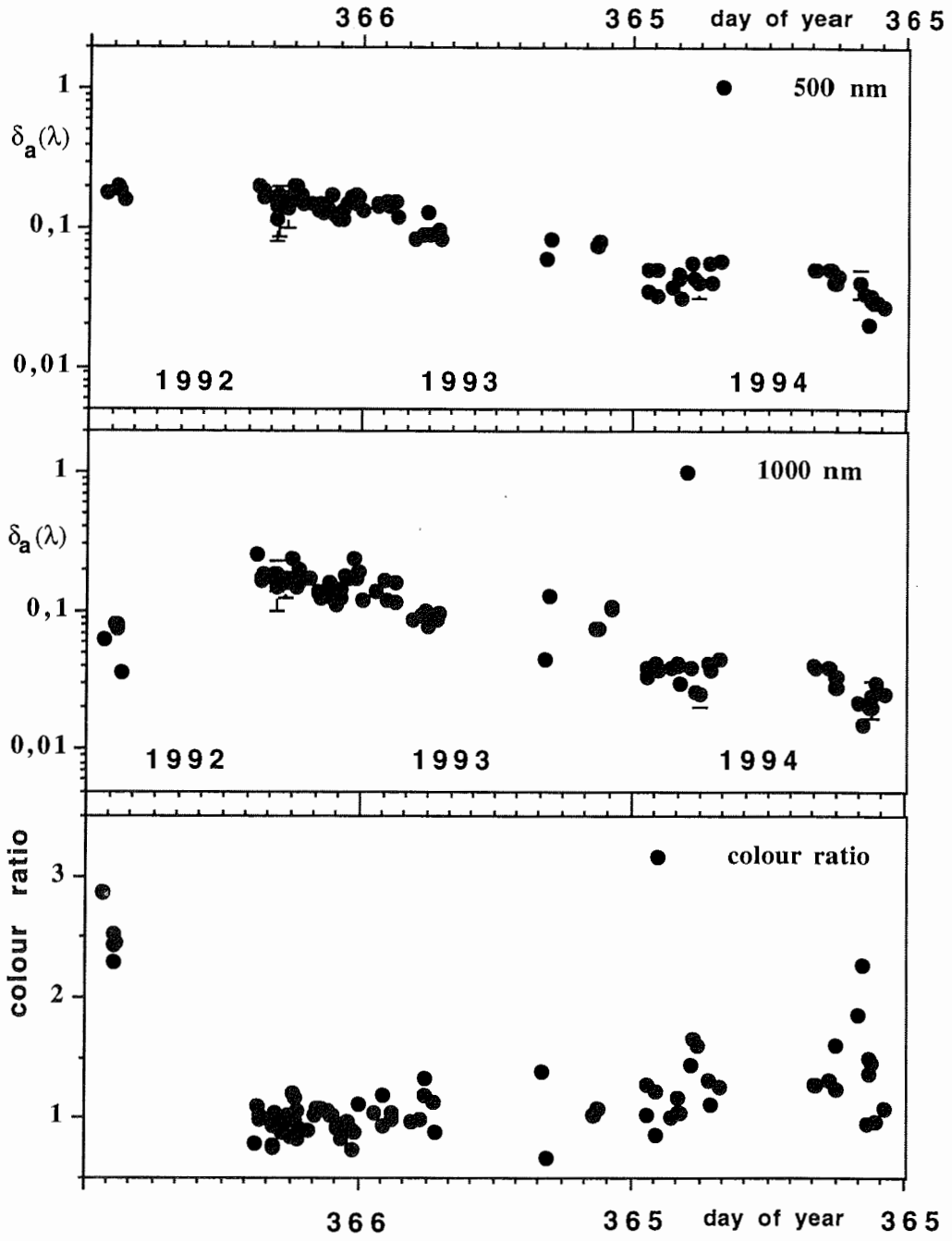

Figs. 44a - 44c Daily mean sunphotometer data:
a - optical depth of aerosol at 500nm,
b - optical depth of aerosol at 1000nm,
c - ratio of 500nm to 1000nm extinction.

In Fig. 44c the so-called colour ratio, i.e. the ratio of the optical depth of 500nm to 1000nm is displayed. High value of the colour ratio (higher than 3) represent a high contribute of small particles ($r < 0.2\mu m$). The colour ratio of approximately 1 means, that bigger particles are dominant ($r > 1.0\mu m$).

In January and February 1992 small particles are dominant. Later, aging processes cause an aggregation of the small to bigger particles (Herber et al., 1993; Russell et al., 1994). In August/September 1992 a colour ration from about 1, typically for aged volcanic aerosol, can be seen. The variable colour ratio in the end of 1994 indicates the decreasing influence of volcanic aerosols in the stratosphere. Tropospheric aerosol begins to dominate the Antarctic aerosol content.

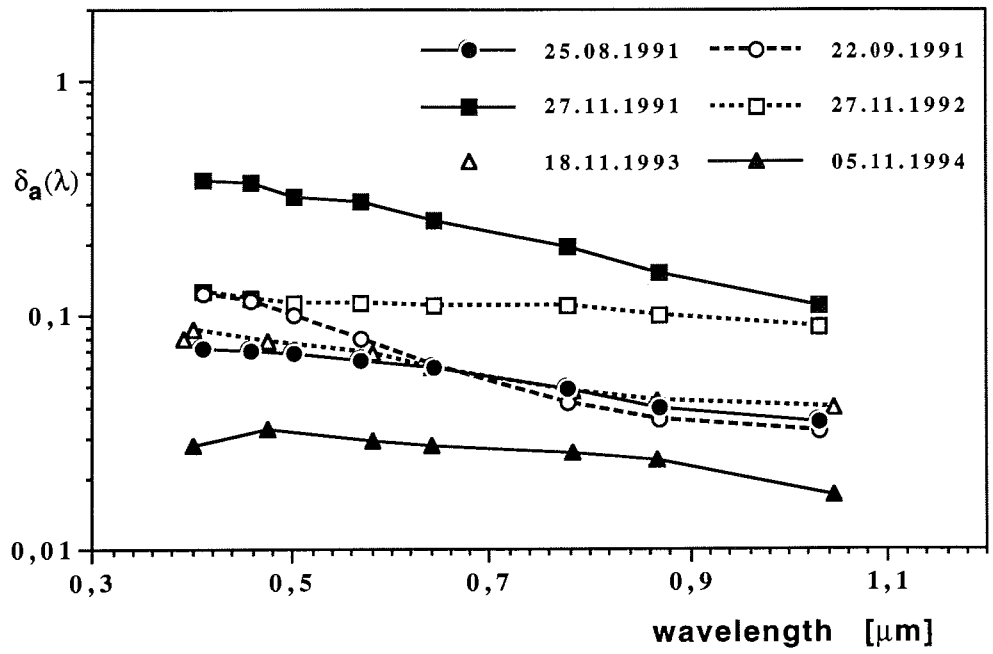

Fig. 45 Spectra of optical depth of aerosol, measured at Georg Forster (70°48' S, 11°51' E): 25.08.1991, 22.09.1991, 27.11.1991; and at Neumayer: 27.11.1992, 18.11.1993, 05.11.1994.

In Fig. 45 some examples of aerosol optical depths for different spectral ranges are shown. The spectra from 27. November 1991 is taken during the maximum of the volcanic pertubation. The measurement from 25. August show the volcanic undisturbed conditions, the measurements from 22. September show the pertubation by Cerro Hudson aerosol. This spectra is typical for reletively fresh volcanic aerosol (Russell et al., 1993). Further spectra from November 1992, 1993 and 1994 represent the step by step decrease of the volcanic pertubation of the southern high latitudes. The sun photometer measurements will be continued.

4.3.6. Time Series based on Monthly Averages

On the basis of the daily averages monthly averages of the radiation values are derived. Data gaps present a particular problem for distinct seasonally varying quantities like the short-wave radiation components. A special treatment for missing daily averages has not been performed.

Between May and July the monthly averaged short-wave fluxes are very low or zero. Thus, no values for the relative global radiation, albedo and relative sunshine duration are displayed in Fig. 46d, 47d, 48d and Tab. 3 - 5.

Negative values of the net radiation components indicate an energy loss and positive values mark an energy gain at the Earth's surface. For intercomparison both, the upward and downward short-wave and long-wave components are presented in the Figures by positive values, disregarding their direction.

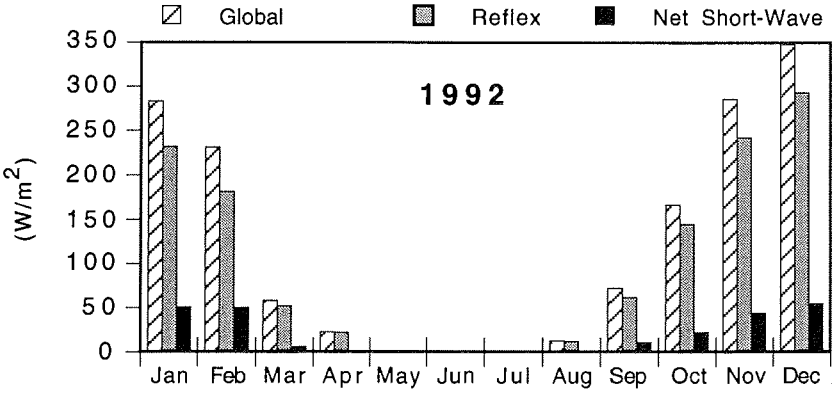

Fig. 46a Monthly averaged global radiation, reflected solar radiation and short-wave radiation balance for 1992.

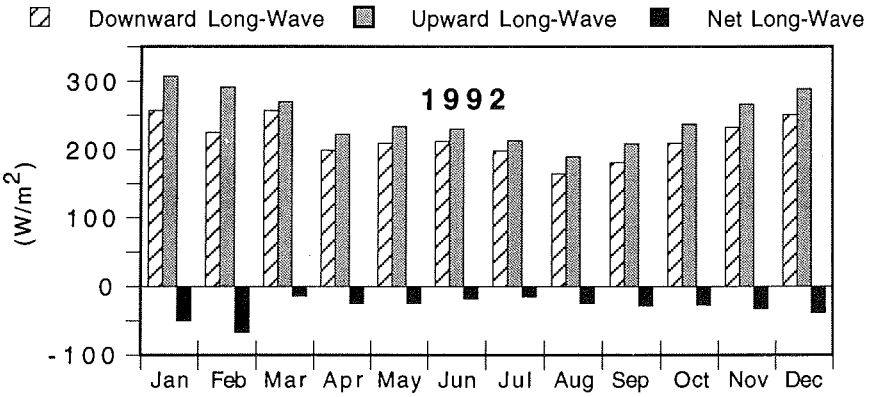

Fig. 46b Monthly averaged downward long-wave radiation, upward long-wave radiation and net long-wave radiation for 1992.

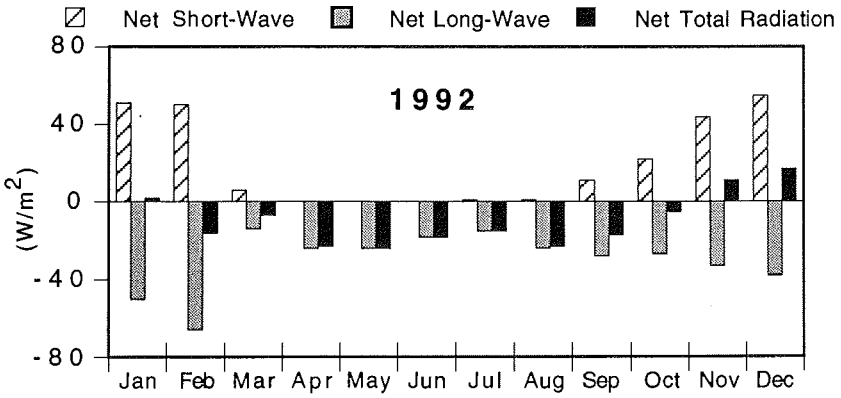

Fig. 46c Monthly averaged net short-wave radiation, net long-wave radiation and net total radiation for 1992.

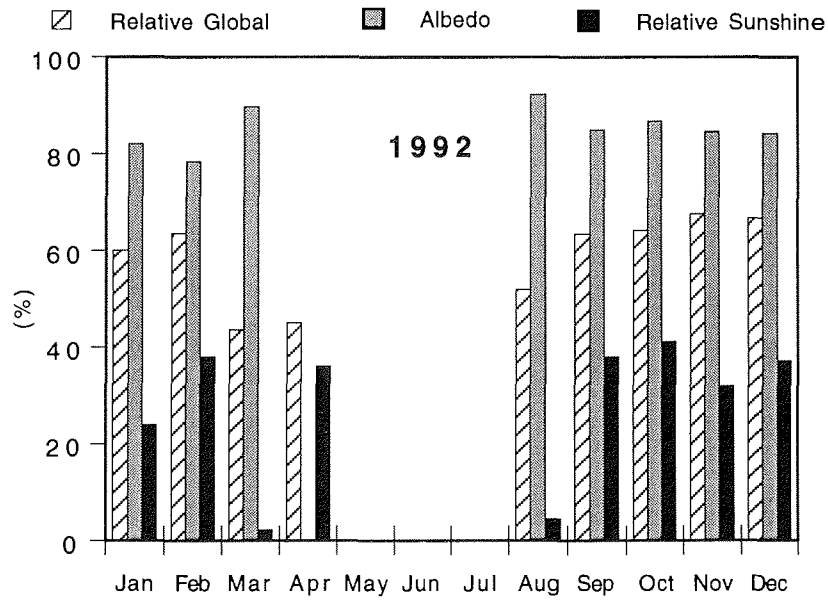

Fig. 46d Monthly averaged relative global radiation (global radiation versus extraterrestrial insolation), albedo and relative sunshine duration (observed sunshine duration versus astronimical sunshine duration) in percent for 1992.

1992	Jan	Feb	Mar	Apr	May	Jun	Jul	Aug	Sep	Oct	Nov	Dec
K⇓	283	231	58	23	0	0	0	13	73	167	286	348
K⇓/G_0	60	64	43	44	-	-	-	52	63	64	68	67
K⇑	232	181	52	22	0	0	0	12	62	145	242	293
K⇑/K⇓	82	78	90	-	-	-	-	89	85	87	85	84
L⇓	257	225	257	199	210	212	198	165	181	210	233	251
L⇑	307	291	270	222	234	230	213	190	209	237	266	289
s	5.6	7.1	0.3	2.8	0.0	0.0	0.0	0.3	4.2	6.5	7.0	8.9
s/S_0	24	38	2	36	-	-	-	4	38	41	32	37
K*	51	50	6	1	0	0	0	1	11	22	44	55
L*	-50	-66	-14	-24	-24	-18	-15	-24	-28	-27	-33	-38
Q*	2	-16	-7	-23	-24	-18	-15	-23	-17	-5	11	17

Tab. 3 Monthly averaged radiation quantities for the year 1992 in W/m^2, % or hours/day. K⇓ = global radiation, G_0 = extraterrestrial insolation, K⇑ = reflected solar radiation, L⇓ = downward long-wave radiation, L⇑ = upward long-wave radiation, s = observed shunshine duration, S_0 = astronomical sunshine duration, K*, L* and Q* net short-wave, net long-wave and net total radiation balance, respectively.

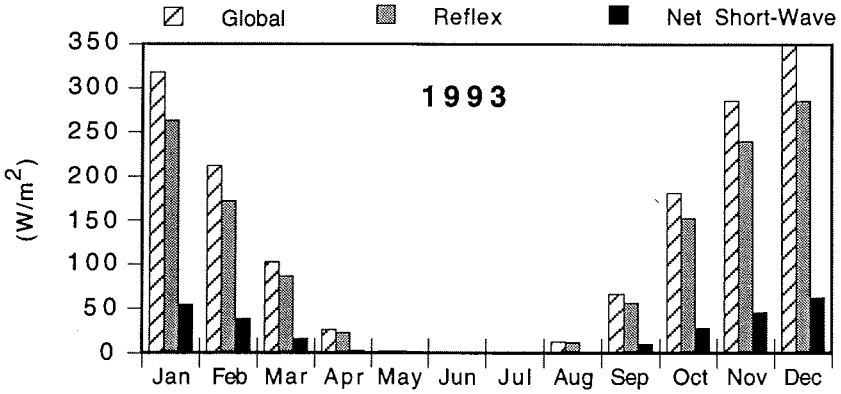

Fig. 47a Monthly averaged global radiation, reflected solar radiation and short-wave radiation balance for 1993.

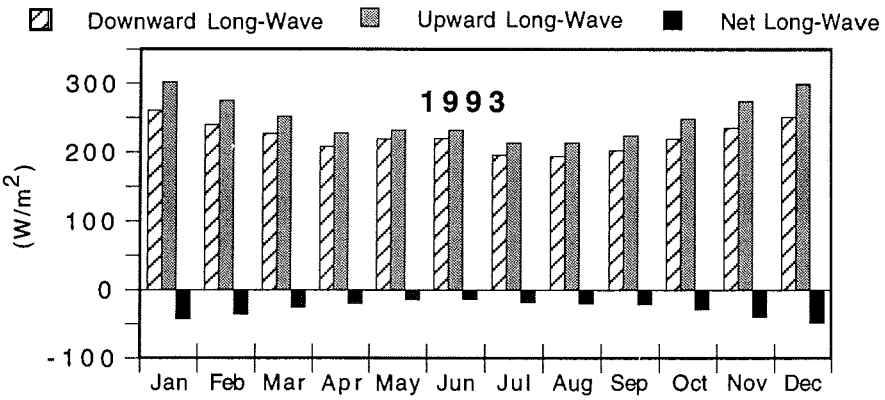

Fig. 47b Monthly averaged downward long-wave radiation, upward long-wave radiation and net long-wave radiation for 1993.

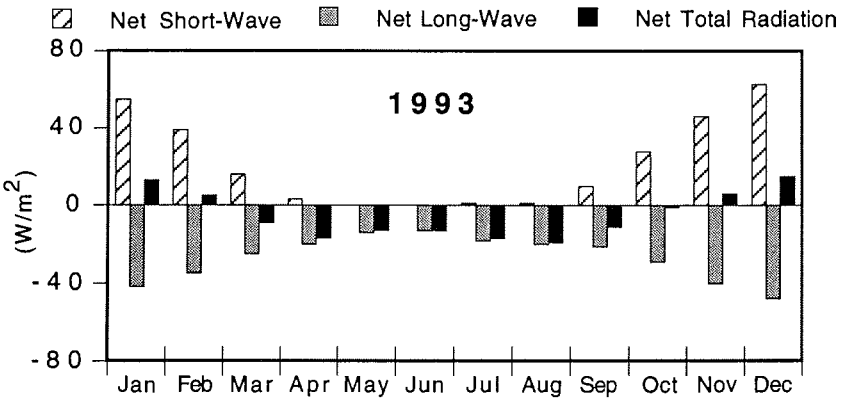

Fig. 47c Monthly averaged net short-wave radiation, net long-wave radiation and net total radiation for 1993.

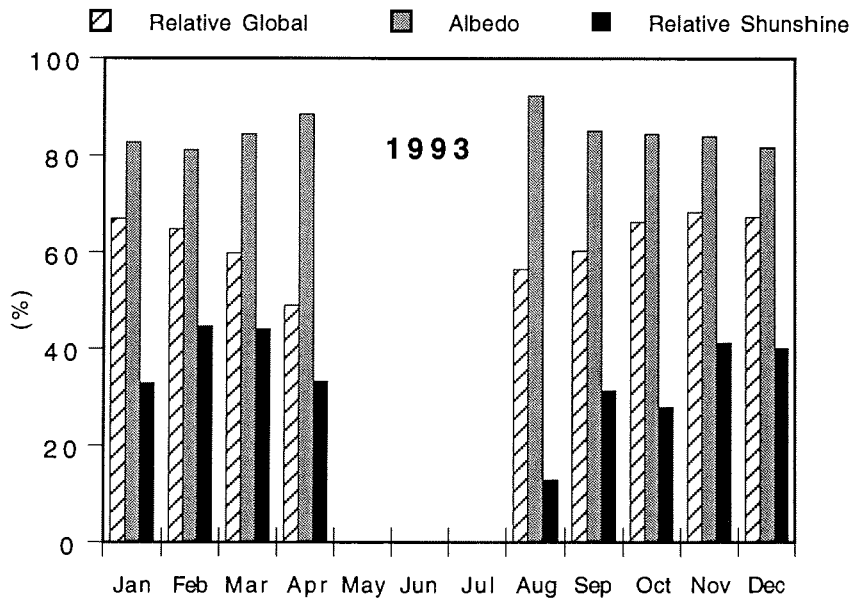

Fig. 47d Monthly averaged relative global radiation (global radiation versus extraterrestrial insolation), albedo and relative sunshine duration (observed sunshine duration versus astronimical sunshine duration) in percent for 1993.

1993	Jan	Feb	Mar	Apr	May	Jun	Jul	Aug	Sep	Oct	Nov	Dec
K⇓	318	212	103	26	2	0	0	13	67	181	286	350
K⇓/G_0	67	65	60	49	-	-	-	58	60	66	69	67
K⇑	263	172	87	23	2	0	0	12	57	153	240	286
K⇑/K⇓	83	81	85	87	-	-	-	89	86	85	84	82
L⇓	260	240	227	208	219	220	196	194	203	219	235	251
L⇑	302	275	252	228	232	232	214	214	224	248	274	299
s	7.7	7.8	5.6	2.6	0.0	0.0	0.0	0.8	3.4	4.5	9.0	9.6
s/S_0	33	45	44	33	-	-	-	13	31	28	41	40
K*	55	39	16	3	0	0	0	1	10	28	46	63
L*	-42	-35	-25	-20	-14	-13	-18	-20	-21	-29	-40	-48
Q*	13	5	-9	-17	-13	-13	-18	-19	-11	-1	6	15

Tab. 4 Monthly averaged radiation quantities for the year 1993 in W/m^2, % or hours/day. K⇓ = global radiation, G_0 = extraterrestrial insolation, K⇑ = reflected solar radiation, L⇓ = downward long-wave radiation, L⇑ = upward long-wave radiation, s = observed shunshine duration, S_0 = astronomical sunshine duration, K*, L* and Q* net short-wave, net long-wave and net total radiation balance, respectively.

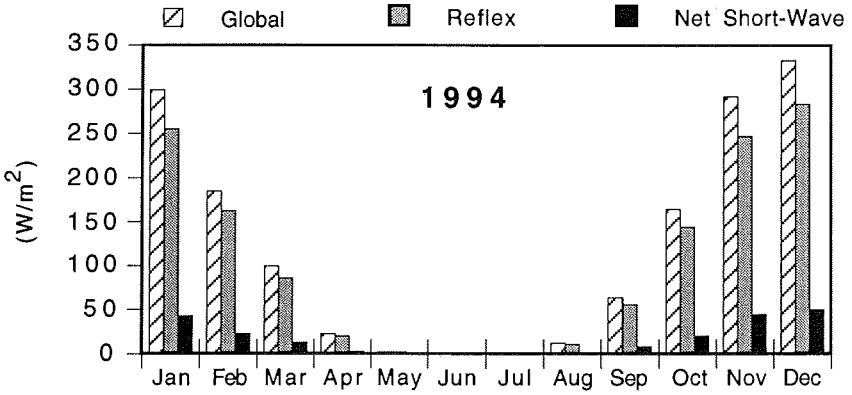

Fig. 48a Monthly averaged global radiation, reflected solar radiation and short-wave radiation balance for 1994.

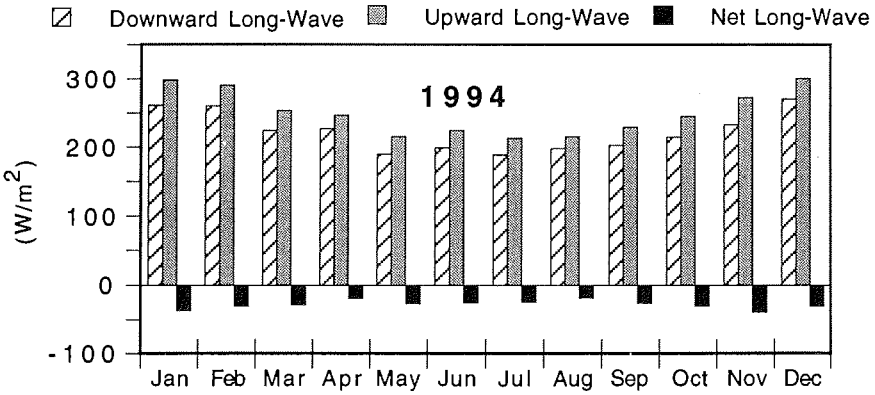

Fig. 48b Monthly averaged downward long-wave radiation, upward long-wave radiation and net long-wave radiation for 1994.

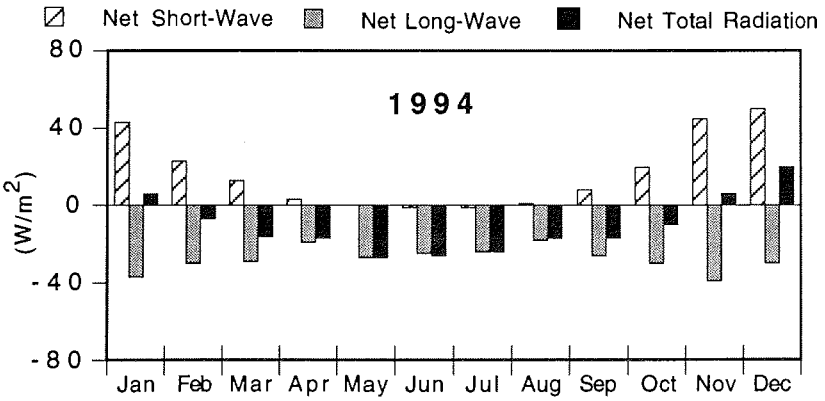

Fig. 48c Monthly averaged net short-wave radiation, net long-wave radiation and net total radiation for 1994.

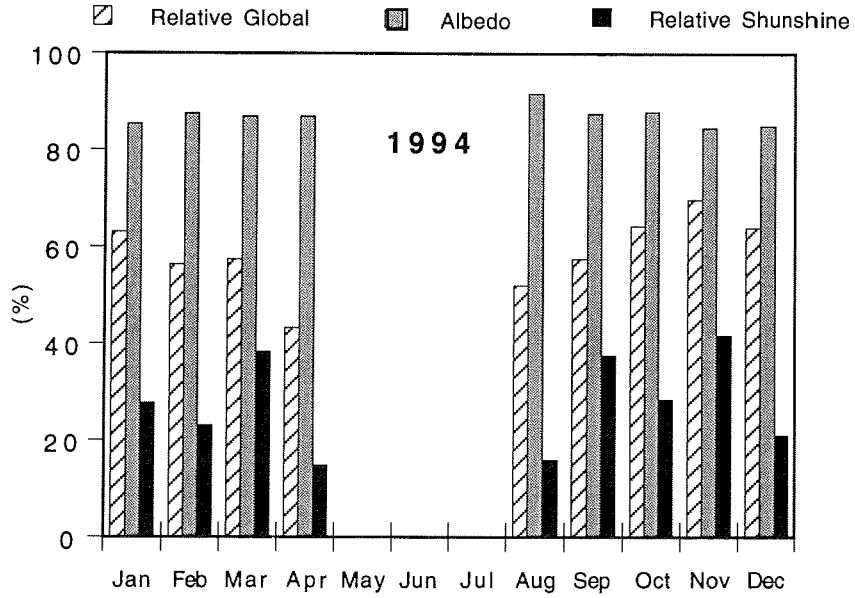

Fig. 48d Monthly averaged relative global radiation (global radiation versus extraterrestrial insolation), albedo and relative sunshine duration (observed sunshine duration versus astronimical sunshine duration) in percent for 1994.

1994	Jan	Feb	Mar	Apr	May	Jun	Jul	Aug	Sep	Oct	Nov	Dec
K⇓	299	185	99	23	2	0	0	12	64	164	292	333
K⇓/G_0	63	57	58	43	-	-	-	52	58	64	70	64
K⇑	255	162	86	20	2	0	0	11	56	144	247	283
K⇑/K⇓	85	88	87	88	-	-	-	91	87	88	85	85
L⇓	261	260	224	227	190	199	189	198	203	215	233	271
L⇑	298	290	253	247	216	224	213	216	229	245	272	301
s	6.5	4.0	4.8	1.2	0.3	0.0	0.0	1.0	4.1	4.4	9.1	5.1
s/S_0	28	23	38	15	-	-	-	16	38	29	42	21
K*	43	23	13	3	0	0	0	1	8	20	45	50
L*	-37	-30	-29	-19	-27	-25	-24	-18	-26	-30	-39	-30
Q*	6	-7	-16	-17	-27	-26	-24	-17	-17	-10	6	20

Tab. 5 Monthly averaged radiation quantities for the year 1994 in W/m², % or hours/day. K⇓ = global radiation, G_0 = extraterrestrial insolation, K⇑ = reflected solar radiation, L⇓ = downward long-wave radiation, L⇑ = upward long-wave radiation, s = observed shunshine duration, S_0 = astronomical sunshine duration, K*, L* and Q* net short-wave, net long-wave and net total radiation balance, respectively.

4.3.7. Yearly Averages

On the basis of the daily averages yearly averages are derived, see Fig. 49 and Tab. 6. Negative values denote an energy loss and positive values an energy gain at the Earth's surface.

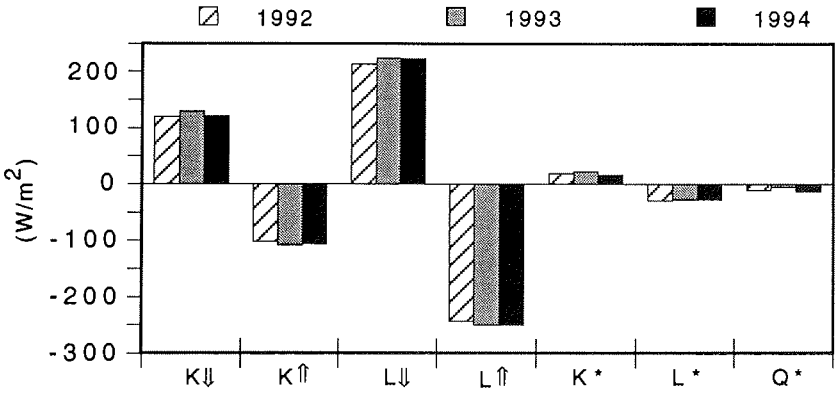

Fig. 49 Yearly averaged radiation quantities for the years 1992, 1993, 1994 in W/m^2. K⇓ = global radiation, K⇑ = reflected solar radiation, L⇓ = downward long-wave radiation, L⇑ = upward long-wave radiation, K*, L* and Q* net short-wave, net long-wave and net total radiation balance.

	1992	1993	1994
K⇓ (W/m^2)	120	129	121
K⇓/G_0 (%)	62	66	62
K⇑ (W/m^2)	-101	-108	-106
K⇑/K⇓ (%)	84	83	87
L⇓ (W/m^2)	214	223	222
L⇑ (W/m^2)	-243	-250	-250
s (hour:min.)	3:41	4:13	3:22
s/S_0 (%)	32	36	29
K* (W/m^2)	19	22	16
L* (W/m^2)	-29	-27	-28
Q* (W/m^2)	-10	-5	-12

Tab. 6 Yearly averaged radiation quantities for the years 1992, 1993, 1994. K⇓ = global radiation, G_0 = extraterrestrial insolation, K⇑ = reflected solar radiation, L⇓ = downward long-wave radiation, L⇑ = upward long-wave radiation, s = observed sunshine duration, S_0 = astronomical shunshine duration, K*, L* and Q* net short-wave, net long-wave and nettotal radiation balance.

5. Acknowledgements

Thanks are due to all wintering crews at Neumayer Station, to Dr. S. El Naggar who took care of the scientific instrumentation and B. Loose who developed the data aquisition and improved the instrumentation of the meteorological observatory of Neumayer.

6. References

Deutscher Wetterdienst (1982):
Wetterschlüsselhandbuch VuB2, Band A+B, Offenbach.

Fröhlich, C. and Shaw, G.E. (1980):
New Determination of Rayleigh Scattering in the Terrestrial Atmosphere, Applied Optics, 19, 1773-1775.

Gube, M. and Obleitner, F. (1986):
The Meteorological Data of the Georg-von-Neumayer Station for 1981 and 1982, Reports on Polar Research 30.

Gube-Lenhardt, M. (1987):
The Meteorological Data of the Georg-von-Neumayer Station for 1983 and 1984, Reports on Polar Research 38.

Helmes, L. (1989):
The Meteorological Data of the Georg-von-Neumayer Station for 1985, 1986 and 1987, Reports on Polar Research 64.

Herber, A., Thomason, L.W., Radionov, V.F. and Leiterer, U. (1993):
Comparison of Trends in the Tropospheric and Stratospheric Aerosol Optical Depths in the Antarctic, J. Geophys. Res., 98, 18441-18447.

Iqbal, M. (1983):
An Introduction to Solar Radiation, Academic Press, Toronto, 390p.

Kasten, F. (1966):
A new Table and Approximation Formula for the Relative Optical Airmass, Arch. Met. Geophys. Biokl. B., 206-223

Kasten, F. and Young, A.T. (1989):
Revised Optical Airmass Table and Approximation Formula, Applied Optics, 28, 4735-4738.

König-Langlo, G. (1992):
The Meteorological Data of the Georg-von-Neumayer Station (Antarctica) for 1988, 1989, 1990 and 1991, Reports on Polar Research 116.

König-Langlo, G. and Augstein, E. (1994):
Parameterization of the Downward Long-Wave Radiation at the Earth's Surface in Polar Regions, Meteorologische Zeitschrift N.F.3 Jg. 1994, H. 6, 343 - 347.

Leiterer, U. and Weller, M. (1988):
Sun Photometer BAS and ABAS for Atmospheric Research, WMO-TD 222, 21-26.

Russell, P.B.; Livingson, L.M.; Dutton, E.G.; Pueschel, R.F.; Reagen, J.A.; Defoor, T.E.; Box, M.A.; Allen, D.; Pilewskie, P.; Herman, B.M.; Kinne, S.A. and Hofmann D.J. (1988):
Pinatubo and Pre-Pinatubo Optical Depth Spectra: Mauna Loa Measurements, Comparisons, Inferred Size Distributions, Radiative Effects, and Relationship to Lidar Data, J. Geophys. Res., 98, 22969 - 22985.

Schmidt, T. and König-Langlo, G. (1994):
Radiation Measurements at the German Antarctic Station Neumayer 1982 - 1992, Reports on Polar Research 146.

Schwerdtfeger, W (1984):
Weather and Climate of the Antarctic, Developements in Atmospheric Sci. 15, Elsevier, The Nederlands, 261 p.

Trepte, C.P., Thomason, L.W. and Kent, G.S. (1994):
Banded Structure in Stratospheric Aerosol Distribution, Geophys. Res. Let., 21, 2397-2400, 1994.

Van Loon, H. and Rogers, J.C. (1984a):
The yearly wave in pressure and zonal geostrophic wind at sea level on the Southern Hemisphere and its interannual variability, Tellus 36 A, pp 348-354.

Van Loon, H. and Rogers, J.C. (1984b):
Interannual variations in the half-yearly cycle of pressure gradients and zonal wind at sea level on the Southern Hemisphere, Tellus 36 A, pp 76-86.

WMO (1983a):
Guide to Climatological Practices, Report No.100, World Meteorological Organization, Geneva.

WMO (1983b):
Guide to Meteorological Instruments and Methods of Observation, Report No. 8, World Meteorological Organization, Geneva.

WMO (1991):
Radiation and Climate. Second Workshop on Implementation of the Baseline Surface Radiation Network, WCRP-64, Report No. 453, World Meteorological Organization, Geneva.

WMO (1995):
Scientific Assessment of Ozone Depletion: 1994, Global Ozone Research and Monitoring Project - Report No 37, World Meteorological Organization, Geneva.